AN INVESTIGATION INTO THE USE OF THE METHOD OF SPHERICAL CURRENTS FOR THE DETERMINATION OF SCATTERED WAVE FIELDS

A thesis submitted to

THE UNIVERSITY OF CAPE TOWN

in fulfilment of the requirements for the degree of

DOCTOR OF PHILOSOPHY

Department of Applied Mathematics
University of Cape Town
September 1976

by
N.M. du Plessis M.Sc.

CONTENTS

ABSTRACT

In this thesis an approximation method, the method of spherical currents, is advanced for the determination of scattered fields (acoustic and electromagnetic) from convex bodies for plane harmonic incident waves. The method is worked out for the scalar (acoustic) case and applied to sound soft and sound hard obstacles of a given shape. The surface fields and backscattering cross sections of these obstacles are calculated according to the method and the results are compared with those of other methods. For the vector (electromagnetic) case only the basic theory is worked out for a perfectly conducting convex body.

CHAPTER I

INTRODUCTION

In this thesis an approximation method, the method of spherical currents, is advanced for the determination of scattered fields (acoustic and electromagnetic) from convex bodies for plane harmonic incident waves. The method is worked out for the scalar (acoustic) case and applied to sound soft and sound hard obstacles of a given shape. The surface fields and back-scattering cross sections of these obstacles are calculated according to the method and the results are compared with those of other methods. For the vector (electromagnetic) case only the basic theory is worked out for a perfectly conducting convex body.

The emphasis on scalar theory is a natural consequence of its greater simplicity compared with electromagnetic theory. During the past few decades however the emphasis in the literature has been mainly on electromagnetic scattering and it is in this field that most of the experimental data is available for comparison. Since the advent of the use of radar as a means of target identification this emphasis on vector theory is understandable, and has in addition led to many experimental results being published in this field.

The limitations imposed above on the incident field and the boundary conditions are not stringent. Not only are they good approximations to a wide variety of practical situations; they are also amenable to analytical treatment. The approximation method investigated here is however not intrinsically limited to plane incident fields and soft or hard or perfectly conducting bodies. As will become clear in the following chapters, the method can be applied to a convex body for arbitrary incident fields and boundary conditions provided that the surface field for a sphere under the same conditions is known. Being based on the solutions for spheres, the method is limited to convex bodies.

In the following paragraph a survey of the field of study is given with particular reference to the scope of this investigation as outlined above.

(1.1) Methods for the determination of scattered fields.

The basic equation of acoustics is the scalar Helmholtz equation

$$\nabla^2 \Phi + k^2 \Phi = 0 \qquad \text{--- (1.1.1),}$$

where Φ is the velocity potential of the sound field and $k = 2\pi/\lambda$ is the wave number.

Two fundamental problems of particular relevance to this investigation is to find solutions of (1.1.1) exterior to a closed, bounded surface S of sufficient smoothness on which either (a) Φ assumes a pre-assigned value on S (the exterior Neumann problem for the Helmholtz equation) or (b) the normal derivative of Φ assumes a pre-assigned value on S (the exterior Dirichlet problem for the Helmholtz equation). It is further required that these solutions satisfy the Sommerfeld radiation conditions

$$|R\Phi| = O(1/R)$$

$$R\left(\frac{\partial \Phi}{\partial R} + ik\Phi\right) = o(1/R) \qquad \text{--- (1.1.2),}$$

to ensure a unique solution in the infinite exterior region.

It can be shown that the second equation of (1.1.2) implies the first.

The Dirichlet and Neumann problems outlined above are the mathematical formulations of the physical problems of finding the scattered fields produced by respectively sound soft and sound hard bounded obstacles. [Hönl, Maue and Westpfahl (1961), Stratton (1941), Kellogg (1929)].

Proofs of the uniqueness and existence of the Dirichlet and Neumann problems proceed from the Helmholtz integral representation of the field, here given for points x_i exterior to S.

$$\underline{\Phi}(x_i) = \frac{1}{4\pi}\oint_S \left[\underline{\Phi}(\eta_i)\frac{\partial G}{\partial n}(x_i,\eta_i) - G(x_i,\eta_i)\frac{\partial \underline{\Phi}}{\partial n}(\eta_i)\right] dS$$

--- (1.1.3)

In (1.1.3) η_i is the point of integration on S and $\partial/\partial n = n_i\, \partial/\partial \eta_i$ is the normal derivative with n_i the outward pointing unit normal on S.

Let ξ_i be a point on S and take the limit $x_i \to \xi_i$ in (1.1.3). The resulting equation makes it clear that it is not possible to assign arbitrary values to Φ and $\partial\Phi/\partial n$ on S. Consequently there must exist a functional relationship between Φ and $\partial\Phi/\partial n$. If however we assign a value to either Φ or $\partial\Phi/\partial n$, the limiting process creates integral equations in resp. $\partial\Phi/\partial n$ and Φ. It is on the uniqueness and existence of the solutions of these integral equations that the uniqueness and existence of the exterior Dirichlet and Neumann problems for the Helmholtz equation ultimately devolve. These problems have received considerable attention and have recently been studied by Ahner (1975), Ursell (1973) and Kleinman and Roach (1974).

Solutions of these integral equations may be substituted into (1.1.3) with the pre-assigned values of Φ or $\partial\Phi/\partial n$ to provide the scattered field exterior to the obstacle. The analytical solution of these integral equations are however limited to but a few obstacles - those for which the scattered field may be determined by the method of separation of variables. The scattered field exterior to a obstacle can be solved by the method of separation of variables for only those cases

where the surface of the obstacle coincides with a coordinate surface in a system of coordinates in which the scalar Helmholtz equation (1.1.1) separates, i.e. in which it is possible to separate the second order partial differential equation into second order ordinary differential equations, each involving a single coordinate as independent variable. Notable examples of closed, bounded obstacles for which exact solutions have been found are the sphere and the spheroid. Even in those cases where an exact solution is obtained, these solutions are of limited practical value for large values of ka, where a is a significant body dimension. This is due to the fact that the solutions are found in the form of infinite series which converge progressively more slowly with increasing ka. To obtain insight in the high frequency behaviour of scattered fields for which an exact solution is known, these exact solutions have to be asymptotically approximated. Basically what is needed here is a series representation of the solution in increasing powers of 1/ka. Asymptotic representations of the exact solutions of the cylinder [Franz (1954)] and sphere [Imai (1954)] problems were obtained by representing the series solution as the sum of the residues of a contour integral, and then applying the Watson transform. Kazarinoff and Ritt (1959) developed an alternative method applicable to separable scalar problems and applied it to the prolate spheroid. Here the theory of complex resolvents of Sims and Philips was used to replace the Watson transform.

By assuming that Φ in (1.1.1) has an asymptotic expansion for $k \to \infty$ of the form

$$\Phi \sim e^{ikS(x_i)} \sum_{n=0}^{\infty} \frac{A_n(x_i)}{(ik)^n}$$

--- (1.1.4),

Keller, Lewis and Seckler (1956) managed to obtain high frequency solutions of a large number of scalar scattering problems, of which the leading term is the geometrical optics solution.

By directly finding the asymptotic expansion it is avoided to first find the exact solution and then expanding it asymptotically. However the calculations involved become laborious except for the simplest geometries, and the results are incomplete where diffracted rays occur. Lee (1975) has generalized and developed this method for the case of electromagnetic scattering from a conducting surface.

On inserting (1.1.4) into (1.1.1) and equating to zero the coefficient of each power of k, the following equations are obtained:

$$\partial_i S \partial_i S = (\nabla S)^2 = 1 \qquad \text{--- (1.1.5)}$$

and $$2\partial_i A_n \partial_i S + A_n \partial_i \partial_i S = -\partial_i \partial_i A_{n-1},$$
$$n = 0, 1, 2, \text{----} \; ; \; A_{-1} = 0$$

Equation (1.1.5) is the eiconal of geometrical optics, and determines the phase function S.

A field of the form (1.1.4) is called a ray field and the functions A_n are amplitude functions. In the case of electromagnetic scattering these coefficients are vectors. The first term in (1.1.4), $A_o e^{ikS}$, is the geometrical acoustics (optics) field, and describes the behaviour of scalar (vector) wave fields in the limit as the wavelength tends to zero. The problem of geometrical optics is therefore to find these phase- and amplitude functions. A brief description of the geometrical optics field as applied to scattering problems is given in sections (2.2) and (3.6). The value of the methods of geometrical optics in the determination of

scattered waves lies chiefly in the near field. The specular returns of the reflected rays in the far field contains a minimum of information about the shape of the scattering object.

The results of geometrical optics may be extended to lower frequencies by general asymptotic methods such as those described above, or by generalizing Fermat's principle so as to include "diffracted" rays. The eiconal (1.1.5) is a direct consequence of Fermat's principle, and if this principle is applied to incident rays not tangentially striking a smooth interface, "reflected rays" are created at the point of incidence in accordance with Snell's laws. These reflected rays are the scattered field of geometrical optics. According to geometrical optics no contribution is made by points on the interface situated (a) where the incident rays are tangential to the surface, (b) at vertices and (c) at edges. Keller (1958) postulated the creation of diffracted rays at such points and generalized Fermat's principle to include them. This method has been applied to a variety of shapes, and a brief description with special reference to the spheroid is given in section (3.6).

Geometrical optics and its extensions into the resonance region are generally referred to as "ray optics", for which even wider applications is being found. Recently particular attention has been paid to the problem of diffraction by a wedge, and the fact that Keller's geometric theory of diffraction solution is not valid near to a shadow boundary. [Lee and Deschamps (1976)].

Apart from asymptotic methods and those of ray optics improvements to the geometric optics solution can be made by utilizing and modifying the surface field predicted by it. The method of spherical currents belongs to this class of approximation method.

According to geometrical optics, the surface field on an ideally reflecting object is twice the incident field on the illuminated region and zero on the shadow side. Physical optics (Kirchhoff theory) uses the surface field predicted by geometrical optics in the Helmholtz integral representation (1.1.3) to predict the field exterior to a scattering object. This method is obviously also a high frequency approximation, but it is a great improvement on geometrical optics, especially as far as the determination of scattered far fields is concerned. The method of physical optics is discussed in section (2.4) and applied in section (3.6) to calculate the backscattering cross section of a hard prolate spheroid for axial incidence. Physical optics has been extensively used for a wide variety of shapes in cross section estimation. In this regard see the survey by Senior (1965) and the reports by Sleator (1964) and Kleinman and Senior (1963).

The main weakness of physical optics is the discrepancy between the assumed surface field and the true surface field. Two aspects may be singled out here. In the first place the surface field assumed by physical optics on the illuminated part of the obstacle is a good approximation only at such points at which the radii of curvature are large compared with the incident wavelength. In this regard see section (2.4). A second weakness lies in the discontinuity of the surface field at the penumbra, i.e. the neighbourhood of the shadow curve.

This is a violation of the true boundary condition, and Jones (1957) avoids this discrepancy by assuming that the penumbra of a smooth convex body is locally that of a cylinder whose generator is tangent to the shadow curve and whose radius of curvature is that of the given body in a plane normal to this tangent. Another method to estimate the contribution of the penumbra was developed

by Fock (1946), and is based on the surface field induced on a paraboloid of revolution.

A third weakness of the surface field assumed by physical optics is that it does not discriminate between objects having identical illuminated surfaces but different shaded surfaces. For example, physical optics predicts the same radar cross section in the backscattered direction for axial incidence for both flatbacked and double-backed cones with identical illuminated surfaces.

According to Blore (1964), Adachi (1960) derived an approximate general solution for the backscattering nose-on cross section of axially symmetric thin bodies having sharp apices. Blore states that "essentially this approximate solution is the physical optics solution, but the physical optics current is assumed over the *whole* surface of the scatterer". Unfortunately the author has not yet received a copy of Adachi's report, but presumably Blore means that the approximation of twice the incident field (for ideal reflectors) is used over the whole surface of the scatterer. If this is the case Adachi's theory removes the latter two of the three weaknesses of the physical optics surface field mentioned above. In this respect see also section (2.4). As the method is applied to long thin bodies, at least one of the principal radii of curvature is large compared to the incident wavelength over most of the surface. This restriction should bring the assumed surface field closer to the true surface field. Blore confirms that for such bodies Adachi's theory gives an accurate prediction of the echo area in the resonance region.

The approximation methods mentioned above are all essentially high frequency methods which to a lesser or greater extent successfully penetrate the resonance region of scattered fields for different bodies.

Dawson and Turner (1960) proposed a cylindrical current method to predict high frequency scattering with greater accuracy than physical optics. This publication is classified, but a condensed version of this method is given in the report by Kleinman and Senior (1963). The method is based on the exact solution for the infinite circular cylinder, is limited to bodies of revolution and cannot be used for axial incidence.

None of these limitations apply to the method of spherical currents, which in addition circumvents the latter two of the three weaknesses in the surface field of physical optics mentioned above, and at least partially, compensates for the finite radii of curvature of smooth convex bodies.

The examples of approximate solutions mentioned above clearly emphasize the importance of exact solutions. Although rigorous solutions of scattering problems have been obtained in but a few examples, many features of these solutions can be applied to more complex shapes.

At the other end of the frequency spectrum we have the Rayleigh region, that is the long wavelength at low frequency region where the wavelength of the incident field is large compared with the body dimensions. A brief outline of Rayleigh theory is given in section (4.1).

Kleinman (1965) gives a definition of the Rayleigh region, and an outline of general methods is given for obtaining successive terms in low frequency expansions. Basically the problem consists of finding a series in ascending powers of k for the scattered field satisfying (1.1.1). The first term in the Rayleigh expansion can be obtained by several methods, notably the empirical method of Siegel (1958).

Low frequency techniques have also been applied successfully to penetrate the resonance region from the low

frequency end of the spectrum, and to provide information in other directions than the backscattered one. In this respect Senior (1973) for scalar scattering from soft and hard objects, and Keller, Kleinman and Senior (1972) for electromagnetic scattering from perfect conductors must be mentioned.

An approximation method not easily categorized is impulse analysis, iniated by Kennaugh and Cosgriff (1958). This method has been applied to predict the radar cross section in the backscattered direction for several shapes, notably the spheroid [Moffatt and Kennaugh (1965)] and the cone sphere [Kennaugh and Moffatt (1962)]. Considerable success has been achieved with this method in the resonance region for some simple shapes [see Blore (1964)]. The limitations of the impulse approximation technique are discussed in the survey by Senior (1965).

Recent attempts [Burnside, Yu and Marhefka (1975)] to bridge the resonance region gap have used the moment method [Harrington (1968)] in combination with Keller's geometric theory of diffraction.

Finally it should be mentioned that although rigorous solutions by analytical means are obtainable for few shapes, the direct numerical solution of the integral equations satisfied by the surface field for other shapes may lead to estimates of scattered fields which for practical purposes could be considered exact.

Over the past few years this problem has received the attention of several authors, e.g. Burton and Miller (1971).

(1.2) Summary of contents.

In Chapter II the method of spherical currents is developed for the scalar scattering of a plane incident wave by bounded convex acoustically soft and hard obstacles.

As the method uses the exact surface fields on spheres, a reasonably detailed account of the scattering of a plane wave by soft and hard spheres is given. The method is then applied to approximate the surface field on arbitrary bounded convex soft and hard obstacles for plane incident waves. The Helmholtz integral representation is then used to obtain expressions for the near and far scattered fields. These results are finally specialized for bodies of revolution for axial incidence.

It was felt to be essential that the method should be compared with results obtained from a shape for which an exact solution exists. Such a body is the spheroid, and the surface field and backscattered cross section for axial incidence by a plane wave according to the method of spherical currents was compared with exact results for the spheroid in Chapter III. In this chapter comparisons are also drawn between the method of spherical currents and physical optics and the geometrical theory of diffraction in the high frequency range.

In Chapter IV the method of spherical currents is applied to the flatbacked cone and the cone sphere and comparisons are made with Siegel's empirical formulae in the Rayleigh region. The method is applied to these shapes to test its applicability in the presence of vertices, edges, plane surfaces and surfaces on which one of the principal radii of curvature become infinite. As results are obtained in the Rayleigh region, it is doubtful whether any meaningful conclusion can be drawn from the way in which edges and vertices are accomodated in the method of spherical currents.

The basic theory of the method in the case of electromagnetic scattering for a plane wave incident on a bounded, convex perfect conductor is developed in Chapter V. The surface current is constructed for the general case and then specialized for the case of an

axially incident wave on a body of revolution. The far field is then derived for bodies of revolution for axial incidence by using the integral representation of the electromagnetic field.

In Chapter VI the results of the previous chapters are summarized and integrated, and some conclusions are drawn from them.

CHAPTER II

THE METHOD OF SPHERICAL CURRENTS - SCALAR CASE.

The main purpose of this chapter is to explain the application of the method of spherical currents to the problem of determining scattered scalar waves, in particular for plane incident waves impinging on acoustically soft and hard convex obstacles. This is done in section (2.4) for the surface field, and in section (2.5) for the exterior field by using the surface field according to the method of spherical currents in the Helmholtz integral representation for the scattered field. As the method of spherical currents is based on the exact solution of the sphere problem, a fairly detailed account of the scattering by hard and soft spheres for plane incident waves is given in section (2.2). As background to this, and partially also because some of the motivation behind the method of spherical currents demands it, it is necessary to give an account of the basic theory of the boundary value problem of acoustics in section (2.1). As it appears in section (2.5), it was not possible to complete analytically the integration over the surface of the scatterer in order to determine the scattered field, far or near. As a consequence of this recourse had to be taken to automatic computation to determine e.g. far fields and cross sections. This involves the computation of the surface fields on spheres and consequently also of spherical Bessel functions and their derivatives over a wide range of argument so as to maximize the frequency range over which the method is applicable. An account of the methods of computation used for the surface fields of spheres and spherical Bessel functions is given in section (2.3).

(2.1) Basic theory - the boundary value problem.

For monochromatic, harmonic scalar waves in isotropic, homogeneous media the wave equation reduces to the scalar Helmholtz equation

$$\nabla^2 \Phi + k^2 \Phi = 0 \qquad \text{--- (2.1.1)}$$

The time dependency of Φ is expressed by the factor $\exp(-i\omega t)$, where $\omega = 2\pi\nu$ is the angular frequency, and ν the frequency. In (2.1.1) $k = 2\pi/\lambda$ is the wave number where λ is the wave length, and Φ represents the velocity potential of acoustics or the scalar potential of electromagnetic theory.

The fundamental problem of the scattering of harmonic waves by bounded obstacles (scatterers) is to find a solution of (2.1.1) exterior to the obstacle of which Φ or its normal derivative (or a linear combination of both), assumes pre-assigned values on the surface S of the obstacle. These boundary conditions may be reduced to two fundamental types:

$$\Phi = 0 \quad \text{on S} \qquad \text{--- (2.1.2s)},$$

or,
$$\frac{\partial \Phi}{\partial n} = 0 \quad \text{on S} \qquad \text{--- (2.1.2h)},$$

where $\partial\Phi/\partial n$ is the normal derivative of Φ on S. If S divides space into an interior region D and an exterior region D', we assume the normal derivative to be taken in the direction pointing away from D.

In acoustics scatterers on which the field exterior to S satisfies (2.1.2s) or (2.1.2h) are respectively referred to as "sound soft" (e.g. air bubble in water) or "sound hard" (e.g. a rigid body in air).

The problem relevant to scattering or diffraction, that is finding a solution of (2.1.1) with the boundary conditions (2.1.2s) or (2.1.2h) at points exterior to S, is referred to as the "exterior problem". It is convenient to approach this problem by way of the "interior" problem: find a solution of (2.1.1) with

boundary conditions (2.1.2s) or (2.1.2h) at points interior to S, i.e. in D.

Let x_i, ($x_i \varepsilon D$) be the point at which a solution of (2.1.1) is sought, and let y_i be any other point such that $y_i \varepsilon D$, then

$$\bar{\nabla}^2 G(x_i, y_i) + k^2 G(x_i, y_i) = 0, \; y_i \neq x_i \text{ --- (2.1.3)},$$

where $$G = \frac{e^{ik|x_i - y_i|}}{|x_i - y_i|} = \frac{e^{ikR}}{R}$$

and $$\bar{\nabla}^2 = \frac{\partial}{\partial y_i} \cdot \frac{\partial}{\partial y_i}$$, in Cartesian tensor notation.

We now apply Green's Theorem to the two scalar fields Φ and G in D bounded by S.

$$\int_D (\bar{\Phi} \bar{\nabla}^2 G - G \bar{\nabla}^2 \bar{\Phi}) d\bar{\tau} = \oint_S (\bar{\Phi} \frac{\partial G}{\partial \eta_i} - G \frac{\partial \bar{\Phi}}{\partial \eta_i}) d f_i$$

--- (2.1.4)

In (2.1.4) $d\bar{\tau}$ is the volume element with y_i as variable of integration, n_i is a point on S and $df_i = n_i df$ is the vectorial surface element where n_i is the unit normal vector to S pointing away from D.

Let σ be a small sphere of radius δ, centred at x_i, with interior region d. Applying (2.1.4) to the region D - d we have:

$$\int_{D-d} (\bar{\Phi} \bar{\nabla}^2 G - G \bar{\nabla}^2 \bar{\Phi}) d\bar{\tau} = \oint_{S+\sigma} (\bar{\Phi} \frac{\partial G}{\partial \eta_i} - G \frac{\partial \bar{\Phi}}{\partial \eta_i}) d f_i$$

--- (2.1.5)

In (2.1.5) η_i now also refers to points on σ, on which n_i points towards x_i. Now (2.1.1) is valid in D, and in D - d

$$\nabla^2 G + k^2 G = 0 \quad ,$$

hence (2.1.5) becomes:

$$\oint_\sigma \left(\bar{\Phi} \frac{\partial G}{\partial \eta_i} - G \frac{\partial \bar{\Phi}}{\partial \eta_i} \right) d\mathcal{f}_i = \oint_S \left(\bar{\Phi} \frac{\partial G}{\partial \eta_i} - G \frac{\partial \bar{\Phi}}{\partial \eta_i} \right) d\mathcal{f}_i \qquad \text{--- (2.1.6)}$$

By introducing spherical polar coordinates centred at x_i for the integral on the left hand side it is easily shown that

$$\lim_{\delta \to 0} \oint_\sigma \left(\bar{\Phi} \frac{\partial G}{\partial \eta_i} - G \frac{\partial \bar{\Phi}}{\partial \eta_i} \right) d\mathcal{f}_i = - 4\pi \, \bar{\Phi}(x_i)$$

Hence, from (2.1.6)

$$\bar{\Phi}(x_i) = - \frac{1}{4\pi} \oint_S \left(\bar{\Phi} \frac{\partial G}{\partial \eta_i} - G \frac{\partial \bar{\Phi}}{\partial \eta_i} \right) d\mathcal{f}_i$$

$$= - \frac{1}{4\pi} \oint_S \left(\bar{\Phi} \frac{\partial G}{\partial n} - G \frac{\partial \bar{\Phi}}{\partial n} \right) d\mathcal{f} \qquad \text{--- (2.1.7)}$$

In (2.1.7) $\dfrac{\partial \bar{\Phi}}{\partial n} = n_i \dfrac{\partial \bar{\Phi}}{\partial \eta_i}$ was used.

For the exterior problem let $x_i \epsilon D'$, where D' is the region exterior to S but interior to the arbitrary closed surface Σ. On applying (2.1.7) to D' bounded by S and Σ, we get:

$$\bar{\Phi}(x_i) = \frac{1}{4\pi} \oint_{S+\Sigma} \left(\bar{\Phi} \frac{\partial G}{\partial n} - G \frac{\partial \bar{\Phi}}{\partial n} \right) d\mathcal{f} \qquad \text{--- (2.1.8).}$$

In (2.1.8) the normals to both S and Σ are directed into D'.

Consider the case where Σ is taken to be a sphere of radius $R = |x_i - \eta_i|$. By choosing spherical polar coordinates centred at x_i it is readily shown that

$$\lim_{R\to\infty} \int_{\Sigma} \left(\underline{\Phi} \frac{\partial G}{\partial n} - G \frac{\partial \underline{\Phi}}{\partial n} \right) d\mathcal{f} = 0,$$

provided that

$$|R\underline{\Phi}| = O(1/R)$$
$$R\left(\frac{\partial \underline{\Phi}}{\partial R} + ik\underline{\Phi} \right) = o(1/R) \qquad \text{--- (2.1.9)}$$

The conditions (2.1.9) are the Sommerfeld radiation conditions which give expression to the physical requirement that there can not be any contribution to the field from infinity. These conditions are also sufficient to guarantee a unique solution of (2.1.1) exterior to S.

Hence, for all fields satisfying the radiation conditions exterior to S, we have

$$\underline{\Phi}(x_i) = \frac{1}{4\pi} \int_{S} \left(\underline{\Phi} \frac{\partial G}{\partial n} - G \frac{\partial \underline{\Phi}}{\partial n} \right) d\mathcal{f} \qquad \text{--- (2.1.10)}$$

The integral on the right hand side of course vanishes identically for all $x_i \in D$.

Let us refer to the prevailing (given) field prior to the introduction of the obstacle as the incident field $\Phi^{(i)}$. By introducing the scatterer this field is modified, and we refer to the resultant field exterior to the obstacle as the total field, $\Phi^{(t)}$. The scattered field $\Phi^{(s)}$ is now defined by

$$\underline{\Phi}^{(t)} = \underline{\Phi}^{(i)} + \underline{\Phi}^{(s)} \qquad \text{--- (2.1.11)}$$

The boundary conditions (2.1.2s) and (2.1.2h) refer to the total field, and they may now be written as:

$$\Phi^{(s)} = -\Phi^{(i)} \quad \text{on S} \qquad \text{--- (2.1.12s)}$$

$$\frac{\partial \Phi^{(s)}}{\partial n} = -\frac{\partial \Phi^{(i)}}{\partial n} \quad \text{on S} \qquad \text{--- (2.1.12h)}$$

It is of course required that all these fields satisfy the scalar Helmholtz equation exterior to S. If the radiation conditions apply to both $\Phi^{(s)}$ and $\Phi^{(i)}$, then (2.1.10) applies to all three fields.

On using (2.1.12s) and (2.1.12h) equation (2.1.10) becomes for the scattered field:

$$\Phi^{(s)}(x_i) = -\frac{1}{4\pi}\oint_S \left(\Phi^{(i)}\frac{\partial G}{\partial n} + G\frac{\partial \Phi^{(s)}}{\partial n}\right) d\xi \qquad \text{--- (2.1.13s)}$$

$$\Phi^{(s)}(x_i) = \frac{1}{4\pi}\oint_S \left(\Phi^{(s)}\frac{\partial G}{\partial n} + G\frac{\partial \Phi^{(i)}}{\partial n}\right) d\xi \qquad \text{--- (2.1.13h)}$$

For the total field we get:

$$\Phi^{(t)}(x_i) = -\frac{1}{4\pi}\oint_S G\,\frac{\partial \Phi^{(t)}}{\partial n}\, d\xi \qquad \text{--- (2.1.14s)}$$

$$\Phi^{(t)}(x_i) = \frac{1}{4\pi}\oint_S \Phi^{(t)}\frac{\partial G}{\partial n}\, d\xi \qquad \text{--- (2.1.14h)}$$

Should the radiation conditions not apply to the incident field, then (2.1.13s and h) continue to hold for the scattered field, but (2.1.14s and h) are no longer valid for the total field. The plane wave is an example of a field which is a solution of (2.1.1), but which does not satisfy the radiation conditions.

However, as it is a good approximation of an incident field reaching a target from a distant source, it is of great importance. Only plane incident waves will be considered here. Let the plane incident wave Ψ be defined by

$$\Psi = e^{ikU_i x_i} \qquad \text{--- (2.1.15),}$$

where u_i is the direction of propagation.

The equations (2.1.9) do not apply to Ψ. It is however easily shown that

$$\lim_{R\to\infty} \oint_{\Sigma} \left(\Psi \frac{\partial G}{\partial n} - G \frac{\partial \Psi}{\partial n} \right) d\mathcal{S} = \Psi \qquad \text{--- (2.1.16)}$$

This may be shown directly or by using (2.1.8) for the incident field. In this case the integral over S is zero - this integral is related by Green's theorem to a volume integral over D which vanishes owing to $x_i \notin D$.

Hence for a plane incident wave (2.1.8) becomes for the total field:

$$\Phi^{(t)}(x_i) = -\frac{1}{4\pi} \oint_S G \frac{\partial \Phi^{(t)}}{\partial n} d\mathcal{S} + \Psi \qquad \text{--- (2.1.17s)}$$

$$\Phi^{(t)}(x_i) = \frac{1}{4\pi} \oint_S \Phi^{(t)} \frac{\partial G}{\partial n} d\mathcal{S} + \Psi \qquad \text{--- (2.1.17h)}$$

On using (2.1.11), (2.1.17s) and (2.1.17h) become for the scattered field:

$$\Phi^{(s)}(x_i) = -\frac{1}{4\pi} \oint_S G \frac{\partial \Phi^{(t)}}{\partial n} d\mathcal{S} \qquad \text{--- (2.1.18s)}$$

$$\Phi^{(s)}(x_i) = \frac{1}{4\pi} \oint_S \Phi^{(t)} \frac{\partial G}{\partial n} d\mathcal{S} \qquad \text{--- (2.1.18h)}$$

Equations (2.1.13s and h) could be used to calculate $\Phi^{(s)}(x_i)$, $x_i \varepsilon D'$, if respectively $\partial\Phi^{(s)}/\partial n$ and $\Phi^{(s)}$ are known on S. In the sound hard case we may find $\Phi^{(s)}(\xi_i)$, $\xi_i \varepsilon S$, from a singular integral equation of the second kind obtained from (2.1.13h) by taking the limit as $x_i \to \xi_i$. Similarly we may obtain an integral equation of the second kind for $\partial\Phi^{(s)}/\partial n\ (\xi_i)$, $\xi_i \varepsilon S$, from (2.1.13s). In this case however we first operate with $n_i\, \partial/\partial x_i$ on both sides of the equation before taking the limit as $x_i \to \xi_i$.

However, we may also use (2.1.18s and h) to calculate $\Phi^{(s)}(x_i)$, $x_i \varepsilon D'$, if we respectively know the values of the normal derivative of the total field and the total field itself on S. These may be obtained from integral equations arising from (2.1.17s and h) as we take the limit as $x_i \to \xi_i$. Owing to the simpler nature of the "free" term (that is the term not containing the unknown function) in (2.1.17s and h) compared with (2.1.13s and h), this latter procedure is followed.

Operate on both sides of (2.1.17s) with $\bar{n}_i\, \partial/\partial x_i$, where $\bar{n}_i$ is the unit normal to S at ξ_i, the line segment $x_i - \xi_i$ being normal to S at ξ_i, and take the limit as $x_i \to \xi_i$ of the resulting equation as well as of (2.1.17h).

Hence we have:

$$\lim_{x_i \to \xi_i} \bar{n}_i \frac{\partial \bar{\Phi}^{(t)}}{\partial x_i} = -\frac{1}{4\pi} \lim_{x_i \to \xi_i} \int_S \bar{n}_i \frac{\partial G}{\partial x_i}(x_i, \eta_i) \frac{\partial \bar{\Phi}^{(t)}}{\partial n}(\eta_i)\, d\mathcal{S} + \lim_{x_i \to \xi_i} \bar{n}_i \frac{\partial \bar{\Psi}}{\partial x_i},$$

or

$$\frac{\partial \bar{\Phi}^{(t)}}{\partial n}(\xi_i) = \frac{\partial \bar{\Psi}}{\partial n}(\xi_i) - \frac{1}{4\pi} \lim_{x_i \to \xi_i} \int_S \bar{n}_i \frac{\partial G}{\partial x_i}(x_i, \eta_i) \frac{\partial \bar{\Phi}^{(t)}}{\partial n}(\eta_i)\, d\mathcal{S}$$

--- (2.1.19s)

and

$$\underline{\Phi}^{(t)}(\xi_i) = \underline{\Psi}(\xi_i) + \frac{1}{4\pi} \lim_{x_i \to \xi_i} \oint_S \frac{\partial G}{\partial n}(x_i, \eta_i)\, \underline{\Phi}^{(t)}(\eta_i)\, d\mathcal{f}$$

--- (2.1.19h)

For the limits of the integrals in (2.1.19s and h) we have (see Hönl, Maue & Westpfahl (1961) pp. 233 - 236 or Kellogg (1967) Chapter VI, Theorems VI and VIII with $G = 1/|x_i - y_i|$):

$$\lim_{x_i \to \xi_i} \oint_S \bar{n}_i \frac{\partial G}{\partial x_i}(x_i, \eta_i) \frac{\partial \underline{\Phi}^{(t)}}{\partial n}(\eta_i)\, d\mathcal{f} = -2\pi \frac{\partial \underline{\Phi}^{(t)}}{\partial n}(\xi_i) + \oint_S \bar{n}_i \frac{\partial G}{\partial \xi_i}(\xi_i, \eta_i) \frac{\partial \underline{\Phi}^{(t)}}{\partial n}(\eta_i)\, d\mathcal{f}$$

$$\lim_{x_i \to \xi_i} \oint_S \frac{\partial G}{\partial n}(x_i, \eta_i) \underline{\Phi}^{(t)}(\eta_i)\, d\mathcal{f} = 2\pi\, \underline{\Phi}^{(t)}(\xi_i) + \oint_S \frac{\partial G}{\partial n}(\xi_i, \eta_i)\, \underline{\Phi}^{(t)}(\eta_i)\, d\mathcal{f}$$

Using these equations (2.1.19s) and (2.1.19h) respectively become:

$$\frac{\partial \underline{\Phi}^{(t)}}{\partial n}(\xi_i) = -\frac{1}{2\pi} \oint_S \bar{n}_i \frac{\partial G}{\partial \xi_i}(\xi_i, \eta_i) \frac{\partial \underline{\Phi}^{(t)}}{\partial n}(\eta_i)\, d\mathcal{f} + 2 \frac{\partial \underline{\Psi}}{\partial n}(\xi_i)$$

--- (2.1.20s)

$$\underline{\Phi}^{(t)}(\xi_i) = \frac{1}{2\pi} \oint_S \frac{\partial G}{\partial n}(\xi_i, \eta_i)\, \underline{\Phi}^{(t)}(\eta_i)\, d\mathcal{f} + 2\, \underline{\Psi}(\xi_i)$$

--- (2.1.20h)

The problem of the exterior boundary value problem with sound soft and sound hard scatterers has therefore been reduced to solving the singular integral equations (2.1.20s) and (2.1.20h). The integrals in these equations, though improper, do exist.

It can be shown that the kernels $\bar{n}_i \, \partial G/\partial \xi_i$ and $\partial G/\partial n = n_i \, \partial G/\partial \eta_i$ have the same properties as the analogous kernels of potential theory where $G = 1/|\xi_i - y_i|$. Kellogg (Kellogg (1929), Chapter XI) has shown that the kernels of potential theory behave like continuous kernels.

Although the equations (2.1.20s and h) are indispensable for proofs of existence and uniqueness, they are of little value where an analytical solution to a particular problem is sought. Other methods, such as separation of the variables, are more convenient for the achievement of such results.

(2.2) Scattering by sound soft and sound hard spheres.

As the method of spherical currents is based upon the exact solution of the scattering problem for spheres, a derivation of this solution is given below. This procedure is that of Hönl, Maue and Westpfahl (Hönl, Maue and Westpfahl (1961), pp. 532 - 535) which ties up with the theory of the preceding paragraph.

Consider a sound soft or sound hard sphere of radius a being illuminated by an incident plane wave. The origin of the system of axes is chosen at the centre of the sphere, and spherical polar coordinates are introduced defined by the equations

$$(x_1, x_2, x_3) = (r \sin\theta\cos\phi, \; r \sin\theta \sin\phi, \; r\cos\theta)$$

$$(\xi_1, \xi_2, \xi_3) = (a \sin\theta\cos\phi, \; a \sin\theta \sin\phi, \; a\cos\theta)$$

$$(\eta_1, \eta_2, \eta_3) = (a \sin\theta'\cos\phi', \; a \sin\theta' \sin\phi', \; a\cos\theta')$$

--- (2.2.1)

The direction of propagation of the incident wave is chosen to be that of the negative 3-axis, hence $(u_1, u_2, u_3) = (0, 0, -1)$ in (2.1.15) and we have

$$\Psi = e^{-ikx_3} = e^{-ikr\cos\theta} \qquad \text{--- (2.2.2)}$$

With this choice of coordinates the equations (2.1.18s and h) for the scattered field, now independent of the azimuthal angle, become:

$$\Phi^{(s)}(r,\theta) = -\frac{a^2}{4\pi}\int_0^{\pi}\frac{\partial\Phi^{(t)}}{\partial n}(\theta')\sin\theta'\,d\theta'\int_0^{2\pi}\frac{e^{ikR}}{R}\,d\phi'$$

--- (2.2.3s)

$$\Phi^{(s)}(r,\theta) = \frac{a^2}{4\pi}\int_0^{\pi}\Phi^{(t)}(\theta')\sin\theta'\,d\theta'\int_0^{2\pi}\frac{\partial}{\partial a}\left(\frac{e^{ikR}}{R}\right)d\phi'$$

--- (2.2.3h)

where

$$R = |x_i - \eta_i| = (x_i x_i + \eta_i\eta_i - 2x_i\eta_i)^{1/2}$$
$$= (r^2 + a^2 - 2ar\cos\Theta)^{1/2},$$

and

$$\cos\Theta = x_i\eta_i/ar = \sin\theta\sin\theta'(\cos\phi\cos\phi' + \sin\phi\sin\phi') + \cos\theta\cos\theta'$$
$$= \cos\theta\cos\theta' + \sin\theta\sin\theta'\cos(\phi - \phi')$$

--- (2.2.4)

Θ is the angle included between the position vectors ξ_i and η_i.

In (2.2.3h) we used $\partial/\partial n = n_i\, \partial/\partial \xi_i = \partial/\partial a$. This result is directly obtained by expressing the gradiënt operator in terms of spherical polar coordinates.

The surface fields $\partial\Phi^{(t)}/\partial n$ and $\Phi^{(t)}$ in (2.2.3s) and (2.2.3h) respectively are now determined by means of (2.1.20s) and (2.1.20h).

With the choice of coordinates (2.2.1), and using (2.2.2) and $\bar{n}_i\, \partial/\partial \xi_i = \partial/\partial a$, (2.1.20s and h) become:

$$\frac{\partial \Phi^{(t)}}{\partial n}(\Theta) = -\frac{a^2}{2\pi}\int_0^{\pi} \frac{\partial \Phi^{(t)}}{\partial n}(\Theta')\sin\Theta' d\Theta' \int_0^{2\pi} \frac{\partial}{\partial a}\left[\frac{e^{ika\sqrt{2-\cos\Theta}}}{a\sqrt{2-\cos\Theta}}\right] d\phi' - 2ik\cos\Theta\, e^{-ika\cos\Theta}$$

--- (2.2.4s)

$$\Phi^{(t)}(\Theta) = \frac{a^2}{2\pi}\int_0^{\pi} \Phi^{(t)}(\Theta')\sin\Theta' d\Theta' \int_0^{2\pi} \frac{\partial}{\partial a}\left[\frac{e^{ika\sqrt{2-\cos\Theta}}}{a\sqrt{2-\cos\Theta}}\right] d\phi' + 2\, e^{-ika\cos\Theta}$$

--- (2.2.4h)

Owing to the similarity of these two equations, only the procedure by means of which the latter is solved is given. The method consists of representing the functions in the integral equations by their expansions in terms of Legendre polynomials. For the kernel of the integral equation this is achieved by means of the expansion.

$$\frac{e^{ikR}}{R} = e^{ik(r^2+a^2-2ar\cos\Theta)^{1/2}} \Big/ (r^2+a^2-2ar\cos\Theta)^{1/2}$$

$$= ik\sum_{n=0}^{\infty}(2n+1)P_n(\cos\Theta)\, j_n(ka)\, h_n^{(1)}(kr), \quad r>a$$

--- (2.2.5)

(Magnus and Oberhettinger (1954), p.21)

In (2.2.5) $P_n(x)$ is the Legendre polynomial of degree n, and $j_n(z)$ and $h_n^{(1)}(z)$ are respectively spherical Bessel functions of the first and third kinds. The function $h_n^{(1)}(z)$ is related to $j_n(z)$ and $y_n(z)$, the spherical Bessel function of the second kind, by means of the equation

$$h_n^{(1)}(z) = j_n(z) + i\, y_n(z) \qquad \text{--- (2.2.6)}$$

These functions can be expressed in terms of the half-order Bessel- and Hankel functions as follows:

$$j_n(z) = \sqrt{\pi/2z}\; J_{n+1/2}(z)$$

$$y_n(z) = \sqrt{\pi/2z}\; Y_{n+1/2}(z)$$

$$h_n^{(1)}(z) = \sqrt{\pi/2z}\; H_{n+1/2}^{(1)}(z)$$

--- (2.2.7)

As series of ascending powers of z, $j_n(z)$ and $y_n(z)$ are defined as follows:

$$j_n(z) = \frac{z^n}{1.3.5\cdots(2n+1)}\left[1 - \frac{(1/2)z^2}{1!(2n+3)} + \frac{(\frac{1}{2}z^2)^2}{2!(2n+3)(2n+5)} - \cdots\right]$$

$$y_n(z) = \frac{1.3.5.\cdots(2n-1)}{z^{n+1}}\left[1 - \frac{\frac{1}{2}z^2}{1!(1-2n)} + \frac{(\frac{1}{2}z^2)^2}{2!(1-2n)(3-2n)} - \cdots\right]$$

--- (2.2.8)

. (Abramowitz and Stegun (1965), Chapter 10)

With the representation (2.2.5) of $G = e^{ikR}/R$, it is necessary to define

$$\frac{\partial}{\partial a}\left[\frac{e^{ika\sqrt{2-\cos\Theta}}}{a\sqrt{2-\cos\Theta}}\right] = \frac{\partial G}{\partial a} \qquad \text{in (2.2.4s and h).}$$

From (2.2.5) we have:

$$\lim_{r\to a} \frac{\partial G}{\partial r} = ik^2 \sum_{n=0}^{\infty} (2n+1) P_n(\cos\Theta) j_n(\epsilon) h_n^{(1)\prime}(\epsilon)$$

and

$$\lim_{r\to a} \frac{\partial G}{\partial a} = ik^2 \sum_{n=0}^{\infty} (2n+1) P_n(\cos\Theta) j_n'(\epsilon) h_n^{(1)}(\epsilon)$$

where

$$\epsilon = ka, \quad j_n'(\epsilon) = \frac{d}{d\epsilon} j_n(\epsilon), \quad \text{etc.}$$

Hence

$$\lim_{r\to a} \frac{\partial G}{\partial r} - \lim_{r\to a} \frac{\partial G}{\partial a} = ik^2 \sum_{n=0}^{\infty} (2n+1) P_n(\cos\Theta) W\{j_n(\epsilon), h_n^{(1)}(\epsilon)\}$$

where

$$W\{j_n(\epsilon), h_n^{(1)}(\epsilon)\} = -i/\epsilon^2 \qquad \text{--- (2.2.9)}$$

is the Wronskian determinant of the functions $j_n(\epsilon)$ and $h_n^{(1)}(\epsilon)$. It follows that

$$\lim_{r\to a} \frac{\partial G}{\partial r} \neq \lim_{r\to a} \frac{\partial G}{\partial a}.$$

We define

$$\left.\frac{\partial G}{\partial a}\right|_{r=a} = \frac{1}{2}\left(\lim_{r\to a} \frac{\partial G}{\partial r} + \lim_{r\to a} \frac{\partial G}{\partial a}\right),$$

$$\therefore \frac{\partial G}{\partial a} = \frac{ik^2}{2} \sum_{n=0}^{\infty} (2n+1) P_n(\cos\Theta) \{j_n(\epsilon) h_n^{(1)\prime}(\epsilon) + j_n'(\epsilon) h_n^{(1)}(\epsilon)\}$$

--- (2.2.10)

With $\cos\Theta$ defined by (2.2.4) the Legendre polynomial $P_n(\cos\Theta)$ may be expanded in terms of associated Legendre polynomials $P_n^{\ell}(\cos\theta)$ and $P_n^{\ell}(\cos\theta')$ by means of the addition theorem for spherical harmonics (Magnus and Oberhettinger (1954), p. 55):

$$P_n(\cos\Theta) = \sum_{\ell=-n}^{n} (-1)^{\ell} P_n^{\ell}(\cos\theta)\, P_n^{-\ell}(\cos\theta')\, e^{i\ell(\phi-\phi')}$$

--- (2.2.11)

By means of (2.2.10) and (2.2.11) and using

$$\int_0^{2\pi} e^{i\ell(\phi-\phi')}\, d\phi' = 2\pi\, \delta_{\ell,0} \qquad \text{, we get}$$

$$\frac{a^2}{2\pi} \int_0^{2\pi} \frac{\partial\theta}{\partial a}\, d\phi' =$$

$$\frac{i\epsilon^2}{2} \sum_{n=0}^{\infty} (2n+1)\left\{ j_n(\epsilon)\, h_n^{(1)\prime}(\epsilon) + j_n'(\epsilon)\, h_n^{(1)\prime}(\epsilon) \right\} P_n(\cos\theta)\, P_n(\cos\theta')$$

--- (2.2.12)

The plane incident wave is expanded in terms of Legendre polynomials as follows:

$$e^{-ikr\cos\theta} = \sum_{n=0}^{\infty} (-i)^n (2n+1)\, j_n(kr)\, P_n(\cos\theta)$$

--- (2.2.13)

For $\Phi^{(t)}$ on the surface we assume an expansion

$$\Phi^{(t)}(\theta) = \sum_{n=0}^{\infty} (-i)^n (2n+1)\, a_n\, P_n(\cos\theta)$$

--- (2.2.14)

We have to find the expansion coefficients as functions of ka = ε. Substitute the expressions for

$$\frac{a^2}{2\pi}\int_0^{2\pi}\frac{\partial G}{\partial a}\,d\phi' \quad , \quad e^{-ika\cos\theta} \qquad \text{and}$$

$\Phi^{(t)}(\theta)$, given respectively by (2.2.12), (2.2.13) and (2.2.14), into (2.2.4h), and then integrate w.r.t. θ', using the orthogonality relation

$$\int_{-1}^{+1} P_n(x)\,P_m(x)\,dx = \frac{2}{2n+1}\cdot\delta_{nm} \qquad \text{--- (2.2.15)}$$

We get, for each n,

$$a_n = i\epsilon^2\left\{j_n(\epsilon)\,h_n^{(1)\prime}(\epsilon) + j_n'(\epsilon)\,h_n^{(1)}(\epsilon)\right\}a_n - 2j_n(\epsilon)$$

Solving for a_n we get, by using (2.2.9):

$$a_n = (i/\epsilon^2)\,h_n^{(1)\prime}(\epsilon) \quad , \quad \text{hence the total surface}$$

field is, from (2.2.4):

$$\underline{\Phi}^{(t)}(\theta) = \frac{i}{\epsilon^2}\sum_{n=0}^{\infty}(-i)^n(2n+1)\frac{P_n(\cos\theta)}{h_n^{(1)\prime}(\epsilon)}$$

--- (2.2.16h)

By following the same procedure we obtain the following expression for $\partial\Phi^{(t)}(\theta)/\partial n$, the normal derivative of the total field on the surface:

$$\frac{\partial\underline{\Phi}^{(t)}}{\partial n}(\theta) = -\frac{ik}{\epsilon^2}\sum_{n=0}^{\infty}(-i)^n(2n+1)\frac{P_n(\cos\theta)}{h_n^{(1)}(\epsilon)}$$

--- (2.2.16s)

The expressions for the surface fields are now substituted into (2.2.3s and h) respectively, and after integration w.r.t. θ' and ϕ' we get the following solutions for the scattered fields exterior to sound soft and sound hard spheres respectively:

$$\underline{\Phi}^{(s)}(r,\theta) = -\sum_{n=0}^{\infty} (-i)^n (2n+1) \frac{j_n(\epsilon)}{h_n^{(1)}(\epsilon)} h_n^{(1)}(kr) P_n(\cos\theta)$$

--- (2.2.17s)

$$\underline{\Phi}^{(s)}(r,\theta) = -\sum_{n=0}^{\infty} (-i)^n (2n+1) \frac{j_n'(\epsilon)}{h_n^{(1)\prime}(\epsilon)} h_n^{(1)\prime}(kr) P_n(\cos\theta)$$

--- (2.2.17h)

The far field S of a field $\Phi(x_i)$ is defined by the equation

$$\lim_{x\to\infty} \underline{\Phi}(x_i) = \frac{e^{ikx}}{kx} \cdot S$$

--- (2.2.18),

where $x = |x_i|$.

Using $h_n^{(1)}(kr) \sim (-i)^{n+1} \frac{e^{ikr}}{kr}, \quad r \gg n$

--- (2.2.19),

the following expressions are found for the far scattered fields of sound soft and sound hard spheres:

$$S(\theta) = i \sum_{n=0}^{\infty} (-1)^n (2n+1) \frac{j_n(\epsilon)}{h_n^{(1)}(\epsilon)} P_n(\cos\theta)$$

--- (2.2.20s)

$$S(\theta) = i \sum_{n=0}^{\infty} (-1)^n (2n+1) \frac{j_n'(\epsilon)}{h_n^{(1)\prime}(\epsilon)} P_n(\cos\theta)$$

--- (2.2.20h)

The backscattered direction is the direction opposite to the direction of incidence, and in this case is defined by $\theta = 0$. Hence, on putting $P_n(1) = 1$, we have for the far field in the backscattered direction:

$$S(0) = i \sum_{n=0}^{\infty} (-1)^n (2n+1) \frac{j_n(t)}{h_n^{(1)}(t)} \qquad \text{--- (2.2.21s)}$$

$$S(0) = i \sum_{n=0}^{\infty} (-1)^n (2n+1) \frac{j_n'(t)}{h_n^{(1)\prime}(t)} \qquad \text{--- (2.2.21h)}$$

The backscattering cross section σ is defined by the equation

$$\sigma = \lim_{r \to \infty} 4\pi r^2 \frac{|W^{(s)}|}{|W^{(i)}|} \qquad \text{--- (2.2.22)}$$

Here $W^{(s)}$ is the power flux density of the scattered field at a distance r from the obstacle in the backscattered direction and $W^{(i)}$ is the power flux density in an incident plane wave field. If $\Phi^{(s)}$ is the scattered wave and Ψ the incident wave, then

$$\frac{|W^{(s)}|}{|W^{(i)}|} = \frac{|\Phi^{(s)} \Phi^{*(s)}|}{|\Psi \Psi^*|}$$, where the asterisk

indicates the complex conjugate. With Ψ defined as in (2.2.2) and using (2.2.18), (2.2.22) becomes

$$\sigma = \frac{4\pi}{k^2} |S(0)|^2 \qquad \text{--- (2.2.23)}$$

It is frequently convenient to use the normalized backscattering cross section σ/σ_0, where σ_0 is the backscattering cross section according to geometrical optics. Hence, if $\Phi_{(GO)}^{(S)}$ is the scattered field calculated according to geometrical optics, then

$$\sigma_o = \lim_{r\to\infty} 4\pi r^2 \frac{|\underline{\Phi}^{(s)}_{(GO)}\, \underline{\Phi}^{*(s)}_{(GO)}|}{|\underline{\Psi}\, \underline{\Psi}^*|} \qquad \text{--- (2.2.24)}$$

In geometrical optics the scattered field at a particular point is the sum of the fields of the reflected rays intersecting at that point. Hence only surface elements perpendicular to the incident beam can contribute to the backscattered field. The points at which the incident direction of propagation is perpendicular to the surface are known as specular points.

smooth convex body has only one such point for a given incident plane wave. Consider a narrow bundle of incident rays striking the surface very nearly perpendicular around the specular point. The area of the surface element containing the specular point can be written as $dS_1 dS_2 = \rho_1 \rho_2 d\theta_1 d\theta_2$, where ρ_1 and ρ_2 are the principal radii of curvature at the specular point, and $dS_1 = \rho_1 d\theta_1$ and $dS_2 = \rho_2 d\theta_2$ are arcs taken along the principal directions which are perpendicular to each other. Each incident ray of the bundle now gives rise to a reflected ray according to Snell's Law.

Hence the rays reflected from the extremities of the arc dS_1 diverge with an angle of $2d\theta_1$, and those reflected from the extremities of the arc dS_2 diverge with an angle $2d\theta_2$. At a distance $r >> \rho_1$ and ρ_2 from the surface element the cross sectional area of the incident bundle remains $dS_1 dS_2 = A^{(i)}$, but the reflected rays now have a cross sectional area of approximately $4r^2 d\theta_1 d\theta_2 = A^{(s)}$. Let $W^{(s)}$ and $W^{(i)}$ respectively be the power flux densities of the reflected (scattered) and incident waves at the distance r from the surface element, then energy conservation demands that $W^{(s)} A^{(s)} = W^{(i)} A^{(i)}$,

$$\therefore \frac{W^{(s)}}{W^{(i)}} = \frac{A^{(i)}}{A^{(s)}} = \frac{dS_1 dS_2}{4r^2 d\theta_1 d\theta_2} = \frac{\rho_1 \rho_2}{4r^2}$$

--- (2.2.25)

From (2.2.22) and (2.2.25) we now have:

$$\sigma_0 = \pi \rho_1 \rho_2 \qquad \text{--- (2.2.26)}$$

$\therefore$ for the sphere $\qquad \sigma_0 = \pi a^2 \qquad$ --- (2.2.27)

From (2.2.23) and (2.2.27) we therefore have for the normalized backscattering cross section

$$\sigma/\sigma_0 = \frac{4}{k^2 a^2} |S(0)|^2 = \frac{4}{\epsilon^2} |S(0)|^2 \qquad \text{--- (2.2.28)}$$

(2.3) <u>The computation of spherical Bessel functions and the surface- and scattered fields of sound hard and sound soft spheres</u>.

As the method of spherical currents is based on the surface fields of spheres it is essential that efficient methods for the numerical computation of these fields be used. The methods have to be accurate over as wide a range of ka as possible, and preferably also uniform.

Fortran programs were written for execution either on the UNIVAC 1106 of the University of Cape Town or the UNIVAC 90/30 of the University of the Western Cape. These programs are listed in Appendix A, and the page numbers are prefixed by an A.

The formulas (2.2.16s and h) were used to compute the surface fields. These involve Legendre polynomials and spherical Bessel functions of the third kind and their derivatives.

The Legendre polynomials were computed by means of the recurrence formula

$$n P_n(x) - (2n-1)\, x\, P_{n-1}(x) + (n-1) P_{n-2}(x) = 0 \qquad \text{--- (2.3.1)}$$

with $\quad P_0(x) = 1 \quad$ and $\quad P_1(x) = x$

The program PLEG is listed on p. A1. Excellent correllation was found between values computed with this subroutine and those listed in existing tables [British Association Math. Tables, Part-volume A, (1946)].
Very close agreement was also found between values of $P_n(x)$ computed by means of PLEG and the subroutine LEGEN from the standard Univac software package MATH-PACK for $-1 \leq x \leq 1$ and $n = 0,1, \ldots 110$.
No restrictions are indicated for LEGEN.

By utilizing (2.2.6) and the equations

$$h_n^{(1)\prime}(z) = j_n'(z) + i\, y_n'(z) \qquad \text{--- (2.3.2)}$$

$$f_n'(z) = f_{n-1}(z) - \frac{(n+1)}{z} f_n(z) \qquad \text{--- (2.3.3)}$$

$$\left(f_n(z) = j_n(z);\ y_n(z);\ h_n^{(1)}(z);\ h_n^{(2)}(z)\right)$$

(Abramowitz and Stegun (1965), Chapter 10), the computation of $h_n^{(1)}(z)$ and $h_n^{(1)\prime}(z)$ is reduced to computing $j_n(z)$, $y_n(z)$, $j_n'(z)$ and $y_n'(z)$.

Initially $j_n(x)$ and $y_n(x)$ (real argument) were computed by using the power series expansions (2.2.8). Computed values (see subroutines PSI and ZETA on pp. A2 and A3) were compared with existing tables (N.B.S. Math. Tables Project, Tables of Spherical Bessel functions, Vols. I and II). For $10^{-2} \leq x \leq 1$ agreement with tabulated values ($0 \leq n \leq 30$) was established up to 8 significant digits. With increasing x the computed values become less reliable - at about $x = 8$ there is agreement to 5 - 6 significant digits (depending on the order) and this decreases to about 4 significant digits at $x = 10$. This error spreading is caused by the iterative factor x^2 when $x > 1$.

The lowest value of x for which $j_n(x)$ and $y_n(x)$ can be computed using PSI and ZETA is determined by the under-

and overflow limits of the computer - $j_0(x)$ diverges as $x \to 0$ and $j_n(x)$, $n \geq 1$ tends to zero more rapidly with increasing order as $x \to 0$. The functions $y_n(x)$ diverge more rapidly with increasing order as $x \to 0$.

The derivatives were computed by using (2.3.3). The subroutines DPSI and DZETA for the respective computation of $j_n'(x)$ and $y_n'(x)$ are listed on pp. A4 and A5. The reliability of these values is entirely dependent on those of $j_n(x)$ and $y_n(x)$.

Subsequently the subroutine BESJ from MATH-PACK was used to compute $j_n(x)$ and $y_n(x)$. The output of BESJ was compared with the tabulated values in the N.B.S. Math. Tables. Excellent correllation was found. The subroutine BESJ basically uses the recurrence equation for regular and irregular Bessel functions $f_\nu(x)$:

$$f_{\nu-1}(x) + f_{\nu+1}(x) = \frac{2\nu}{x} f_\nu(x) \qquad \text{--- (2.3.4)}$$

[Goldstein and Thaler (1959)].

For large values of the argument the so called phase-amplitude method is employed. [Goldstein and Thaler (1958)]. The definition of the Hankel functions (or Bessel functions of the third kind) in terms of $J_\nu(x)$ and $Y_\nu(x)$ viz.

$$H_\nu^{(1)}(x) = J_\nu(x) + i\, Y_\nu(x)$$

$$H_\nu^{(2)}(x) = J_\nu(x) - i\, Y_\nu(x) ,$$

suggest an alternative definition in terms of an amplitude function $A_\nu(x)$ and a phase function $\Phi_\nu(x)$:

$$H_\nu^{(1)} = A_\nu e^{i\Phi_\nu}$$

$$H_\nu^{(2)} = A_\nu e^{-i\Phi_\nu}$$

It then follows that

$$J_\nu(x) = A_\nu \cos\Phi_\nu \quad , \quad Y_\nu(x) = A_\nu \sin\Phi_\nu$$

Differential equations are obtained for A_ν and Φ_ν from Bessel's differential equation and the Wronskian of J_ν and Y_ν. It turns out that these equations are readily solved for large x.

It was found that subroutine BESJ gave incorrect values of $J_\nu(x) = J_{n+\frac{1}{2}}(x)$ for $x > 50$, $n \gtrsim 64$ - for these values of x the magnitude of the computed values of $J_{n+\frac{1}{2}}(x)$ increased with increasing n where it should decrease as n increases. This is clearly seen from (2.2.7) and (2.2.8) with $\nu = n + \frac{1}{2}$. In fact, if $\nu >> x/2$, the function $J_\nu(x) \sim (2\nu/x)^{-\nu}$ decreases very rapidly with increasing order. Hence if given $J_\nu(x)$ and $J_{\nu+1}(x)$, (2.3.4) will give poor accuracy for $J_{\nu+n}(x)$. On the other hand if $Y_\nu(x)$ and $Y_{\nu+1}(x)$ are given then (2.3.4) can be used to generate $Y_{\nu+n}(x)$ as for $\nu >> x/2$, $Y_\nu(x) \sim (2\nu/x)^{\nu}$ increases extremely rapidly with increasing order.

If however one is given $J_{\nu+n}(x)$ and $J_{\nu+n+1}(x)$ where $n >> (x/2)$, one might recur without loss of accuracy provided it is done in the direction of decreasing order. Such a method is derived by Goldstein and Thaler (1959) on which BESJ is based. However, for $x > 50$ it was neglected in BESJ to recur for $J_\nu(x)$ in the direction of decreasing order. This explained the erroneous values of $J_\nu(x)$ and the correct values of $Y_\nu(x)$ for $\nu >> x/2$, $x > 50$, as computed by using BESJ. The subroutine BESJ was then modified to ensure recurrence in the direction of decreasing order for $J_\nu(x)$. The output of the modified BESJ (pp. A6 - A8) for $x > 50$ was then compared with the Debye asymptotic approximations of $j_n(x)$ and $y_n(x)$ (Hönl, Maue and Westpfahl (1961) pp. 501 - 503):

$$j_n(x) \sim \begin{cases} (1-t^2)^{-1/4} \dfrac{\cos\sigma}{x} & (n < x - \frac{1}{2}) \\ (t^2-1)^{-1/4} \, e^{-\tau}/2x & (n > x - \frac{1}{2}) \end{cases} \qquad (2.3.5)$$

$$y_n(x) \sim \begin{cases} (1-t^2)^{-1/4} \dfrac{\sin\sigma}{x} & (n < x - \frac{1}{2}) \\ -(t^2-1)^{-1/4} \, e^{\tau}/x & (n > x - \frac{1}{2}) \end{cases} \qquad (2.3.6)$$

In (2.3.5) and (2.3.6)

$$\left.\begin{aligned} t &= (2n+1)/x \\ \sigma &= x\left(\sqrt{1-t^2} - t \arccos t\right) - \pi/4 \\ \tau &= x\left(t \ln\left(t + \sqrt{t^2-1}\right) - \sqrt{t^2-1}\right) \end{aligned}\right\} \qquad (2.3.7)$$

These asymptotic approximations are obtained by applying the Saddle point method to the Sommerfeld integral representations of the Bessel functions.

The computed values of $y_n(x)$ for $x > 50$ using the modified BESJ were the same as the values computed when using the original BESJ and agreed with values obtained by using (2.3.6) to two significant digits. The computed values of $j_n(x)$ for $x > 50$ using the modified BESJ displayed the expected behaviour of decreasing with increasing order when $\nu >> x/2$ and agreed with values obtained from (2.3.5) to two significant digits. In BESJ the restriction $0 < x < 88.028$ is placed on x, and it is mentioned that care should be exercised when calculating Bessel functions of high orders for $x \leq 2$.

The derivatives $j_n'(x)$ and $y_n'(x)$ were computed by means of the subroutine DBES (p. A9) based on (2.3.3).

The surface fields on hard spheres were calculated by means of the subroutine POTAS (p. A10) based on (2.2.16h). The output of POTAS is QR and QI respectively, the real and imaginary parts of the surface field. As the terms

of the real and imaginary parts of the surface field involve the same functions, and as the two series converge at roughly the same rate, they are computed in the same subroutine and the two series are terminated by a single convergence criterion. To be able to apply the method of spherical currents to surfaces with vertices [see section (2.4)], it is essential to compute surface fields for very small values of ka, if possible including $\varepsilon = ka = 0$. Owing to the restriction on the argument of the Bessel functions, this cannot be achieved by using (2.2.16h). However from (2.2.16h) a power series expansion in increasing powers of ka may be obtained by taking the inverse of the power series expansion of $j_n'(x) + iy_n'(x)$. This expansion (2.3.8) was used, neglecting terms of the fifth and higher degrees in ka, to compute the surface field for $0 \leq ka \leq .01$

$$\Phi^{(t)}(\theta) \approx \left[1 + (1/2 - \tfrac{5}{9} P_2(\cos\theta))\epsilon^2 + (\tfrac{1}{8} - \tfrac{1}{4}\cos\theta - \tfrac{5}{162} P_2(\cos\theta) + \tfrac{9}{525} P_4(\cos\theta)\right]$$

$$+ i\epsilon\left[\tfrac{3}{2}\cos\theta - (\tfrac{1}{3} + \tfrac{7}{60} P_3(\cos\theta)\epsilon^2\right]$$

--- (2.3.8)

Surface fields computed using POTAS were compared with existing tables [Schwarz (1943)]. Complete agreement with the tabulated values of the real and imaginary parts of the surface field was established. In Fig. (3.1) the graph of the surface field amplitude of a sound hard sphere (ka = 5) is plotted as a function of the polar angle.

For sound hard spheres the normalized backscattering cross section was computed by utilizing (2.2.28) and (2.2.21h), the latter equation giving the far field amplitude in the backscattered direction. Subroutine

SP on p. A11 generates PR and PI, respectively the real and imaginary parts of the far field amplitude. The graph of the normalized backscattering cross section for sound hard spheres for $0 \leq ka \leq 10$ is given in Fig. (3.6). As far as can be judged, this graph is identical to the one given by Senior (1966), Fig. 5 p. 660.

For sound soft spheres the normal derivative of the surface field (real and imaginary parts) was computed by means of subroutine PUT, p. A12, based on equation (2.2.16s). The normalized backscattering cross section for sound soft spheres was computed by using subroutine SPS, p. A13, to generate PR and PI, respectively the real and imaginary parts of the far field amplitude. This subroutine is based on equation (2.2.21s). The graph of the normalized backscattering cross section of soft spheres as a function of ka ($0 \leq ka \leq 10$) is given in Fig. (3.5). This graph agrees with that given by Senior (Senior (1961) Fig. 1, p. 657).

(2.4) The method of spherical currents - the surface field.

In what follows a method is described by means of which the surface field of an obstacle is approximated by utilizing the surface field of spheres with the same physical properties as the given obstacle and illuminated by the same incident field. For this reason the method is referred to as the method of spherical currents. The particular way in which the surface fields of spheres are used to approximate the surface field of a given body makes it clear that the method is applicable only to convex bodies possessing a continuously defined normal except at certain isolated points (vertices) or lines (edges). Methods are devised to deal with the field at vertices and edges. As far as physical properties (apart from shape) and incident fields are concerned the method is limited only in as far as the corresponding

problem for the sphere has been solved.

The method of spherical currents is outlined below for sound hard convex bodies impinged upon by a plane incident wave. A similar argument applies to convex bodies with different surface properties subject to different incident waves.

Consider a sound hard obstacle scattering a plane incident wave. If $\Phi(\xi_i)$ and $\Psi(\xi_i)$ are respectively the total and incident fields at a point ξ_i on the surface S of the obstacle, then $\Phi(\xi_i)$ satisfies the integral equation (2.1.20h):

$$\Phi(\xi_i) = \frac{1}{2\pi} \oint_S \frac{\partial G}{\partial n}(\xi_i, \eta_i) \Phi(\eta_i) d\mathcal{f} + 2\Psi(\xi_i)$$

--- (2.4.1)

In view of the singularity of the integrand at $\eta_i = \xi_i$, the major contribution to the integral in (2.4.1) can be attributed to a surface element σ of S ($\xi_i, \eta_i \varepsilon \sigma$) of which the points η_i are situated in the immediate proximity of ξ_i.

Hence $\Phi(\xi_i) \approx U(\xi_i)$ --- (2.4.2),

where $U(\xi_i)$ satisfies the integral equation

$$U(\xi_i) = \frac{1}{2\pi} \oint_\sigma \frac{\partial G}{\partial n}(\xi_i, \eta_i) U(\eta_i) d\mathcal{f} + 2\Psi(\xi_i)$$

--- (2.4.3)

In (2.4.3) $G(\xi_i, \eta_i) = \frac{e^{ikR}}{R}$, $R = |\xi_i - \eta_i|$.

$$\therefore \frac{\partial G}{\partial n} = n_i \frac{\partial G}{\partial \eta_i} = \frac{e^{ikR}}{R^3}(ikR - 1)(\eta_i - \xi_i) n_i$$

--- (2.4.4)

Should σ be a plane surface element, then $(\eta_i - \xi_i)\, n_i = 0$, and (2.4.3) becomes

$$U(\xi_i) = 2\Psi(\xi_i) \qquad \text{--- (2.4.5)}.$$

The assumption that $(\eta_i - \xi_i)\, n_i = 0$ has approximate validity over the whole of the convex surface only to the extent to which the radii of curvature at ξ_i can be considered as large compared with the wavelength. Under these conditions we may write

$$\Phi(\xi_i) \approx 2\Psi(\xi_i) \qquad \text{--- (2.4.6)}$$

The approximation (2.4.6) for the surface field is based on local considerations. In physical optics the approximation (2.4.6) for the surface field is used only on the illuminated part of the convex body. On the part in the geometrical shadow of the body the surface field is taken to be zero. Hence physical optics, while using the correct form of Huyghens' principle [equation (2.1.18h)] for the scattered field exterior to the hard obstacle, approximates the surface field by that predicted by geometrical optics, i.e. zero in the shadow region and twice the incident field in the illuminated region, in accordance with Snell's laws.

Equation (2.4.3) defines an approximation of the surface field at the point ξ_i of an arbitrary, smooth convex body. It follows that any two bodies with identical boundary properties sharing the same surface element σ at ξ_i will have the same approximated surface field at ξ_i. Construct a sphere passing through ξ_i with its centre in the region interior to S and situated on the normal to S at ξ_i. The radius ρ of the sphere is now chosen in such a manner that if σ be taken small enough, it can be considered as common to both S and the sphere, henceforth referred to as the representative sphere. The equation (2.4.3) now defines the same approximate surface field for the obstacle and the representative

sphere at ξ_i. The method of spherical currents now consists of approximating the surface field of S at ξ_i by the surface field of the representative sphere at ξ_i, thus compensating in a sense for non-local effects which would be ignored should the approximate field as defined by (2.4.3) be used. Hence

$$\Phi(\xi_i) \approx \Phi_{(sc)}(\xi_i) \qquad \text{--- (2.4.7),}$$

where, on using (2.2.16h)

$$\Phi_{(sc)}(\xi_i) = \frac{i}{k^2\rho^2} \sum_{n=0}^{\infty} (2n+1) i^n \frac{P_n(\cos\alpha)}{h_n^{(1)\prime}(k\rho)} \qquad \text{--- (2.4.8)}$$

In (2.4.8) ρ is the radius of the representative sphere (as yet undefined) and α is the angle between the normal to the representative sphere (and S) at ξ_i and the direction of propagation of the plane incident wave. In the special case where S is the surface of a hard sphere of radius a and the incident wave is propagated in the direction of the negative 3-axis (origin at centre of sphere), then $\cos\alpha = \cos(\pi-\theta)$, where θ is the polar angle, and (2.4.8) reduces to (2.2.16h), after using

$$P_n(\cos(\pi-\theta)) = P_n(-\cos\theta) = (-1)^n P_n(\cos\theta).$$

The choice of ρ, the radius of the representative sphere, must obviously depend upon the principal radii of curvature at the point ξ_i on S. As a first approximation σ can be considered as so small that for all $\eta_i \varepsilon \sigma$, $(\eta_i - \xi_i)\, n_i = 0$. As one moves away from ξ_i, the most rapid deviation from planeness will occur in the principal direction associated with the least of the principal radii of curvature. Hence a sensible choice for ρ would be the least of the principal radii of curvature. In addition, surface fields of sound hard spheroids were computed by the method of spherical

currents using the least principal radius, the maximum principal radius and the Gaussian curvature. These surface fields are graphically compared with those obtained from exact solutions for sound hard spheroids in Figures (3.1) to (3.3). The choice of least principal radius of curvature for the surface field according to the method of spherical currents gives the best approximation of the surface field on sound hard spheroids. The least principal radius of curvature is also chosen when one of the principal radii of curvature tends to infinity. At vertices or sharp points both principal radii of curvature tend to zero. At such points and in their immediate neighbourhood the low frequency expansion of (2.4.8) is used. From (2.3.8) we then have

$$\Phi_{(sc)}(\xi_i) \approx \left[1+\left(\frac{1}{2}-\frac{5}{9}P_2(\cos\alpha)\right)k^2\rho^2+\left(\frac{1}{8}+\frac{1}{4}\cos\alpha-\frac{5}{162}P_2(\cos\alpha)+\frac{9}{525}P_4(\cos\alpha)\right)k^4\rho^4\right]$$

$$+ik\rho\left[-\frac{3}{2}\cos\alpha-\left(\frac{1}{3}-\frac{7}{60}P_3(\cos\alpha)\right)k^2\rho^2\right]$$

--- (2.4.9)

At points where the surface of the scatterer is locally flat, that is where both principal radii of curvature tend to infinity, the approximation (2.4.6) for the surface field is used.

As far as edges are concerned, a surface field will be assigned to points in the neighbourhood of the edge in accordance with the procedure outlined above. The presence of an edge will therefore introduce a discontinuous change of surface field across the edge. By the same reasoning as outlined above it follows that in the sound soft case the normal derivative of the surface

field is given by

$$\frac{\partial \Phi^{\pm}(\xi_i)}{\partial n} = \frac{-ik}{k^2\rho^2} \sum_{n=0}^{\infty} \frac{(2n+1)\, i^n P_n(\cos\alpha)}{h_n^{(1)}(k\rho)} \qquad \text{--- (2.4.10)}$$

For a sphere (2.4.10) becomes (2.2.16s) with $\alpha = \pi - \theta$.

It now remains to derive expressions for $\cos\alpha$ and ρ for an arbitrary convex scatterer with a continuously defined normal except at certain isolated points and lines (edges).

Choose a Cartesian system of axes with origin in the interior of S. Let η_i be an arbitrary point on S with polar angles θ and ϕ, then the parametric equations of S can be written as

$$\left.\begin{aligned} \eta_1 &= \eta(\theta,\phi)\sin\theta\cos\phi \\ \eta_2 &= \eta(\theta,\phi)\sin\theta\sin\phi \\ \eta_3 &= \eta(\theta,\phi)\cos\theta \end{aligned}\right\} \qquad \text{--- (2.4.11),}$$

where η is the distance from the origin of the coordinate system to the point η_i.

Every point on S is uniquely characterized by a pair of parameters θ and ϕ of which the respective parametric lines are ϕ = const. and θ = const.

The tangent vectors $\partial\eta_i/\partial\theta$ and $\partial\eta_i/\partial\phi$ along the parametric lines satisfy the equation

$$\frac{\partial \eta_i}{\partial\theta}\frac{\partial \eta_i}{\partial\phi} = \frac{\partial \eta}{\partial\theta}\frac{\partial \eta}{\partial\phi} \qquad \text{--- (2.4.12)}$$

The vector product of the vectors $\partial\eta_i/\partial\theta$ and $\partial\eta_i/\partial\phi$, respectively the tangent vectors to the parametric lines ϕ = const. and θ = const., in this order, defines an outward pointing normal vector

$$N_i = \varepsilon_{ijk} \frac{\partial \eta_j}{\partial \theta} \frac{\partial \eta_k}{\partial \phi} \qquad \text{--- (2.4.13)}$$

The outward pointing unit normal vector n_i is defined by

$$n_i = N_i / \left| \varepsilon_{ijk} \frac{\partial \eta_j}{\partial \theta} \frac{\partial \eta_k}{\partial \phi} \right| \qquad \text{--- (2.4.14)}$$

If the incident plane wave is propagated in the direction of the unit vector u_i, then

$$\Psi(x_i) = e^{ik u_i x_i} \qquad \text{--- (2.4.15),}$$

and $$\cos\alpha = u_i n_i \qquad \text{--- (2.4.16)}$$

In the particular case of an axi-symmetric obstacle we choose the 3-axis of the coordinate system to coincide with the symmetry axis. Now η is a function of θ only, and (2.14.12) becomes

$$\frac{\partial \eta_i}{\partial \theta} \frac{\partial \eta_i}{\partial \phi} = 0 \qquad \text{--- (2.4.17).}$$

If in addition the incident direction of propagation is parallel to the 3-axis, i.e. $(u_i) = (0, 0, \pm 1)$, then (2.4.16) simplifies to:

$$\cos\alpha = \frac{\pm \eta' \sin\theta + \eta \cos\theta}{\sqrt{\eta^2 + \eta'^2}} \qquad \text{--- (2.4.18)}$$

In (2.4.18) the positive sign is taken if the incident field is propagated along the positive 3-axis, and the negative sign is taken if the incident field is propagated along the negative 3-axis. The prime indicates differentiation w.r.t. θ. It follows that in this case $\cos\alpha$ is independent of ϕ.

The curvature of a surface at a given point can be investigated by considering the radii of curvature of the normal plane curves of the surface at the given point. These curves are the intersections of the surface with

those planes containing the normal line through the given point.

From the differential geometry of surfaces we have that the reciprocals of the roots of the 2nd degree equation in λ below are the least and greatest radii of curvature of the normal plane curves (i.e. the principal radii of curvature) with parametric equations $\eta_i = \eta_i(\theta,\phi)$ at the point (θ,ϕ) on the surface. It can be shown that these roots are real. This equation has the form:

$$(LN-M^2)-\lambda(EN-2FM+GL)+\lambda^2(EG-F^2)=0 \qquad \text{--- (2.4.19)}$$

(Duschek and Hochrainer (1961) pp. 37 - 44).

In (2.4.19)

$$\left.\begin{aligned} E &= \frac{\partial \eta_i}{\partial\theta}\frac{\partial \eta_i}{\partial\theta}, \quad F = \frac{\partial \eta_i}{\partial\theta}\frac{\partial \eta_i}{\partial\phi}, \quad G = \frac{\partial \eta_i}{\partial\phi}\frac{\partial \eta_i}{\partial\phi} \\ L &= \frac{\partial^2 \eta_i}{\partial\theta^2} n_i, \quad M = \frac{\partial^2 \eta_i}{\partial\theta\,\partial\phi} n_i, \quad N = \frac{\partial^2 \eta_i}{\partial\phi^2} n_i \end{aligned}\right\} \text{--- (2.4.20)}$$

The vector n_i is the unit normal to the surface defined by (2.4.14) and (2.4.13). With this choice of unit normal the roots of (2.4.18) will be negative. This is due to the fact that n_i has an opposite orientation to

$$H_i = \frac{d^2\eta_i}{ds^2} \Big/ \left|\frac{d^2\eta_i}{ds^2}\right|,$$

the unit normal to the normal plane curves at the given point. Let λ_1 and λ_2 ($|\lambda_1| \le |\lambda_2|$ be the roots of (2.4.18), then the greatest and least principal radii of curvature, resp. ρ_1 and ρ_2, are given by

$$\rho_1 = -1/\lambda_1, \quad \rho_2 = -1/\lambda_2 \qquad \text{--- (2.4.21)}$$

In case of axial symmetry with the choice of axes as above, η in (2.4.10) is not a function of ϕ. All the quantities in (2.4.20) become independent of ϕ, and in

addition, F, G, M and N simplify considerably.

The unit normal now becomes

$$(n_i) = \frac{1}{\sqrt{\eta^2+\eta'^2}}\left(-\frac{d}{d\theta}(\eta\cos\theta)\cos\phi, -\frac{d}{d\theta}(\eta\cos\theta)\sin\phi, \frac{d}{d\theta}(\eta\sin\theta)\right)$$

--- (2.4.22)

As $\left(\frac{\partial^2 \eta_i}{\partial\theta^2}\right) = \left(\frac{\partial^2}{\partial\theta^2}(\eta\sin\theta)\cos\phi, \frac{\partial^2}{\partial\theta^2}(\eta\sin\theta)\sin\phi, \frac{\partial^2}{\partial\theta^2}(\eta\cos\theta)\right)$,

the scalar product

$$L = \frac{1}{\sqrt{\eta^2+\eta'^2}}\left(-\frac{\partial^2}{\partial\theta^2}(\eta\sin\theta)\frac{\partial}{\partial\theta}(\eta\cos\theta) + \frac{\partial^2}{\partial\theta^2}(\eta\cos\theta)\frac{\partial}{\partial\theta}(\eta\sin\theta)\right)$$

is independent of ϕ.

Also

$$\left(\frac{\partial^2 \eta_i}{\partial\theta\partial\phi}\right) = \frac{\partial}{\partial\theta}(\eta\sin\theta)(-\sin\phi, \cos\phi, 0),$$

$$\therefore \frac{\partial^2 \eta_i}{\partial\theta\partial\phi} = \frac{\partial}{\partial\theta}(\eta\sin\theta)\frac{\partial \eta_i}{\partial\phi} / \eta\sin\theta$$

As n_i involves the vector product of $\partial n_i/\partial\phi$ with $\partial n_i/\partial\theta$, it follows that

$$M = \frac{\partial^2 \eta_i}{\partial\theta\partial\phi} \cdot n_i = 0$$

From (2.4.12) we have that $F = \frac{\partial \eta_i}{\partial\theta}\frac{\partial \eta_i}{\partial\phi} = 0$

For axial symmetry (2.4.20) becomes:

$$E = \eta^2 + \eta'^2 \quad , \quad F = 0 \quad , \quad G = \eta^2 \sin^2\theta$$

$$L = \frac{1}{\sqrt{\eta^2+\eta'^2}}\left(\frac{\partial^2}{\partial\theta^2}(\eta\cos\theta)\frac{\partial}{\partial\theta}(\eta\sin\theta) - \frac{\partial^2}{\partial\theta^2}(\eta\sin\theta)\frac{\partial}{\partial\theta}(\eta\cos\theta)\right),$$

$$M = 0 \quad , \quad N = \frac{1}{\sqrt{\eta^2+\eta'^2}}\,\eta\sin\theta\,\frac{\partial}{\partial\theta}(\eta\cos\theta) \qquad \text{--- (2.4.23)}$$

For axial symmetry the coefficients in (2.4.19) are independent of ϕ and it follows that the principal radii of curvature are independent of ϕ. Consequently, bearing (2.4.18) in mind, we have from (2.4.8) and (2.4.10) that the surface fields are also independent of ϕ.

(2.5) The scattered field.

The equations (2.1.18s) and (2.1.18h) respectively define the scattered fields exterior to sound soft and sound hard obstacles illuminated by a plane incident disturbance.

$$\Phi^{(s)}(x_i) = -\frac{1}{4\pi}\oint_S G\,\frac{\partial \Phi^{(t)}}{\partial n}\,df \qquad \text{--- (2.1.18s)}$$

$$\Phi^{(s)}(x_i) = \frac{1}{4\pi}\oint_S \Phi^{(t)}\,\frac{\partial G}{\partial n}\,df \qquad \text{--- (2.1.18h)}$$

In these equations $G = \dfrac{e^{ik|x_i-\eta_i|}}{|x_i-\eta_i|} = e^{ikR}/R$,

x_i is exterior to S, η_i is the point of integration on S, df is the surface element and $\partial\Phi^{(t)}(\eta_i)/\partial n$ and $\Phi^{(t)}(\eta_i)$ are respectively the normal derivative of the surface field in the sound soft case and the surface field in the sound hard case.

We now introduce a system of axes as in the previous section. Then

$$(x_i) = (r\sin\theta\cos\phi, r\sin\theta\sin\phi, r\cos\theta)$$

$$(\eta_i) = (\eta\sin\theta'\cos\phi', \eta\sin\theta'\sin\phi', \eta\cos\theta')$$

--- (2.5.1)

In general η is a function of θ' and ϕ'.

With this choice of coordinates we have $df = |df_i|$, where df_i is the vectorial surface element defined by

$$df_i = \varepsilon_{ijk}\frac{\partial\eta_j}{\partial\theta'}\frac{\partial\eta_k}{\partial\phi'}d\theta'd\phi' = N_i\,d\theta'd\phi' \qquad \text{--- (2.5.2)}$$

$$\therefore df = \left|\varepsilon_{ijk}\frac{\partial\eta_j}{\partial\theta'}\frac{\partial\eta_k}{\partial\phi'}\right| d\theta'd\phi' \qquad \text{--- (2.5.3)}$$

$$G = e^{ikR}/R,$$

where $R = (r^2+\eta^2-2r\eta(\sin\theta\sin\theta'\cos(\phi-\phi')+\cos\theta\cos\theta'))^{1/2}$

--- (2.5.4)

Also

$$\frac{\partial G}{\partial n}(x_i,\eta_i) = n_i\frac{\partial G}{\partial\eta_i} = n_i\frac{\partial G}{\partial R}\frac{\partial R}{\partial\eta_i},$$

where n_i is the outward unit normal to S.
Hence, from (2.4.14) and using

$$\frac{\partial G}{\partial R} = \frac{e^{ikR}}{R^2}(ikR-1)$$

and $\dfrac{\partial R}{\partial\eta_i} = (\eta_i - x_i)/R$, we have:

$$\frac{\partial G}{\partial n} = \frac{1}{\left|\varepsilon_{ijk}\frac{\partial\eta_j}{\partial\theta'}\frac{\partial\eta_k}{\partial\phi'}\right|}\cdot\varepsilon_{ijk}(\eta_i-x_i)\frac{\partial\eta_j}{\partial\theta'}\frac{\partial\eta_k}{\partial\phi'}\frac{e^{ikR}}{R^3}(ikR-1)$$

--- (2.5.5)

We now replace $\partial\Phi^{(t)}/\partial n$ and $\Phi^{(t)}$ in (2.1.18s and h) by their values calculated according to the method of spherical currents. These functions are defined by (2.4.10) and (2.4.8) respectively and are in both cases indicated by $F(\theta',\phi')$.

Hence

$$F(\theta',\phi') = \frac{i}{k\rho^2}\sum_{n=0}^{\infty}\frac{(2n+1)\,i^n\,P_n(\cos\alpha)}{h_n^{(1)}(k\rho)} \qquad \text{--- (2.5.6s)}$$

in the sound soft case and

$$F(\theta',\phi') = \frac{i}{k^2\rho^2}\sum_{n=0}^{\infty}\frac{(2n+1)\,i^n\,P_n(\cos\alpha)}{h_n^{(1)\prime}(k\rho)} \qquad \text{--- (2.5.6h)}$$

in the sound hard case.

If the scattered fields according to the method of spherical currents are indicated by $\Phi_{(sc)}(r,\theta,\phi)$, then we have from (2.1.18s and h), (2.5.6s and h), (2.5.3) and (2.5.5)

$$\Phi_{(sc)}(r,\theta,\phi) = -\frac{1}{4\pi}\int_0^{\pi}\int_0^{2\pi}\frac{e^{ikR}}{R}F(\theta',\phi')\left|\varepsilon_{ijk}\frac{\partial\eta_j}{\partial\theta'}\frac{\partial\eta_k}{\partial\phi'}\right|d\theta'd\phi'$$

--- (2.5.7s)

in the sound soft case and

$$\Phi_{(sc)}(r,\theta,\phi) = \frac{1}{4\pi}\int_0^{\pi}\int_0^{2\pi}\frac{e^{ikR}}{R^3}(ikR-1)F(\theta',\phi')\varepsilon_{ijk}(\eta_i-x_i)\frac{\partial\eta_j}{\partial\theta'}\frac{\partial\eta_k}{\partial\phi'}d\theta'd\phi'$$

--- (2.5.7h)

in the sound hard case.

These equations are now specialized for the case where a plane wave travelling in the direction of the negative 3-axis [$(u_i) = (0, 0, -1)$] impinges on an axi-symmetric obstacle with choice of axes as in the previous section.

$\cos\alpha$ is now given by (2.4.18), taking the negative sign. Also, ρ is now independent of ϕ', and consequently the surface fields in (2.5.7s and h) are independent of ϕ' and indicated by $F(\theta')$. The integration w.r.t. ϕ' can be performed if the representation (2.2.5) for the Green's function is used in (2.5.7s) and in (2.5.7h) before taking the normal derivative. In (2.5.7s) put

$$\frac{e^{ikR}}{R} = ik \sum_{n=0}^{\infty} (2n+1) P_n(\cos\Theta) j_n(k\eta) h_n^{(1)}(kr) \quad , \quad r > \eta$$

--- (2.5.8)

where $\cos\Theta = \cos\theta\cos\theta' + \sin\theta\sin\theta'\cos(\phi-\phi')$ and,

according to (2.2.11),

$$P_n(\cos\Theta) = \sum_{\ell=-n}^{n} (-1)^{\ell} P_n^{\ell}(\cos\theta) P_n^{-\ell}(\cos\theta') e^{i\ell(\phi-\phi')} .$$

In the axi-symmetric case

$$(N_i) = \left(\varepsilon_{ijk} \frac{\partial \eta_j}{\partial \theta'} \frac{\partial \eta_k}{\partial \phi'}\right)$$

$$= \eta \sin\theta' \left(-\frac{d}{d\theta}(\eta\cos\theta')\cos\phi', -\frac{d}{d\theta'}(\eta\cos\theta')\sin\phi', \frac{d}{d\theta'}(\eta\sin\theta')\right)$$

--- (2.5.9)

$$\therefore |N_i| = \left|\varepsilon_{ijk} \frac{\partial \eta_j}{\partial \theta'} \frac{\partial \eta_k}{\partial \phi'}\right| = \eta \sin\theta' \left(\eta^2 + \left(\frac{d\eta}{d\theta'}\right)^2\right)^{1/2}$$

--- (2.5.10)

On using (2.5.8) in the sound hard case the normal derivative $\partial/\partial n = n_i\, \partial/\partial \eta_i$ must be expressed i.t.o. the variables η, θ' and ϕ'. In the case of axial symmetry n_i is defined by (2.4.22). In spherical polar coordinates (η, θ', ϕ')

$$\frac{\partial}{\partial \eta_i} = e^{\eta}_i \frac{\partial}{\partial \eta} + \frac{1}{\eta} e^{\theta'}_i \frac{\partial}{\partial \theta'} + \frac{1}{\eta \sin\theta'} e^{\phi'}_i \frac{\partial}{\partial \phi'} \qquad \text{--- (2.5.11),}$$

where

$$\left.\begin{aligned} (e^{\eta}_i) &= (\sin\theta'\cos\phi', \sin\theta'\sin\phi', \cos\theta') \\ (e^{\theta'}_i) &= (\cos\theta'\cos\phi', \cos\theta'\sin\phi', -\sin\theta') \\ (e^{\phi'}_i) &= (-\sin\phi', \cos\phi', 0) \end{aligned}\right\} \qquad \text{--- (2.5.12)}$$

From (2.4.22), (2.5.11) and (2.5.12) we have

$$\frac{\partial}{\partial n} = n_i \frac{\partial}{\partial \eta_i} = \frac{1}{\sqrt{\eta^2 + \left(\frac{d\eta}{d\theta'}\right)^2}} \left(\eta \frac{\partial}{\partial \eta} - \frac{1}{\eta} \frac{d\eta}{d\theta'} \frac{\partial}{\partial \theta'} \right)$$

--- (2.5.13)

On substituting for e^{ikR}/R and $|\varepsilon_{ijk} \frac{\partial \eta_j}{\partial \theta'} \frac{\partial \eta_k}{\partial \phi'}|$ according to (2.5.8) and (2.5.10) and integrating w.r.t. ϕ' where $\int_0^{2\pi} e^{il(\phi - \phi')} d\phi' = 2\pi \delta_{l,0}$ is used, (2.5.7s) becomes:

$$\Phi_{(sc)}(r,\theta) = -\frac{ik}{2} \int_0^{\pi} \left\{ \sum_{n=0}^{\infty} (2n+1) A_n(\theta') P_n(\cos\theta) h_n^{(1)}(kr) \right\} d\theta'$$

$$A_n(\theta') = P_n(\cos\theta') j_n(k\eta) F(\theta') \sqrt{\eta^2 + \left(\frac{d\eta}{d\theta'}\right)^2}\, \eta \sin\theta' \qquad \text{---(2.5.14s)}$$

$(r > \eta)$

For the sound hard case we get for the external field according to the method of spherical currents from (2.1.18h), on using (2.5.3), (2.5.10), (2.5.8), (2.5.13) and integrating w.r.t. ϕ':

$$\Phi_{(sc)}(r,\theta) = \frac{ik}{2}\int_0^{\pi}\left\{\sum_{n=0}^{\infty}(2n+1)A_n(\theta')P_n(\cos\theta)h_n^{(1)}(kr)\right\}d\theta'$$

$$A_n(\theta') = \left(k\eta^2 P_n(\cos\theta')j_n'(k\eta) + \sin\theta'\frac{d\eta}{d\theta'}P_n'(\cos\theta')j_n(k\eta)\right)F(\theta')\sin\theta'$$

$(r>\eta)$

--- (2.5.14h)

Equations (2.5.14s and h) can also be written in the following form by interchanging the processes of integration and summation.

$$\Phi_{(sc)}(r,\theta) = -\frac{ik}{2}\sum_{n=0}^{\infty}(2n+1)B_n P_n(\cos\theta)h_n^{(1)}(kr)$$

$$B_n = \int_0^{\pi}A_n(\theta')d\theta',$$

--- (2.5.15s)

where $A_n(\theta')$ is defined in (2.5.14s).

$$\Phi_{(sc)}(r,\theta) = \frac{ik}{2}\sum_{n=0}^{\infty}(2n+1)B_n P_n(\cos\theta)h_n^{(1)}(kr)$$

$$B_n = \int_0^{\pi}A_n(\theta')d\theta',$$

--- (2.5.15h)

where $A_n(\theta')$ is defined in (2.5.14h).

Hence, in agreement with symmetry considerations, the exterior field is independent of the azimuthal angle.

(2.6) The far field.

The far fields can be obtained from (2.1.18s) and (2.1.18h)

by replacing G and $\partial G/\partial n$ by their asymptotic values for $|x_i| >> |\eta_i|$

$$G = \frac{e^{ik|x_i - \eta_i|}}{|x_i - \eta_i|} \sim \frac{e^{ikr}}{r} \cdot e^{-ik\eta_i e_i^r} \qquad \text{--- (2.6.1)}$$

$$\frac{\partial G}{\partial n} \sim -ik\frac{e^{ikr}}{r} n_i e_i^r e^{-ik\eta_i e_i^r} \qquad \text{--- (2.6.2)}$$

In (2.6.1) and (2.6.2) $r = |x_i|$, $e_i^r = x_i/r$ and n_i is the outward unit normal vector to the obstacle surface S. If the far field amplitude [see (2.2.18)] by the method of spherical currents is denoted by $S_{(sc)}(\theta,\phi)$, we get from (2.1.18s and h), using (2.6.1), (2.6.2) and (2.5.3):

$$S_{(sc)}(\theta,\phi) = -\frac{k}{4\pi}\int_0^{\pi}\int_0^{2\pi} e^{-ik\eta_i e_i^r} F(\theta',\phi') \left|\varepsilon_{ijk}\frac{\partial \eta_j}{\partial \theta'}\frac{\partial \eta_k}{\partial \phi'}\right| d\theta' d\phi'$$

--- (2.6.3s)

$$S_{(sc)}(\theta,\phi) = -\frac{ik^2}{4\pi}\int_0^{\pi}\int_0^{2\pi} n_i e_i^r e^{-ik\eta_i e_i^r} F(\theta',\phi') \left|\varepsilon_{ijk}\frac{\partial \eta_j}{\partial \theta'}\frac{\partial \eta_k}{\partial \phi'}\right| d\theta' d\phi'$$

--- (2.6.3h)

These results are now specialized for axially symmetric obstacles with the incident plane wave travelling in the direction of the negative 3-axis coinciding with the axis of symmetry. On using (2.5.10), (2.4.22) and (e_i^r) = (SinθCosϕ, SinθSinϕ, Cosθ), (2.6.3s and h) become:

$$S_{(sc)}(\theta) = -\frac{k}{4\pi}\int_0^{\pi} I_1(\theta,\theta') F(\theta') e^{-ik\eta \mathrm{Cos}\theta \mathrm{Cos}\theta'} \sqrt{\eta^2 + \left(\frac{d\eta}{d\theta'}\right)^2}\, \eta \,\mathrm{Sin}\theta' d\theta'$$

--- (2.6.4s)

$$S_{(sc)}(\theta) = \frac{-ik^2}{4\pi}\int_0^{\pi}\left\{I_1(\theta,\theta')\frac{d}{d\theta'}(\eta\sin\theta')\cos\theta - I_2(\theta,\theta')\frac{d}{d\theta'}(\eta\cos\theta')\sin\theta\right\}\times F(\theta')\,e^{-ik\eta\cos\theta\cos\theta'}\,\eta\sin\theta'\,d\theta' \quad \text{--- (2.6.4h)}$$

In (2.6.4s and h)

$$I_1(\theta,\theta') = \int_0^{2\pi} e^{-ik\eta\sin\theta\sin\theta'\cos(\phi-\phi')}\,d\phi',$$

$$I_2(\theta,\theta') = \int_0^{2\pi}\cos(\phi-\phi')\,e^{-ik\eta\sin\theta\sin\theta'\cos(\phi-\phi')}\,d\phi'.$$

In Appendix B it is shown that

$$I_1(\theta,\theta') = -2\pi\sum_{n=1}^{\infty}\frac{(-1)^n}{((n-1)!)^2}\left(\frac{k\eta}{2}\sin\theta\sin\theta'\right)^{2n-2} \quad \text{--- (2.6.5)}$$

$$I_2(\theta,\theta') = 2\pi i\sum_{n=1}^{\infty}\frac{(-1)^n}{n!(n-1)!}\left(\frac{k\eta}{2}\sin\theta\sin\theta'\right)^{2n-1} \quad \text{--- (2.6.6)}$$

From (2.6.4s and h), (2.6.5) and (2.6.6) it follows that the far field amplitude is independent of ϕ.

Formulae for the far field can also be obtained from (2.5.14s and h) by using $h_n^{(1)}(kr) \sim (-i)^{n+1} e^{ikr}/kr$,

but the equations (2.6.4s and h) are simpler and more suitable for automatic computation.

CHAPTER III

SCALAR SCATTERING BY A PROLATE SPHEROID.

(3.1) The exact solution.

In scattering problems the prolate spheroidal shape occupies a position of prominence. Not only does it approximate a finite rod (a simple antenna) in its limiting form, but since the advent of radar its importance has increased as many aerodynamically efficient shapes are more or less prolate spheroidal.

Perhaps most important of all, the prolate spheroid can be identified with a coordinate surface belonging to a set of coordinates, the prolate spheroidal coordinates, which separate both the scalar- and electromagnetic wave equations.

The prolate spheroidal coordinates ξ, η, ϕ are related to the Cartesian coordinates x_1, x_2, x_3 of a point by the transformations

$$\left.\begin{aligned} x_1 &= F[(\xi^2-1)(1-\eta^2)]^{1/2}\cos\phi \\ x_2 &= F[(\xi^2-1)(1-\eta^2)]^{1/2}\sin\phi \\ x_3 &= F\xi\eta \end{aligned}\right\} \qquad \text{--- (3.1.1)}$$

with $1 \le \xi \le \infty$, $-1 \le \eta \le 1$, $0 \le \phi \le 2\pi$.

The surfaces ξ = const., η = const. and ϕ = const. are respectively confocal prolate spheroids of major axis $2a = 2F\xi$ and minor axis $2b = 2F(\xi^2 - 1)^{\frac{1}{2}}$, two-sheeted hyperboloids (one sheet corresponds to a positive η, other to a negative η), and azimuthal planes originating in the z-axis.

Let the surface of the prolate spheroidal obstacle be defined by the equation

$$\xi = \xi_0 \qquad \text{--- (3.1.2),}$$

then $$\xi_0 = \frac{1}{\epsilon} = \frac{a}{\sqrt{a^2 - b^2}} \qquad \text{--- (3.1.3)}$$

where ε is the eccentricity and a and b are resp. the semi-major and semi-minor axes. The interfocal distance, 2F, is related to a and b by the equation

$$F = ae = \sqrt{a^2 - b^2} \qquad \text{--- (3.1.4)}$$

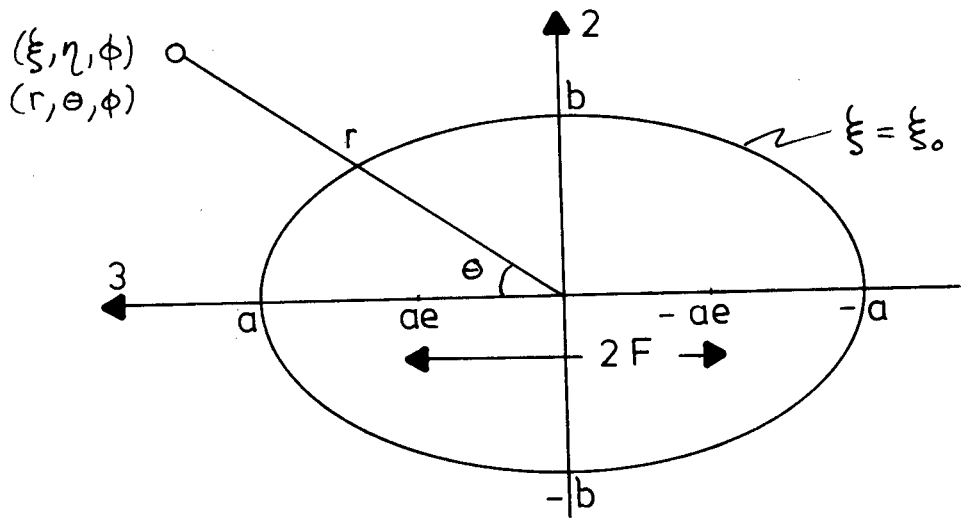

In the prolate spheroidal coordinate system the scalar Helmholtz equation $\nabla^2\Phi + k^2\Phi = 0$ becomes:

$$\left[\frac{\partial}{\partial\xi}(\xi^2-1)\frac{\partial}{\partial\xi} + \frac{\partial}{\partial\eta}(1-\eta^2)\frac{\partial}{\partial\eta} + \frac{\xi^2-\eta^2}{(\xi^2-1)(1-\eta^2)}\frac{\partial^2}{\partial\varphi^2} + c^2(\xi^2-\eta^2)\right]\Phi = 0$$

--- (3.1.5)

The separation of (3.1.5) is achieved by putting $\Phi(\xi,\eta,\phi) = U(\xi)V(\eta)W(\phi)$.

The resulting ordinary differential equations may be written as follows:

$$\frac{d}{d\xi}\left[(\xi^2-1)\frac{dU}{d\xi}\right] - \left[\lambda_{mn} - c^2\xi^2 + \frac{m^2}{\xi^2-1}\right]U = 0$$

--- (3.1.6)

$$\frac{d}{d\eta}\left[(1-\eta^2)\frac{dV}{d\eta}\right] + \left[\lambda_{mn} - c^2\eta^2 - \frac{m^2}{1-\eta^2}\right]V = 0 \qquad \text{--- (3.1.7)}$$

$$\frac{d^2W}{d\phi^2} + m^2 W = 0 \qquad \text{--- (3.1.8),}$$

$$c = kF \qquad \text{--- (3.1.9).}$$

The functions $W(\phi)$ are therefore of the type $e^{im\phi}$, where m is an integer to ensure single-valuedness. In the notation of Flammer (1957)

$$\left.\begin{aligned} U(\xi) &= R_{mn}(c,\xi) \\ V(\eta) &= S_{mn}(c,\eta) \end{aligned}\right\} \qquad \text{--- (3.1.10)}$$

where the prolate spheroidal wave functions $R_{mn}(c,\xi)$ and $S_{mn}(c,\eta)$ are respectively referred to as the radial and angular solutions. The separation constants λ_{mn} are to be determined so that $R_{mn}(c,\xi)$ and $S_{mn}(c,\eta)$ are finite at $\xi = \pm 1$ and $\eta = \pm 1$ resp.

The incident and scattered fields are now expanded in prolate spheroidal wave functions and the unknown coefficients of expansion for the scattered wave are determined by means of the boundary conditions (2.1.12s and h) which, for the prolate spheroid (3.1.2) become:

$$\left.\Phi^{(s)}\right|_{\xi=\xi_0} = -\left.\Phi^{(i)}\right|_{\xi=\xi_0} \qquad \text{--- (3.1.11s)}$$

$$\left.\frac{\partial\Phi^{(s)}}{\partial\xi}\right|_{\xi=\xi_0} = -\left.\frac{\partial\Phi^{(i)}}{\partial\xi}\right|_{\xi=\xi_0} \qquad \text{--- (3.1.11h)}$$

With a time-dependency $\exp(-i\omega t)$, the incident plane wave travelling along the 3-axis in the negative direction

is defined by

$$\Phi^{(i)} = e^{-ikx_3} = e^{-ikF\xi\eta} \qquad \text{--- (3.1.12)}$$

The expansion of this wave in terms of prolate spheroidal wave functions is given by

$$e^{-ic\xi\eta} = \sum_{n=0}^{\infty} (2n+1)(-i)^n S_n^{o(1)}(\xi, c)\, ps_n^o(\eta, c^2)\, ps_n^o(1, c^2) \qquad \text{--- (3.1.13)}$$

(Jones (1964), p. 89).

The notation used in (3.1.13) is that of Meixner and Schäfke (Meixner and Schäfke (1954)).

$S_n^{0(1)}(\xi,c)$ is the radial solution of the first kind and is denoted by $R_{0n}^{(1)}(c,\xi)$ in Flammer's notation. The angular solution $ps_n^0(\eta,c^2)$ is denoted by $S_{0n}(c,\eta)$ in Flammer's notation. The normalization convention for the angular functions differs in the two schemes. (Abramowitz and Stegun (1965), Chapter 21).

In the Meixner-Schäfke scheme

$$\int_{-1}^{+1} [ps_n^o(\eta, c^2)]^2 d\eta = \frac{2}{2n+1}.$$

In the Flammer scheme

$S_{0n}(c,0) = P_n(0)$ if n even,

$S'_{0n}(c,0) = P'_n(0)$ if n odd,

and $$\int_{-1}^{+1} [S_{on}(c,\eta)]^2 d\eta = N_{on}.$$

Hence in the Flammer scheme (3.1.13) becomes:

$$e^{-ic\xi\eta} = 2\sum_{n=0}^{\infty} \frac{(-i)^n S_{on}(c,1)\, S_{on}(c,\eta)\, R^{(1)}_{on}(c,\xi)}{N_{on}} \qquad \text{--- (3.1.14)}$$

Let the expansion for the scattered field $\Phi^{(s)}$ be given by

$$\Phi^{(s)}(\xi,\eta) = 2\sum_{n=0}^{\infty} \frac{(-i)^n A_n\, S_{on}(c,\eta)\, R^{(3)}_{on}(c,\xi)}{N_{on}} \qquad \text{--- (3.1.15)}$$

Here

$$R^{(3)}_{on}(c,\xi) = R^{(1)}_{on}(c,\xi) + i\, R^{(2)}_{on}(c,\xi) \qquad \text{--- (3.1.16)}$$

is the radial function of the 3rd kind and $R^{(2)}_{0n}(c,\xi)$ is the radial function of the 2nd kind. The choice of $R^{(3)}_{0n}$ as radial function in (3.1.15) is dictated by the radiation conditions which $R^{(3)}_{0n}$ satisfies.

For large $c\xi$

$$R^{(1)}_{on}(c,\xi) \sim \frac{1}{c\xi}\cos\left[c\xi - \tfrac{1}{2}(n+1)\pi\right]$$

$$R^{(2)}_{on}(c,\xi) \sim \frac{1}{c\xi}\sin\left[c\xi - \tfrac{1}{2}(n+1)\pi\right] \qquad \text{--- (3.1.17)}$$

Hence, from (3.1.16) and (3.1.17) it follows

$$\left.\begin{aligned} R^{(3)}_{on}(c,\xi) &\sim \frac{(-i)^{n+1}}{c\xi}\, e^{ic\xi} \\ &\sim \frac{(-i)^{n+1}}{kr}\, e^{ikr} \end{aligned}\right\} \qquad \text{--- (3.1.18),}$$

where $c\xi \sim kr$ follows from (3.1.1) ($r^2 = x_i x_i$).

From (3.1.14), (3.1.15) and the boundary conditions (3.1.11s and h) we get

$$A_n = -\frac{S_{on}(C,1)\, R^{(1)}_{on}(C,\xi_o)}{R^{(3)}_{on}(C,\xi_o)} \qquad \text{--- (3.1.19s)}$$

$$A_n = -\frac{S_{on}(C,1)\, \partial R^{(1)}_{on}(C,\xi_o)/\partial \xi_o}{\partial R^{(3)}_{on}(C,\xi_o)/\partial \xi_o} \qquad \text{--- (3.1.19h)}$$

These latter equations give with (3.1.15) the following expressions for the scattered fields:

$$\underline{\Phi}^{(s)}(\xi,\eta) = -2 \sum_{n=0}^{\infty} \frac{(-i)^n S_{on}(C,1) R^{(1)}_{on}(C,\xi_o)}{N_{on} R^{(3)}_{on}(C,\xi_o)} S_{on}(C,\eta) R^{(3)}_{on}(C,\xi) \qquad \text{--- (3.1.20s)}$$

$$\underline{\Phi}^{(s)}(\xi,\eta) = -2 \sum_{n=0}^{\infty} \frac{(-i)^n S_{on}(C,1) \partial R^{(1)}_{on}(C,\xi_o)/\partial \xi_o}{N_{on} \partial R^{(1)}_{on}(C,\xi_o)/\partial \xi_o} S_{on}(C,\eta) R^{(3)}_{on}(C,\xi) \qquad \text{--- (3.1.20h)}$$

Let $\Phi^{(t)}(\eta)$ be the surface field in the sound hard case, then

$$\underline{\Phi}^{(t)}(\eta) = \underline{\Phi}^{(i)}(\xi_o,\eta) + \underline{\Phi}^{(s)}(\xi_o,\eta),$$

and from (3.1.14) and (3.1.20h) we have

$$\Phi^{(t)}(\eta) = 2\sum_{n=0}^{\infty} \frac{(-i)^n S_{on}(c,1)\, S_{on}(c,\eta)\, W(R_{on}^{(1)}, R_{on}^{(3)})}{N_{on}\, \partial R_{on}^{(3)}(c,\xi_0)/\partial \xi_0}\Bigg|_{\xi=\xi_0}$$

--- (3.1.21),

where

$$W(R_{on}^{(1)}, R_{on}^{(3)}) = R_{on}^{(1)} \frac{\partial R_{on}^{(3)}}{\partial \xi} - R_{on}^{(3)} \frac{\partial R_{on}^{(1)}}{\partial \xi}$$

--- (3.1.22)

is the Wronskian of $R_{0n}^{(1)}$ and $R_{0n}^{(3)}$.

From (3.1.16) we have

$$W(R_{on}^{(1)}, R_{on}^{(3)}) = i\, W(R_{on}^{(1)}, R_{on}^{(2)}) \qquad \text{--- (3.1.23)}$$

It is easily shown that if ω_1 and ω_2 are two independent solutions of

$$\frac{d^2\omega}{dz^2} + p(z)\frac{d\omega}{dz} + q(z)\omega = 0,$$

then $$\frac{dW(\omega_1,\omega_2)}{dz} = -p(z)W$$

$$\therefore W = k\, e^{-\int p\, dz}$$

, where k is a constant. From (3.1.6) we have that for the radial functions

$$p(\xi) = \frac{d}{d\xi}(\xi^2-1)/(\xi^2-1),$$

$$\therefore W = k/(\xi^2-1) \qquad \text{--- (3.1.24)}$$

It remains to find k for the two solutions $R_{0n}^{(1)}$ and $R_{0n}^{(2)}$ of (3.1.6).

On using (3.1.17) we find for $c\xi \to \infty$

$$W(R_{on}^{(1)}, R_{on}^{(2)}) \sim c/\xi^2 \quad , \text{ hence,}$$

comparing with the asymptotic value of the right hand side of (3.1.24), we have $k = 1/c$.

$$\therefore W(R_{on}^{(1)}, R_{on}^{(2)}) = 1/c(\xi^2 - 1),$$

and from (3.1.23)

$$W(R_{on}^{(1)}, R_{on}^{(3)}) = i/c(\xi^2 - 1) \qquad \text{--- (3.1.25)}$$

Hence, using (3.1.25) in (3.1.21) we get for the surface field on a sound hard spheroid

$$\Phi^{(t)}(\eta) = \frac{2i}{c(\xi_o^2 - 1)} \sum_{n=0}^{\infty} \frac{(-i)^n S_{on}(c,1) S_{on}(c,\eta)}{N_{on} \partial R_{on}^{(3)}(c,\xi_o)/\partial \xi_o}$$

--- (3.1.26)

The far field amplitudes [see (2.2.18)] are obtained from (3.1.20s and h) using (3.1.18) and $\eta \sim \cos\theta$ for $r \to \infty$.

$$\therefore S(\theta) = 2i \sum_{n=0}^{\infty} \frac{(-1)^n R_{on}^{(1)}(c,\xi_o) S_{on}(c,1) S_{on}(c,\cos\theta)}{N_{on} R_{on}^{(3)}(c,\xi_o)}$$

--- (3.1.27s)

$$S(\theta) = 2i \sum_{n=0}^{\infty} \frac{(-1)^n \partial R_{on}^{(1)}(c,\xi_o)/\partial \xi_o \cdot S_{on}(c,1) S_{on}(c,\cos\theta)}{N_{on} \partial R_{on}^{(3)}(c,\xi_o)/\partial \xi_o}$$

--- (3.1.27h)

(3.2) The method of spherical currents applied to the spheroid.

Let η_i be the Cartesian coordinates of a point on the surface of the prolate spheroid $\xi = \xi_0$, where ξ_0 is related to the semi-major and semi-minor axes a and b through (3.1.3). With the choice of axes as in the previous paragraph the Cartesian equation of the spheroid is given by:

$$\frac{\eta_1^2}{b^2} + \frac{\eta_2^2}{b^2} + \frac{\eta_3^2}{a^2} = 1 \qquad \text{--- (3.2.1)}$$

Now (2.4.11) becomes:

$$\left.\begin{aligned} \eta_1 &= \eta(\theta)\,\sin\theta\,\cos\phi \\ \eta_2 &= \eta(\theta)\,\sin\theta\,\sin\phi \\ \eta_3 &= \eta(\theta)\,\cos\theta \end{aligned}\right\} \qquad \text{--- (3.2.2)}$$

where (η,θ,ϕ) are the spherical polar coordinates of a point on the spheroid. From (3.2.1) and (3.2.2) the equation of the spheroid in spherical polar coordinates is obtained:

$$\eta = \frac{ab}{(a^2\sin^2\theta + b^2\cos^2\theta)^{1/2}} \qquad \text{--- (3.2.3)}$$

The normal derivative of the surface field in the sound soft case and the surface field in the sound hard case are respectively defined by (2.4.10) and (2.4.8), now written as:

$$\frac{\partial \Phi_{(sc)}(\theta)}{\partial n} = \frac{-i}{k\rho^2} \sum_{n=0}^{\infty} \frac{i^n (2n+1) P_n(\cos\alpha)}{h_n^{(1)}(k\rho)}$$

--- (3.2.4s)

$$\Phi_{(sc)}(\theta) = \frac{i}{k^2\rho^2} \sum_{n=0}^{\infty} \frac{i^n (2n+1) P_n(\cos\alpha)}{h_n^{(1)\prime}(k\rho)} .$$

--- (3.2.4h)

It remains to calculate Cosα and ρ for the prolate spheroid.

For the incident plane wave propagated parallel to the 3-axes and in the negative direction, we get from (2.4.18) and (3.2.3)

$$\cos\alpha = \frac{-b^2\cos\theta}{(a^4\sin^2\theta + b^4\cos^2\theta)^{1/2}} \qquad \text{--- (3.2.5)}$$

The principal radii of curvature are found as functions of θ by solving (2.4.19). Using (3.2.3), the equations (2.4.23) become:

$$E = a^2b^2(a^4\sin^2\theta+b^4\cos^2\theta)(a^2\sin^2\theta+b^2\cos^2\theta)^{-3}$$
$$F = 0$$
$$G = a^2b^2\sin^2\theta\,(a^2\sin^2\theta + b^2\cos^2\theta)^{-1}$$
$$L = -a^3b^3(a^4\sin^2\theta+b^4\cos^2\theta)^{-1/2}(a^2\sin^2\theta+b^2\cos^2\theta)^{-3/2}$$
$$M = 0$$
$$N = -a^3b\sin^2\theta(a^4\sin^2\theta+b^4\cos^2\theta)^{-1/2}(a^2\sin^2\theta+b^2\cos^2\theta)^{-1/2}$$

--- (3.2.6)

On substituting these expressions for E, F, G, L, M and N into (2.4.19) and solving for λ we get:

$$\lambda_1 = -ab\left[\frac{a^2\sin^2\theta + b^2\cos^2\theta}{a^4\sin^2\theta + b^4\cos^2\theta}\right]^{3/2}$$

$$\lambda_2 = -\frac{a}{b}\left[\frac{a^2\sin^2\theta + b^2\cos^2\theta}{a^4\sin^2\theta + b^4\cos^2\theta}\right]^{1/2},$$

and hence from (3.4.21)

$$\rho_1 = \frac{1}{ab}\left[\frac{a^4\sin^2\theta + b^4\cos^2\theta}{a^2\sin^2\theta + b^2\cos^2\theta}\right]^{3/2}$$

$$\rho_2 = \frac{b}{a}\left[\frac{a^4\sin^2\theta + b^4\cos^2\theta}{a^2\sin^2\theta + b^2\cos^2\theta}\right]^{1/2}$$

$$\bar{\rho} = \frac{1}{a}\left[\frac{a^4\sin^2\theta + b^4\cos^2\theta}{a^2\sin^2\theta + b^2\cos^2\theta}\right] \qquad \text{--- (3.2.7),}$$

where $\bar{\rho} = \sqrt{\rho_1\rho_2}$ is the Gaussian curvature.

The scattered fields according to the method of spherical currents are defined by (2.5.14s and h), with η defined by (3.2.3). These equations now become:

$$\underline{\Phi}_{(sc)}(r,\theta) = -\frac{ik}{2}\int_0^{\pi}\left\{\sum_{n=0}^{\infty}(2n+1)A_n(\theta')P_n(\cos\theta)h_n^{(1)}(kr)\right\}d\theta'$$

$$A_n(\theta') = \frac{F(\theta')P_n(\cos\theta')j_n(k\eta)\,a^2b^2(a^4\sin^2\theta' + b^4\cos^2\theta')^{1/2}}{(a^2\sin^2\theta' + b^2\cos^2\theta')^2}$$

$$F(\theta') = \partial\underline{\Phi}_{(sc)}^{(t)}(\theta')/\partial n \,.$$

--- (3.2.8s)

$$\underline{\Phi}_{(sc)}(r,\theta) = \frac{ik}{2}\int_0^{\pi}\left\{\sum_{n=0}^{\infty}(2n+1)A_n(\theta')P_n(\cos\theta)h_n^{(1)}(kr)\right\}d\theta'$$

$$A_n(\theta') = \left[k\eta^2 P_n(\cos\theta')j_n'(k\eta) + \frac{P_n'(\cos\theta')j_n(k\eta)ab(b^2-a^2)\sin^2\theta'\cos\theta'}{(a^2\sin^2\theta' + b^2\cos^2\theta')^{3/2}}\right]F(\theta')\sin\theta'$$

$$F(\theta') = \underline{\Phi}_{(sc)}^{(t)}(\theta')$$

--- (3.2.8h)

The far field amplitudes are obtained from (2.6.4s and h) in conjunction with (3.2.3). We get:

$$S_{(sc)}(\theta) = \frac{-k}{4\pi} \int_0^{\pi} A(\theta,\theta') F(\theta') e^{-ik\eta \cos\theta \cos\theta'} \eta \sin\theta' d\theta'$$

$$A(\theta,\theta') = \frac{\eta^3}{a^2 b^2} (a^4 \sin^2\theta' + b^4 \cos^2\theta')^{1/2} I_1(\theta,\theta')$$

$$F(\theta') = \partial \bar{\Phi}^{(t)}_{(sc)}(\theta')/\partial n$$

--- (3.2.9s)

$$S_{(sc)}(\theta) = -\frac{ik^2}{4\pi} \int_0^{\pi} A(\theta,\theta') F(\theta') e^{ik\eta \cos\theta \cos\theta'} \eta \sin\theta' d\theta'$$

$$A(\theta,\theta') = \frac{\eta^3}{a^2 b^2} \left(a^2 \sin\theta \sin\theta' I_2(\theta,\theta') + b^2 \cos\theta \cos\theta' I_1(\theta,\theta') \right)$$

$$F(\theta') = \bar{\Phi}^{(t)}_{(sc)}(\theta')$$

--- (3.2.9h)

In (3.2.9s and h) $I_1(\theta,\theta')$ and $I_2(\theta,\theta')$ are defined by equations (2.6.5) and (2.6.6).

(3.3) <u>The surface field on a sound hard prolate spheroid</u>.

In this section surface fields on sound hard prolate spheroids computed by means of the exact expression given by (3.1.26) are graphically compared with those computed by means of the method of spherical currents. The graphs of the surface field amplitudes according to (3.1.26) given in Figures (3.1) - (3.3) are from

Senior (1966), Fig. 7. The expression used by Senior in this paper differs from (3.1.26) in that i should be replaced by -i. This is due to assuming a time dependency $\exp(-i\omega t)$.

The graphs of the surface field amplitudes in Figures (3.1) - (3.3) are plotted as functions of the angular position η on the surface for c = 5 and a:b = 2:1; 5:1 and 10:1 ($\therefore$ from (3.1.3) ξ_0 = 1,155; 1,021 and 1,005 resp.) This choice of c is in the resonance region, at least as far as the major dimensions of the spheroids are concerned.

For the method of spherical currents the surface field amplitudes were computed by means of equation (3.2.4h) with $\cos\alpha$ given by (3.2.5) and ρ by the equations (3.2.7). The real and imaginary parts of the surface field were computed as the output of subroutine POTAS (p. A10). The main program calls on subroutine RAG (p. A14) to provide the different radii of curvature and $\cos\alpha$ as functions of c, b:a and η as input for POTAS. Subroutine RAG is based on the formulas (3.2.5) and (3.2.7) with

$$\cos\Theta = \frac{\xi_0 \eta}{(\xi_0^2 + \eta^2 - 1)}$$

On comparing the surface field amplitudes according to the method of spherical currents with those according to the exact theory for the various eccentricities it is immediately apparent that the choice of least principal radius of curvature as radius for the representative sphere affords the best approximation under the given conditions. With this choice of ρ the following correspondences with the graphs according to the exact theory are observed:

For a given eccentricity (or choice of a:b) the surface field amplitude has a maximum at the front tip ($\eta = 1$) where the incident wave is perpendicular to the surface.

As η decreases, so does the surface amplitude decrease at progressively more glancing incidence of the impinging plane wave. Apart from slight undulations this decrease continues nearly monotonically until well in the geometrical shadow region ($\eta < 0$) where the surface field amplitude reaches a minimum just before the rear tip ($\eta = -1$) after which it rises more sharply to a value ≈ 1 at $\eta = -1$.

With increasing eccentricity the surface field curves level out, the amplitudes near the front tip dropping most rapidly. The slight undulations referred to above are more apparent in the fatter obstacles, but they are still visible on the curve of the 10:1 spheroid in Fig. (3.3). According to Senior these undulations are due to interference with a backwards travelling wave on the surface. With increasing a:b the minimum in the surface field amplitude in the geometrical shadow region near the rear tip becomes less pronounced.

The main differences between the surface field amplitudes as resp. calculated according to exact theory and the method of spherical currents using the least principal radius of curvature are the following: (a) For a given eccentricity the intensity of surface activity in the shadow region relative to the illuminated region is greater in the case of the method of spherical currents than in the exact theory; (b) the decrease in surface field amplitude with increasing eccentricity is much more rapid in the method of spherical currents than in the exact theory. At the front tip the surface field amplitudes for a:b = 5:1 and 10:1 are both practically equal to 1 according to the method of spherical currents - below the front tip surface field amplitude according to exact theory for the 10:1 body.

The fact that the surface field amplitude is relatively more intense according to the method of spherical currents

may be accounted for as follows. The point at which the surface field is calculated is closer to the shadow boundary of the representative sphere measured along the surface than the shadow boundary of the spheroid; consequently waves travelling along the surface from the shadow boundary suffer less attenuation on the representative sphere than on the spheroid to reach the same point in the shadow region.

The principal radii of curvature of the prolate spheroid have their (equal) minimum values at $\theta = 0,\pi$ and their maximum values at $\theta = \pi/2$ [see eq. (3.2.7)]. For

$c = 5$, $a:b = 2$: $1,44 \leq k\rho_1 \leq 11,54$

$1,44 \leq k\rho_2 \leq 2,89$

$c = 5$, $a:b = 5$: $0,20 \leq k\rho_1 \leq 25,5$

$0,20 \leq k\rho_2 \leq 1,02$

$c = 5$, $a:b = 10$: $0,05 \leq k\rho_1 \leq 50,3$

$0,05 \leq k\rho_2 \leq 0,50.$

With increasing eccentricity the method of spherical currents utilizing the greatest principal radius of curvature therefore involves progressively more of the high frequency behaviour of spheres, while the choice of least principal radius of curvature tends to involve more of the low frequency behaviour of spheres.

The effect of creeping waves on spheres, though noticeable at fairly low frequencies becomes more prominent at higher frequencies. This accounts for the more undulating behaviour and sharper fall-off of the surface field amplitudes.

For all subsequent calculations the least principal radius of curvature will be used as radius of the representative sphere in the method of spherical currents.

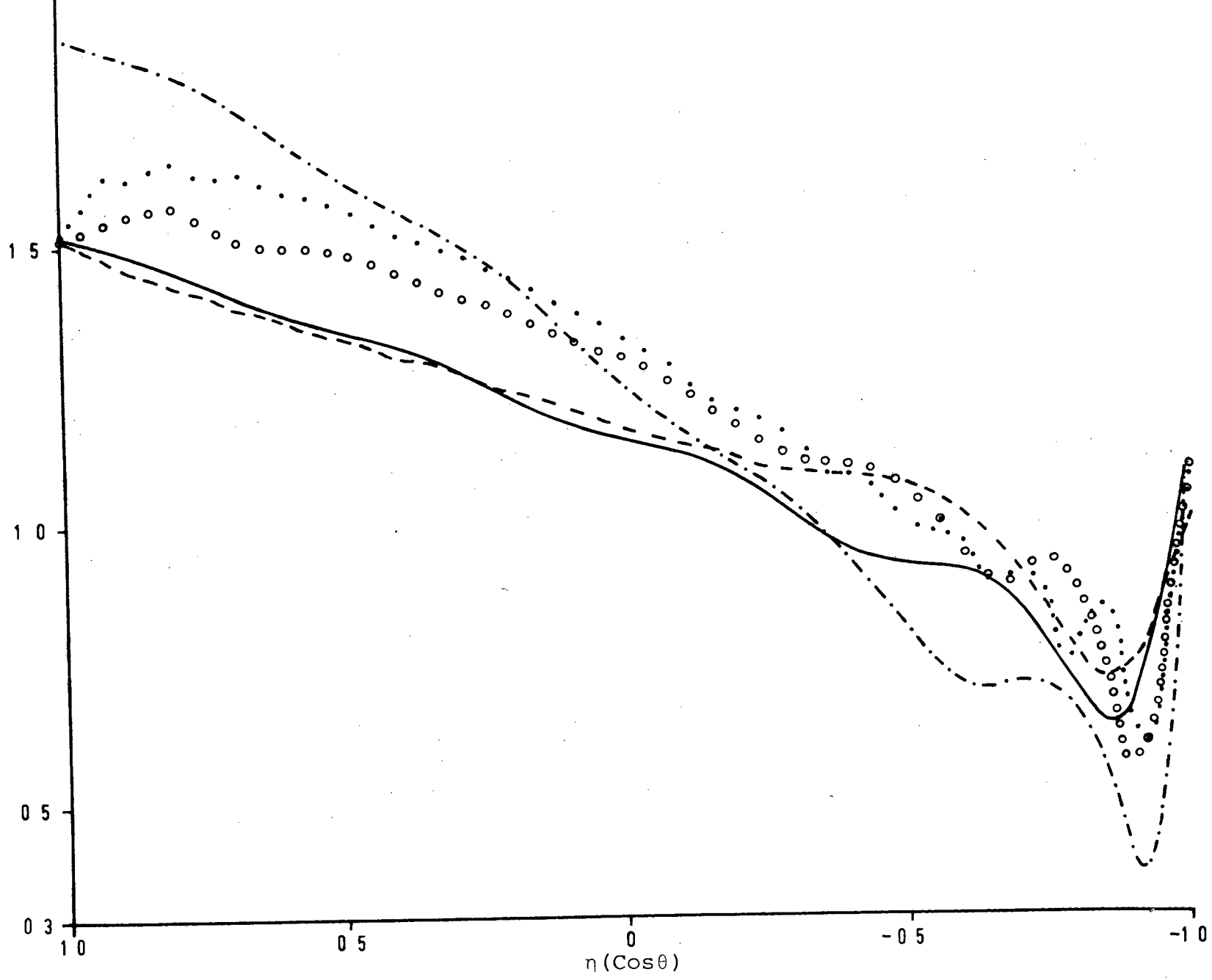

Fig. (3.1) Surface field amplitude for a sphere with ka = 5 (-·-·-) and a 2:1 spheroid with c = 5 according to Senior (——) and the method of spherical currents: least principal radius of curvature (---), Gaussian curvature (ooo), greatest principal radius of curvature (···)

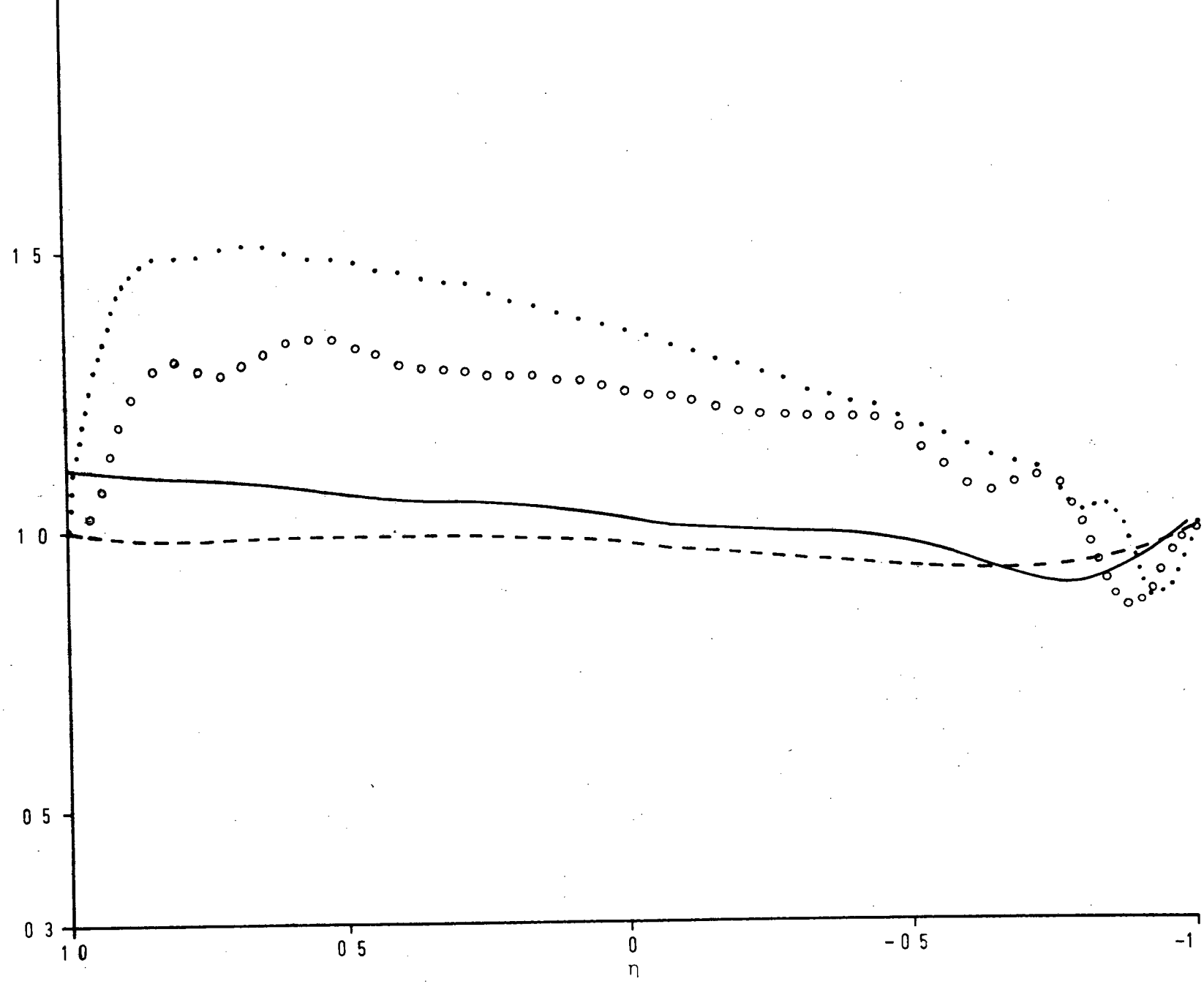

Fig. (3.2)

Surface field amplitude for a 5:1 spheroid with c = 5 according to Senior (——) and the method of spherical currents: least principal radius of curvature (---), Gaussian curvature (∘∘∘), greatest

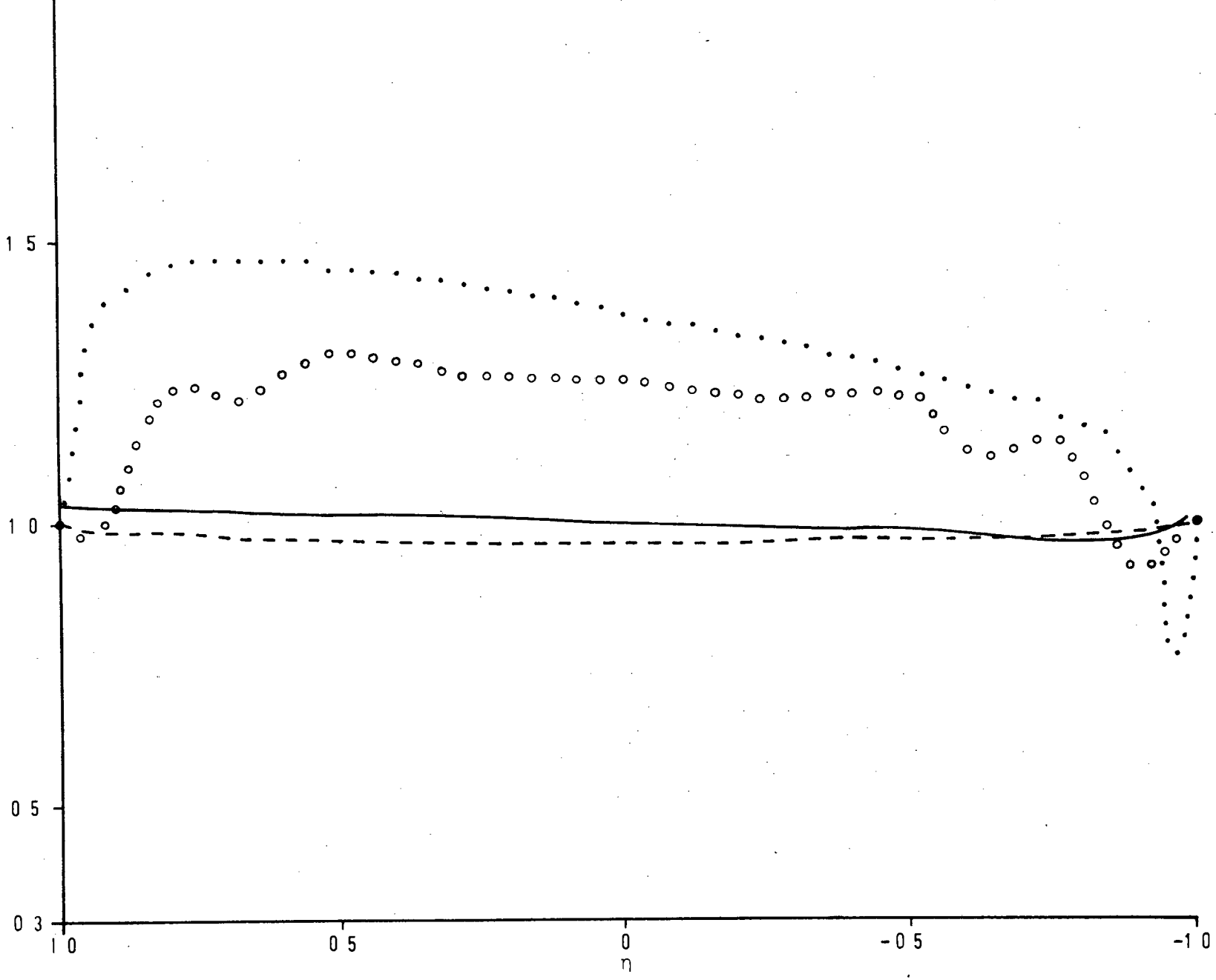

g. (3.3) Surface field amplitude for a 10:1 spheroid with c = 5 according to Senior (——) and the method of spherical currents: least principal radius of curvature (---), Gaussian curvature (∘∘∘), greatest principal radius of curvature (···)

(3.4) Scattering patterns of hard prolate spheroids for axial incidence.

In Fig. (3.4) scattering patterns, which show the directional behaviour of the scattered radiation, are reproduced. The curves give $|S(\theta)|/c\xi_0 = |S(\theta)|/ka$ as a function of θ for different values of ξ_0 and c. The solid lines are the scattering patterns according to Spence and Granger (1951) and are based on the exact expression for the far field amplitude $S(\theta)$ given by equation (3.1.27h). The notation for the prolate spheroidal wave functions used by Spence and Granger is that of Stratton, Morse, Chu and Hutner (1941).

The dashed curves represent the scattering patterns according to the method of spherical currents with $S(\theta)$ given by (3.2.9h). The spheroids chosen are $\xi_0 = 1{,}020$ (a:b = 5,07) and $\xi_0 = 1{,}077$ (a:b = 2,69) with c values of 1,2 and 3. For $\xi_0 = 1{,}020$, $1{,}020 < c\xi_0 = ka < 3{,}06$ and for $\xi_0 = 1{,}077$, $1{,}077 < c\xi_0 = ka < 3{,}23$, hence just beyond the Rayleigh region for spheroids.

On putting $\cos\theta' = z$, (3.2.9h) can be written in the form

$$S_{(sc)}(\theta) = \int_{-1}^{1} \left(FR(D, b/a, \theta, z) + i\, FI(D, b/a, \theta, z) \right) dz$$

--- (3.4.1)

where

$$FR + FI = \left(QR(D, b/a, z) + i\, QI(D, b/a, z) \right)\left(HR(D, b/a, \theta, z) + i\, HI(D, b/a, \theta, z) \right)$$

--- (3.4.2),

and $D = ka$.

In (3.4.2) QR and QI are the real and imaginary parts of the surface field $F(\theta') = \Phi^{(t)}_{(sc)}(\theta')$. This is the output of subroutine POTAS (p. A10).

Furthermore

$$HR = \frac{(k\eta)^4}{2(ka)^2}\left\{\beta\cos(k\eta z\cos\theta) - \alpha\sin(k\eta z\cos\theta)\right\}$$

$$HI = -\frac{(k\eta)^4}{2(ka)^2}\left\{\alpha\cos(k\eta z\cos\theta) + \beta\sin(k\eta z\cos\theta)\right\}$$

--- (3.4.3)

where

$$\alpha = -z\cos\theta\sum_{n=1}^{\infty}\frac{(-1)^n}{((n-1)!)^2}\left[\frac{k}{2}\eta\sqrt{1-z^2}\sin\theta\right]^{2n-2}$$

$$\beta = \left(\frac{a}{b}\right)^2\sqrt{1-z^2}\sin\theta\sum_{n=1}^{\infty}\frac{(-1)^n}{n!\,(n-1)!}\left[\frac{k}{2}\eta\sqrt{1-z^2}\sin\theta\right]^{2n-1}$$

--- (3.4.4)

The functions HR and HI are computed as the output of subroutine HASH (p. A16) which calls on subroutine RAD (p. A15) to provide $k\eta$ as a function of D, b/a and z. The real and imaginary parts of the integrand in (3.4.1) are computed by subroutine GRIND (p. A17) which calls on HASH and POTAS to provide HR, HI, QR and QI as input. GRIND also calls on RAD to provide $k\rho$ and $\cos\alpha$ as functions of D, b/a and z, as input for POTAS.

In subroutine GREAT (p. A18) the real and imaginary parts of the integral in (3.4.1) are computed using Simpson's 1/3-rule. The summation process is terminated by applying a convergence criterion to the sum of the squares of the real and imaginary parts, which forms the output of

GREAT as a function of D, b/a, θ and the limits of integration.

The main program calls on GREAT to provide $|S_{(sc)}(\theta)|^2$ as input and computes $|S_{(sc)}(\theta)|/D$ as a function of c, ξ_0 and θ by utilizing the equations

$$D = ka = c\xi_0$$

and

$$b/a = \frac{\sqrt{\xi_0^2 - 1}}{\xi_0} \qquad \text{--- (3.4.5)}$$

which are readily obtained from (3.1.9), (3.1.4) and (3.1.3).

It is clear from Fig. (3.4) that the best correspondence between the scattering patterns according to exact theory and those according to the method of spherical currents are obtained for the lowest frequency (c = 1) on the illuminated side of the scatterer. Except for c = 1, $0^\circ < \theta < 90^\circ$, $|S(\theta)|/D$ is less than $|S_{(sc)}(\theta)|/D$. The fact that $|S_{(sc)}(\theta)|/D > |S(\theta)|/D$ for $90^\circ < \theta < 180^\circ$ for all values of c could be attributed to the relatively greater surface field intensity in the shadow region in the case of the method of spherical currents, observed in the previous section.

The method of spherical currents displays the lobed structure of the scattering patterns, but to a much less marked degree than the exact theory.

The computation of the scattering patterns according to the method of spherical currents were checked by computing $|S_{(sc)}(\theta)|/ka$ with ka = 1 and a = b and comparing the results with $|S(\theta)|/ka$, where $S(\theta)$ is the far field of the sound hard sphere defined by (2.2.20h). Good correlation was established.

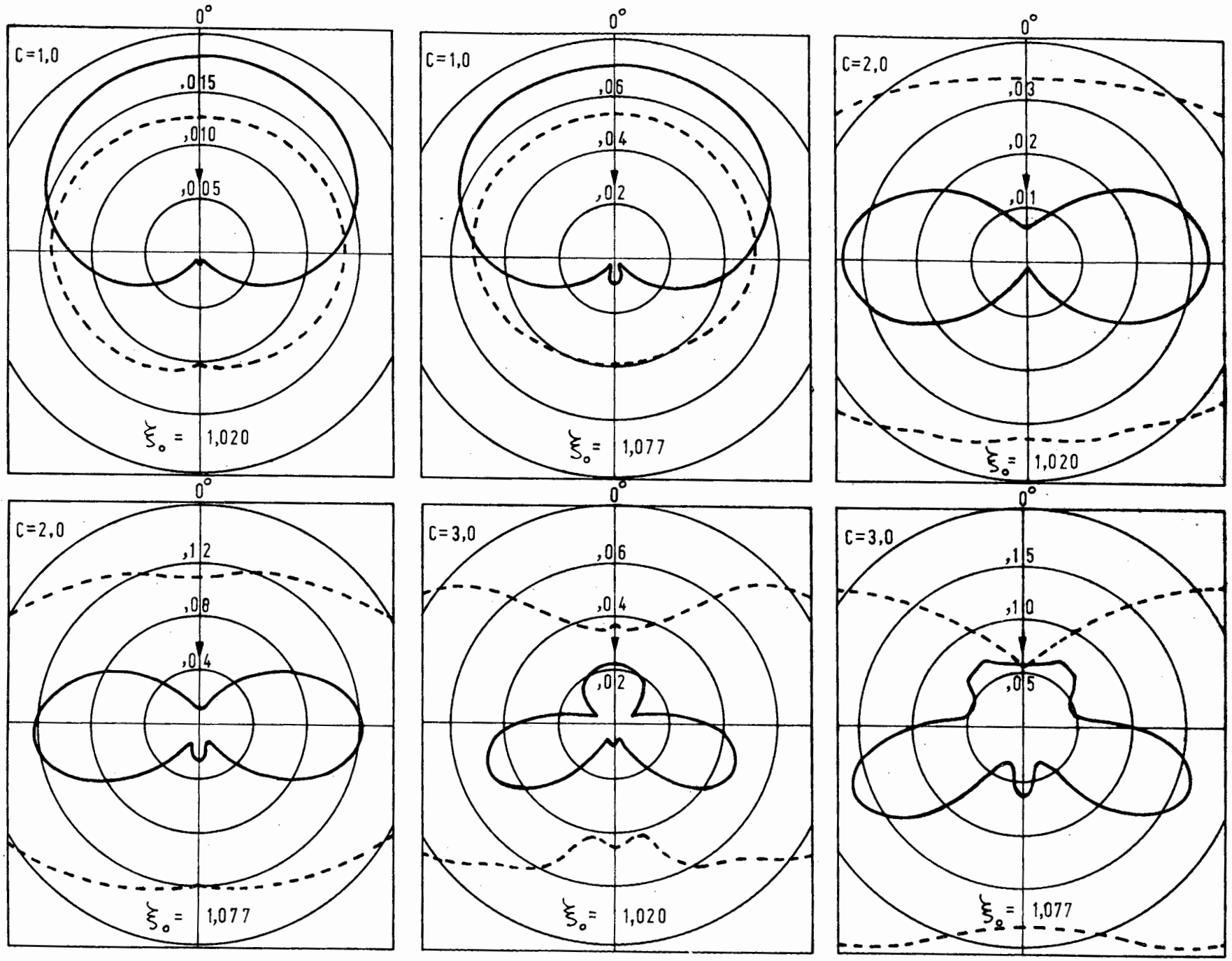

Fig. (3.4) $|S(\theta)|/ka$ as a function of θ for $\xi_0 = 1{,}020$ and $1{,}077$, $c = 1, 2, 3$.

(3.5) Backscattering cross sections for sound soft and sound hard prolate spheroids for axial incidence.

The backscattering cross section according to geometrical optics, σ_0, is defined by (2.2.26) where ρ_1 and ρ_2 are the principal radii of curvature at the specular point. For axial incidence on a prolate spheroid we have from (3.2.7) for $\theta = 0$ (the specular point) $\rho_1 = \rho_2 = b^2/a$, hence (2.2.26) becomes for both hard and soft spheroids:

$$\sigma_0 = \pi b^4/a^2 \qquad \text{--- (3.5.1)}$$

The backscattering cross section according to the exact theory of section (3.1) is denoted by σ and defined by (3.2.23):

$$\sigma = \frac{4\pi}{k^2}|S(0)|^2 \qquad \text{--- (3.5.2)}$$

In (3.5.2) S(0) is the far field in the backscattered direction and is obtained for the soft and hard cases from (3.1.27s and h) by putting $\theta = 0$:

$$S(0) = 2i \sum_{n=0}^{\infty} \frac{(-1)^n R_{on}^{(1)}(c,\xi_0)}{N_{on} R_{on}^{(3)}(c,\xi_0)} \{S_{on}(c,1)\}^2$$

--- (3.5.2s)

$$S(0) = 2i \sum_{n=0}^{\infty} \frac{(-1)^n \partial R_{on}^{(1)}(c,\xi_0)/\partial\xi_0}{N_{on} \partial R_{on}^{(3)}(c,\xi_0)/\partial\xi_0} \{S_{on}(c,1)\}^2$$

--- (3.5.2h)

From (3.5.2) and (3.5.3) we get for the normalized backscattering cross section σ/σ_0:

$$\sigma/\sigma_0 = \frac{4}{D^2(b/a)^4}\,|S(0)|^2 \qquad \text{--- (3.5.3)}$$

where $D = ka = c\xi_0$.

The normalized backscattering cross sections of soft and hard spheroids were calculated by Senior (1966) using (3.5.2s and h) and are shown as functions of D, $0 \leq D \leq 10$, for a/b = 2, 5 and 10 in Figure (3.5) for soft spheroids and Figures (3.7) - (3.9) for hard spheroids.

Using the method of spherical currents the normalized backscattering cross section is indicated by $\sigma_{(sc)}/\sigma_0$ and defined by

$$\sigma_{(sc)}/\sigma_0 = \frac{4}{D^2(b/a)^4}\,|S_{(sc)}(0)|^2 \qquad \text{--- (3.5.4)}$$

where $S_{(sc)}(0)$ is the far field in the backscattered direction and is obtained from (3.2.9s) and (3.2.9h) by putting $\theta = 0$. These equations become:

$$S_{(sc)}(0) = -\frac{k}{2b^2}\int_0^{\pi} F(\theta')\, e^{-ik\eta\cos\theta'}\, \rho\eta^3 \sin\theta'\, d\theta'$$

$$F(\theta') = -\frac{i}{k\rho^2}\sum_{n=0}^{\infty} i^n (2n+1)\frac{P_n(\cos\alpha)}{h_n^{(1)}(k\rho)} \qquad \text{--- (3.5.5s)}$$

and

$$S_{(sc)}(0) = \frac{-ik^2}{2a^2}\int_0^{\pi} F(\theta')\, e^{-ik\eta\cos\theta'}\, \eta^4 \cos\theta' \sin\theta' \, d\theta'$$

$$F(\theta') = \frac{i}{k^2\rho^2} \sum_{n=0}^{\infty} i^n (2n+1) P_n(\cos\alpha) \frac{}{h_n^{(1)\prime}(k\rho)}$$

--- (3.5.5h)

The graphs of σ/σ_0 in Fig. (3.5) with S(0) given by (3.5.2s) are taken from Senior (1966), Fig. 1. $\sigma_{(sc)}/\sigma_0$ was calculated using $S_{(sc)}(0)$ in (3.5.5s) after putting $\cos\theta' = z$. From (3.5.5s) we then get:

$$S_{(sc)}(0) = \int_{-1}^{+1} \{\varphi R(D, b/a, z) + i\varphi I(D, b/a, z)\}\{HR(D, b/a, z) + i HI(D, b/a, z)\} dz$$

--- (3.5.6),

where

$$HR = \frac{(k\eta)^3}{2D^2(b/a)^2} \cos(k\eta z)$$

$$HI = \frac{-(k\eta)^3}{2D^2(b/a)^2} \sin(k\eta z)$$

--- (3.5.7)

and QR and QI are the real and imaginary parts of $-\rho F(\theta') = -\rho \partial\Phi^{(t)}(\theta')/\partial n$.

$$\therefore \varphi R + i\varphi I = \frac{i}{k\rho} \sum_{n=0}^{\infty} i^n (2n+1) P_n(\cos\alpha) \frac{}{h_n^{(1)}(k\rho)}$$

--- (3.5.8)

The functions QR and QI are computed as the output of subroutine PUT (p. A19). PUT calls on subroutines PSI (p. A2) and ZETA (p. A3) to provide the spherical Bessel functions. As mentioned in section (2.3) PSI and ZETA are accurate to only four significant digits at an argument value of about 10. However the largest value attained by $k\rho$ is 5 for a:b = 2:1 at $\theta = \pi/2$ with D = 10.

Subroutine HURI (p. A20) calls on RAD (p. A15) to provide $k\eta$ as a function of D, b/a and z, and has HR and HI of (3.5.7) as output.

The subroutine SYMINT (p. A21) calls PUT and HURI to compute the integrand of (3.5.6) and then integrates this function by using Simpson's 1/3-rule. In SYMINT use was made of the fact that HR is symmetric in z and HI anti-symmetric in z. This did not lead to a significant reduction of CPU time. The summation is terminated by the same method as in GREAT (p. A18). The output of SYMINT is $|S_{(sc)}(0)|^2$ as a function of D and b/a. The main program calls on SYMINT and computes σ/σ_0. The subroutines involved in computing σ/σ_0 for soft spheroids were checked by computing σ/σ_0 for a = b and comparing this with the output of subroutine SPS (p. A13) which gives σ/σ_0 for a soft sphere as a function of D. Very good agreement was found. The normalized backscattering cross section for a sphere as a function of ka is reproduced in Fig. (3.5).

The following points of agreement between the curves of σ/σ_0 and $\sigma_{(sc)}/\sigma_0$ can be observed in Fig. (3.5). For a given eccentricity the normalized cross sections have a maximum at D = 0 and display a sharp fall-off with increasing D. The oscillations in the curves also tend to flatten out progressively with increasing D. With increasing a:b the normalized cross sections

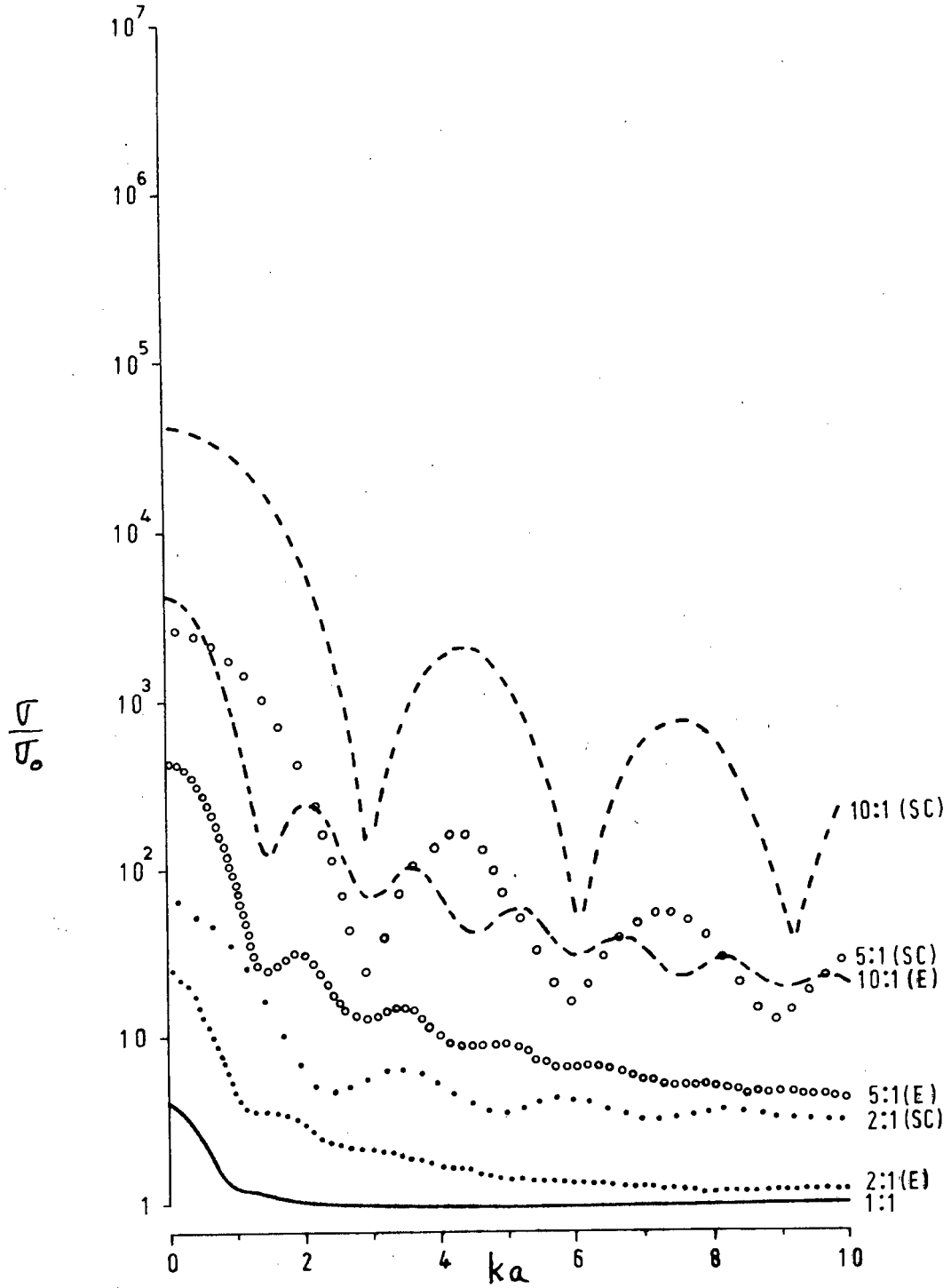

Fig. (3.5) Normalized backscattering cross sections of soft spheroids according to exact theory (E) and the method of spherical currents (SC). Sphere (——), 2:1 (···), 5:1 (°°°) 10:1 (---).

increase (in the case of σ/σ_0 this is entirely due to the normalization) and the oscillations become more pronounced. The separation (in D) between adjacent maxima and minima also tend to become more constant after the first maximum is ignored.

The main differences between σ/σ_0 and $\sigma_{(sc)}/\sigma_0$ is firstly that $\sigma_{(sc)}/\sigma_0 > \sigma/\sigma_0$ - this difference increases with increasing eccentricity - and secondly that the separation between adjacent maxima and minima differs considerably in the two cases for fixed a:b. It is a peculiar fact that the separation distance for $\sigma_{(sc)}/\sigma_0$ is very nearly double that of σ/σ_0 - this is especially noticeable in the thinner bodies (a:b = 5 and 10).

In spite of these differences it is perhaps fair to say that the method of spherical currents discriminates between the various soft spheroids in qualitatively the same way as exact theory.

In Figures (3.7) to (3.9) the normalized backscattering cross sections for hard spheroids according to Senior (1966) (Figures 4, 3 and 2 resp. in this paper) are plotted as functions of D for $0 \leq D \leq 10$. The far field in the backscattered direction is defined by (3.5.2h).

$\sigma_{(sc)}/\sigma_0$ for hard spheroids was calculated using $S_{(sc)}(0)$ as defined in (3.5.5h). On putting $z = \cos\theta'$ in (3.5.5h) we get:

$$S_{(sc)}(0) = \int_{-1}^{+1} \{ FR(D, b/a, z) + i\, FI(D, b/a, z) \}\, dz$$

--- (3.5.9)

where

$$FR + FI = (\varphi R + i\,\varphi I)(HR + i\,HI)$$

--- (3.5.10)

In (3.5.10) QR and QI are the real and imaginary parts of $\Phi^{(t)}_{(sc)}(\theta')$ and form the output of POTAS (p. A10).

$$HR = -\frac{(k\eta)^4 z}{2D^2}\,Sin(k\eta z)$$

$$HI = -\frac{(k\eta)^4 z}{2D^2}\,Cos(k\eta z) \qquad \text{--- (3.5.11)}$$

The functions HR and HI are computed by means of subroutine FAR (p. A22) which calls on RAD (p. A15) to provide $k\eta$ as a function of D, b/a and z. The real and imaginary parts of the integrand in (3.5.9) are computed by subroutine GRAND (p. A23) which calls on FAR and POTAS to provide HR, HI, QR and QI as input. GRAND also calls on RAD to provide $k\rho$ and $\cos\alpha$ as functions of D, b/a and z as input for POTAS.

In subroutine GRATE on p. A23 the real and imaginary parts of the integral in (3.5.9) are computed and combined in the single output $|S_{(sc)}(0)|^2$. This subroutine is very similar to GREAT (p. A18) which has been discussed in section (3.4). The main program calls on GREAT to provide $|S_{(sc)}(0)|^2$ as function of D and b/a and then computes $\sigma_{(sc)}/\sigma_0$.

The subroutines involved in computing $\sigma_{(sc)}/\sigma_0$ for hard prolate spheroids were checked by computing $\sigma_{(sc)}/\sigma_0$ for a = b and comparing the result with σ/σ_0 for spheres, using (2.2.28) and (2.2.21h). Subroutine SP (p. A11) has the real and imaginary parts of the far field in the backscattered direction as output. The graph of σ/σ_0 for a hard sphere as a function of D is shown in Fig. (3.6). This agrees well with $\sigma_{(sc)}/\sigma_0$ with a = b. For purposes of comparison the graph of $\sigma_{(sc)}/\sigma_0$ for a a:b = 100:99 hard spheroid as a function of D is also shown in Fig. (3.6).

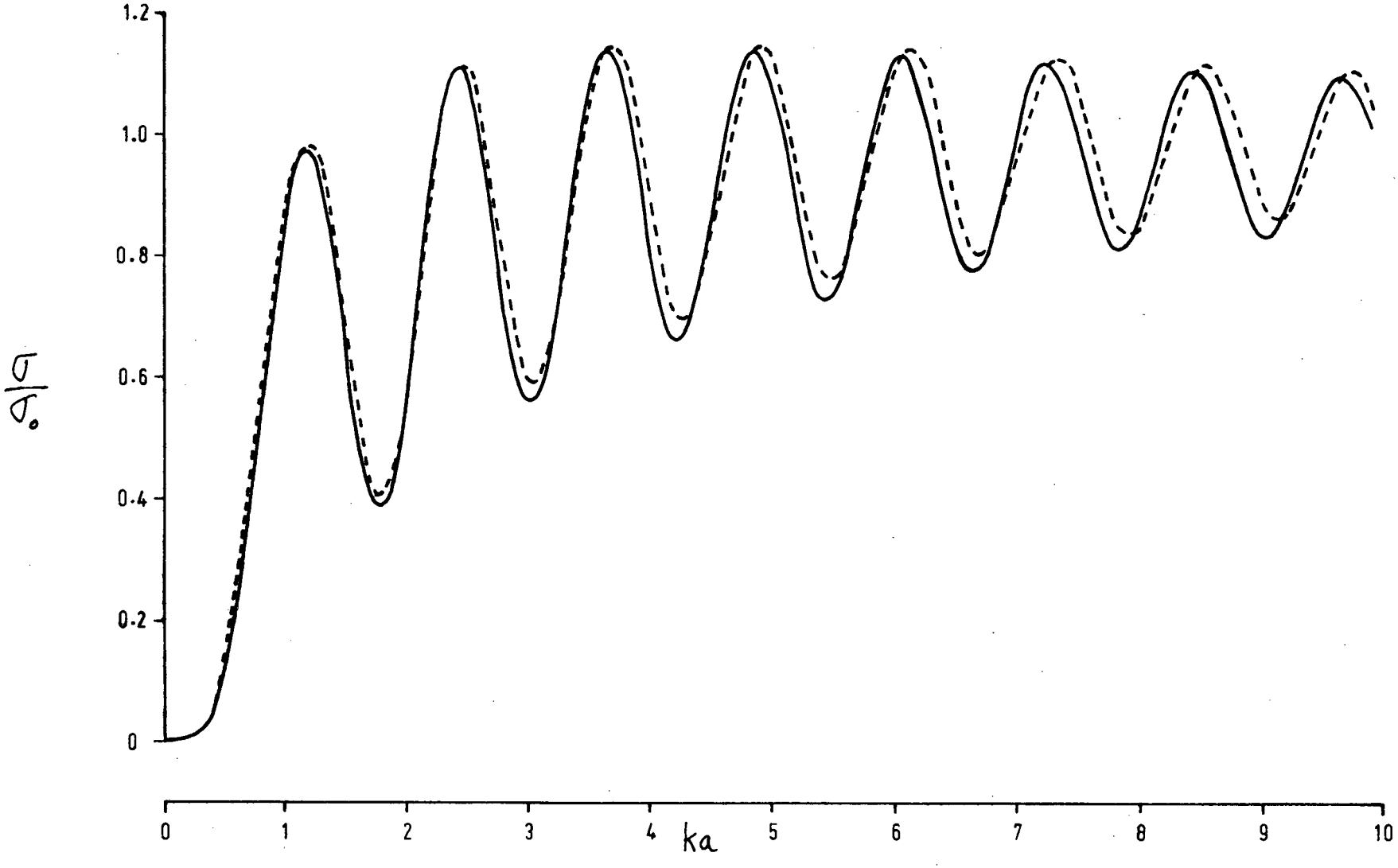

Fig. (3.6) Normalized backscattering cross sections for a hard sphere (——) and a 100:99 spheroid using the method of spherical currents (---)

In Fig. (3.7) σ/σ_0 and $\sigma_{(sc)}/\sigma_0$ are shown plotted as functions of D, while in Figures (3.8) and (3.9) σ/σ_0 and $\sigma_{(sc)}/2\sigma_0$ are plotted as functions of D.

Superficially the differences in backscattering cross sections according to the two methods employed are quite marked. There is however a fair agreement for $ka < 1$, hence in the Rayleigh region, which improves as the spheroids become fatter - for the 2:1 spheroid [see Fig. (3.7)] there is close agreement for $ka < 1$.

Regarding the curves of σ/σ_0 against D, Senior [Senior (1966)] comments as follows:

"Taking first the 10:1 spheroid, we observe that the curve oscillates between maxima that, after the first, are slowly decreasing in magnitude as $c\xi_0(ka)$ increases, and minima that are indistinguishable from zero. The oscillation is extremely regular and if the first maximum is ignored, the seperation (in $c\xi_0$) of adjacent maxima and minima averages 0,780 with a standard deviation of only 0,008. This value is compatible with the interference between two individual sources of scattering whose phase centres are coincident with the ends of the spheroid. If the phase of excitation were the same as that of the incident field, the separation of the maxima and minima would be 0,785 (i.e. $\pi/4$). This is quite close to the value deduced from the data, and since the distance from tip to tip measured along the surface exceeds the straight line distance by only a factor 1,016, it is almost impossible to distinguish between direct excitation of the rear tip and the excitation through a travelling wave supported by the surface.

The results of the 5:1 spheroid are similar, but the maxima now decrease more rapidly and the minima are no longer zero. When a:b = 2, the differences from the thin

body behaviour are very marked, and since the minima increase with $c\xi_0$, the two dominant sources of the scattering are no longer of equal magnitude".

The conclusion is that for the fatter spheroids the scattering is no longer determined by travelling waves whose attenuation can be ignored. Here one must turn to the sphere where a second contribution (the first is the specular return) arises from waves creeping along the surface from the shadow boundary and back again.

Concerning the curves of $\sigma_{(sc)}/\sigma_0$ against D, much the same remarks may be made. For the 10:1 spheroid this curve also oscillates between maxima that, after the first, are slowly decreasing in magnitude with increasing D and minima that are indistinguishable from zero. If the first maximum is ignored the oscillation is very regular. However here the separation between adjacent maxima and minima average about double that of exact theory. This value is compatible with the interference between two individual scattering sources separated by an optical path length of 2ka and not 4ka (i.e at the tips of the spheroid) as is the case in exact theory.

The results for the 5:1 spheroid are similar to that of the 10:1 spheroid. As in the case of exact theory we observe that the maxima now decrease more rapidly and the minima are no longer zero. Again, the average separation between adjacent maxima and minima is about double that of exact theory.

For the 2:1 spheroid we find, as in the case of exact theory, an initial decrease of maxima followed by an increase, and a steady increase in minima with increasing ka. The separation is also less constant than in the case of the thinner spheroids, but here too we find that the separation is roughly double that of exact theory.

For the three spheroids considered here the corresponding maxima and minima of σ/σ_0 and $\sigma_{(sc)}/\sigma_0$ can be brought practically in phase by plotting $\sigma_{(sc)}/\sigma_0$ against ka/2 on the same system where σ/σ_0 is plotted against ka.

Although the maxima of σ/σ_0 and $\sigma_{(sc)}/\sigma_0$ differ markedly and increasingly so as the bodies become thinner, there is nevertheless, for a particular eccentricity, a fairly constant relationship between these maxima.

Let the i-th maxima of σ/σ_0 and $\sigma_{(sc)}/\sigma_0$ resp. be denoted by a_i and A_i for a fixed value of a:b. It is then found that for

a:b = 10 : $A_1/a_1 = 3,85$; $A_2/a_2 = 3,82$; $A_3/a_3 = 3,80$
a:b = 5 : $A_1/a_1 = 3,56$; $A_2/a_2 = 3,43$; $A_3/a_3 = 3,36$
a:b = 2 : $A_1/a_1 = 2,35$; $A_2/a_2 = 2,15$; $A_3/a_3 = 2,40$

By affecting two simple scale transformations it is therefore possible to bring $\sigma_{(sc)}/\sigma_0$ and σ/σ_0 into fairly close correspondence for a particular value of a:b over the range $0 \leq ka \leq 10$. This correspondence should increase with increasing a:b.

It should also be noted that as the only difference between exact theory and the method of spherical currents lies in the surface field, there should be close correspondence between the backscattering cross sections if there is a small variation between the surface fields. In Figures (3.1) to (3.5) the surface fields are shown with $c = kF = k\sqrt{a^2 - b^2} = 5$ for a:b = 2, 5 and 10 respectively. The respective values of D = ka are 5,77, 5,10 and 5,03, and the respective values of $\sigma_{(sc)}/\sigma_0 - \sigma/\sigma_0$ are approximately 0,07, 1,9 and 0,58. For a:b = 2 and c = 5 it can be seen that there is a close correspondence between the surface fields, especially in the illuminated region. For a:b = 5 the variation between the surface fields is larger and this is reflected in the larger value of $\sigma_{(sc)}/\sigma_0 - \sigma/\sigma_0$. For a:b = 10 there is a

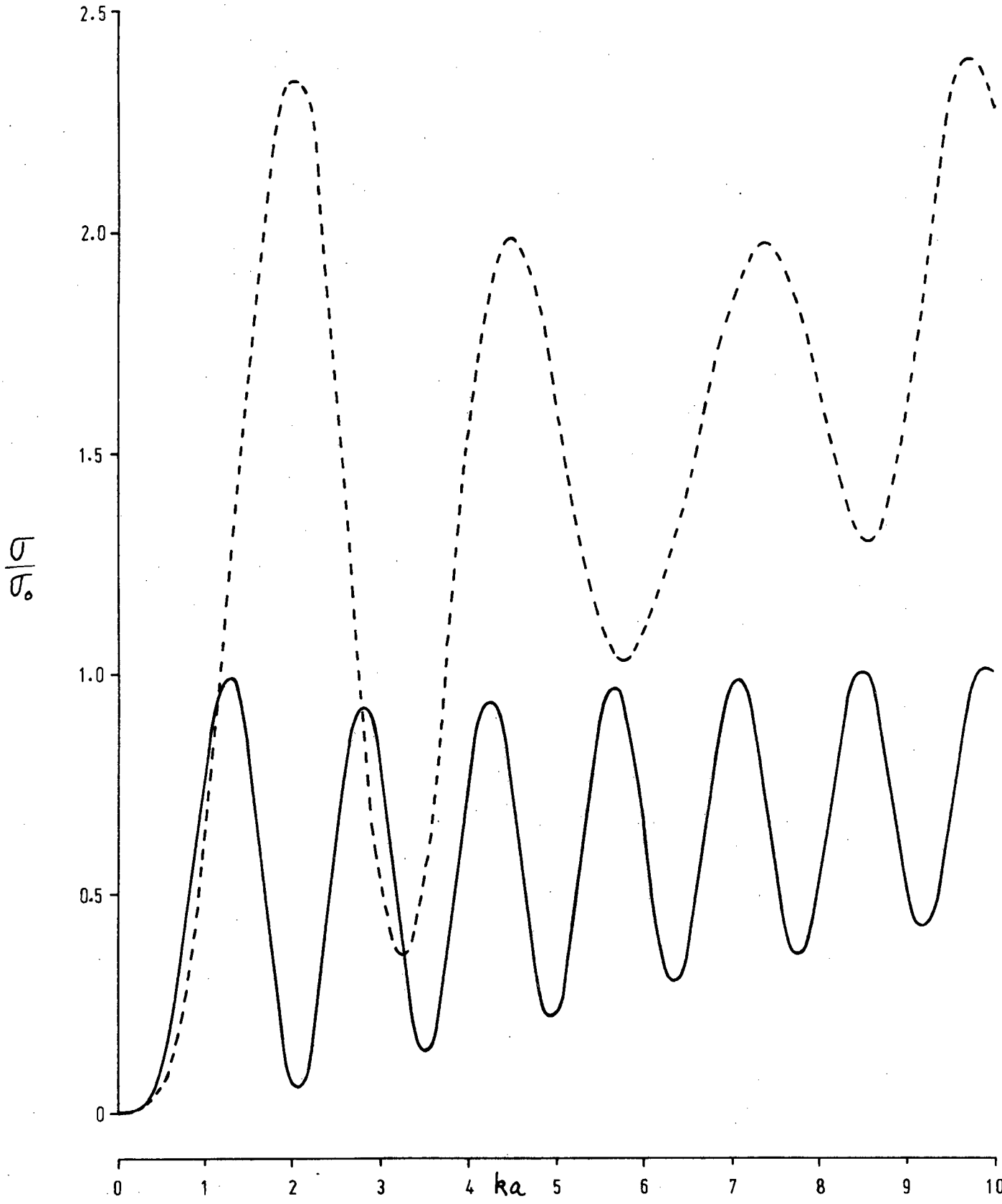

Fig. (3.7) Normalized backscattering cross sections of hard 2:1 spheroids. Senior 1966 (——), method of spherical currents (---)

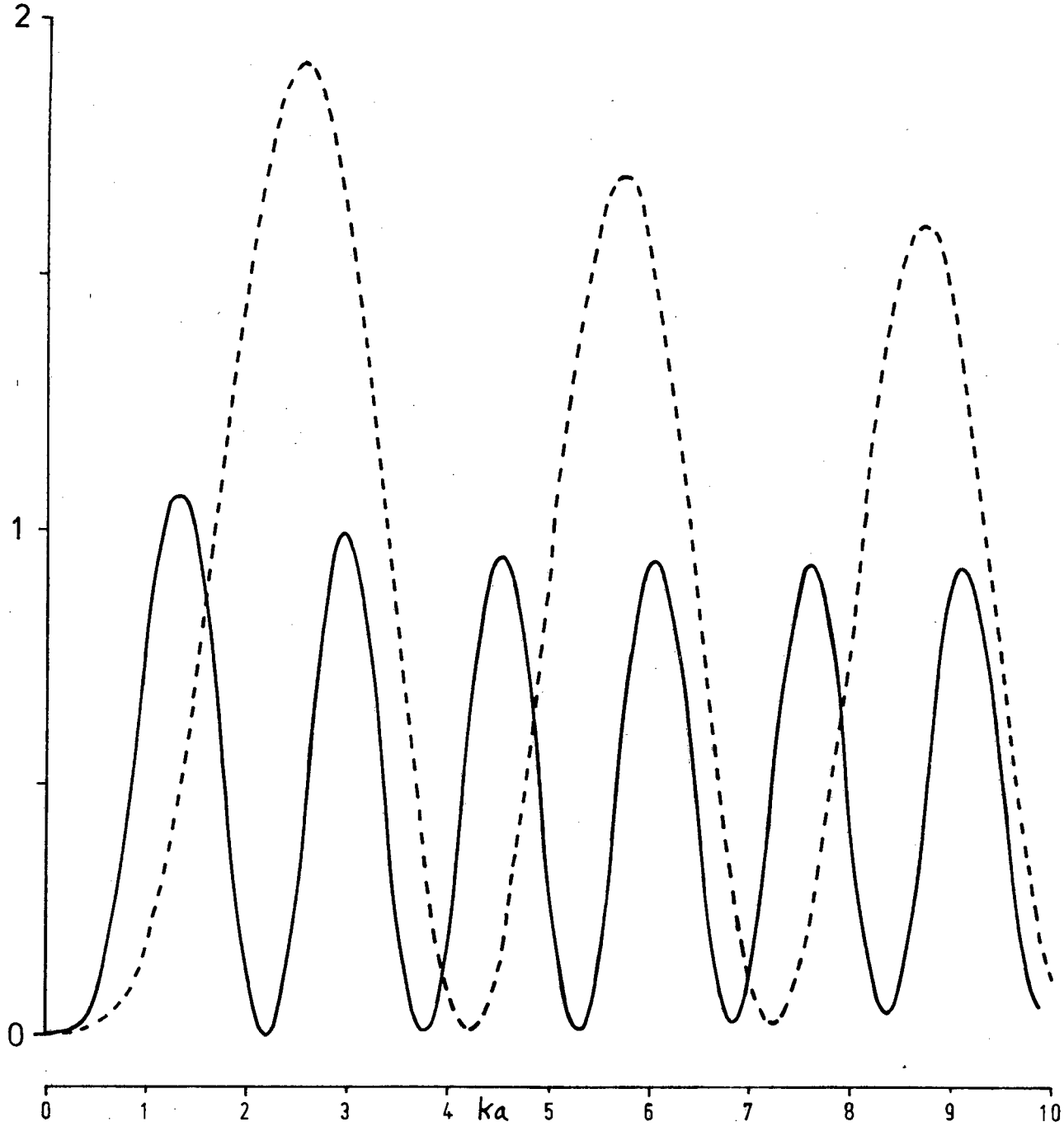

Fig. (3.8) Normalized backscattering cross sections of hard (5:1) spheroids
σ/σ_0 according to Senior 1966 (——), $\sigma_{(sc)}/2\sigma_0$ according to the
method of spherical currents (---)

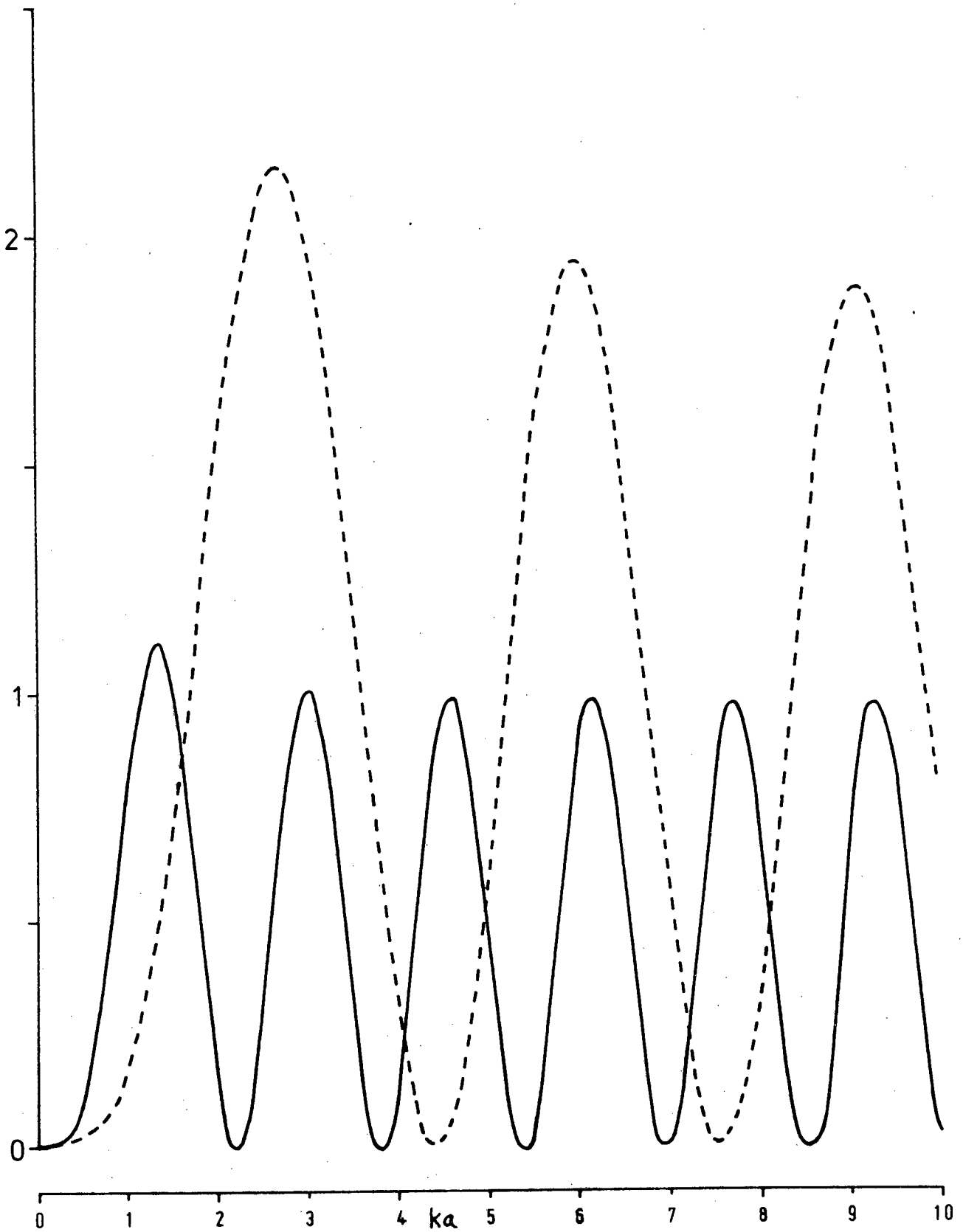

Fig. (3.9) Normalized backscattering cross sections of hard 10:1 spheroids. σ/σ_0 according to Senior 1966 (——), $\sigma/2\sigma_0$ according to the method of spherical currents (---)

smaller variation between the surface fields than in the 5:1 case and the normalized backscattering cross sections have a corresponding smaller difference.

Finally it can be said that the method of spherical currents discriminates between hard prolate spheroids of different eccentricity in qualitatively the same way as exact theory.

(3.6) Backscattering cross sections of hard prolate spheroids at high frequencies for axial incidence.

One of the classical high frequency scattering theories is physical optics or Kirchhoff theory. As explained in section (2.4), this consists of replacing the surface field with twice the incident field on the illuminated side and zero on the dark side of the scattering object. Let the direction of propagation of the plane incident field be u_i, then we have from (2.1.18h):

$$\Phi^{(s)}_{(po)}(x_i) = \frac{1}{2\pi} \oint_{S'} e^{ik u_i x_i} \frac{\partial G(x_i, \eta_i)}{\partial n} df$$

--- (3.6.1),

where S' is the illuminated part of the surface S of the sound hard obstacle.

With $(u_i) = (0,0,-1)$ and using the asymptotic expression for $\partial G/\partial n$ given by (2.6.2), the following equation for the far field according to physical optics is obtained:

$$S_{(po)} = -\frac{ik^2}{2\pi} \oint_{S'} (n_i \vec{e}_i)\, e^{-ik(\eta_3 + \eta_i \vec{e}_i)}\, df$$

--- (3.6.2)

In the backscattered direction [$(e_i^r) = (0,0,1)$] this becomes

$$S_{(PO)}^{(0)} = -\frac{ik^2}{2\pi} \oint_{S'} \eta_3 e^{-2ik\eta_3} d\mathbf{f} \qquad \text{--- (3.6.3)}$$

If the obstacle has axial symmetry, we choose the 3-axis to coincide with the axis of symmetry.

The equation of the surface of the obstacle is defined by

$$\left.\begin{aligned} &\eta_3 = g(\rho) \\ &\text{where} \quad \rho^2 = \eta_1^2 + \eta_2^2 = \eta^2 \sin^2\theta \end{aligned}\right\} \qquad \text{--- (3.6.4)}$$

Now

$$\eta_3 \, d\mathbf{f} = \varepsilon_{3jk} \frac{\partial \eta_j}{\partial \rho} \frac{\partial \eta_k}{\partial \phi} d\rho \, d\phi = \rho \, d\rho \, d\phi \qquad \text{--- (3.6.5)},$$

and (3.6.3) becomes after integration w.r.t. ϕ:

$$S_{(PO)}^{(0)} = -ik^2 \int_{\alpha}^{\beta} e^{-2ikg(\rho)} \rho \, d\rho \qquad \text{--- (3.6.6)}$$

The limits of integration α and β are so chosen that the integration extends only over S', the illuminated part of S.

Equation (3.6.6) is now specialized for a prolate spheroid with centroid at the origin, semi-major axis a and semi-minor axis b. In the form (3.6.4) the equation of the spheroid is

$$\eta_3 = \frac{a}{b}\sqrt{b^2 - \rho^2} \qquad \text{--- (3.6.7)},$$

and (3.6.6) becomes

$$S_{(PO)}(0) = -ik^2 \int_0^b e^{-2ik(a/b)\sqrt{b^2-\rho^2}}\, \rho\, d\rho$$

After integrating w.r.t. ρ we get:

$$S_{(PO)}(0) = \frac{ib^2}{4a^2}\left[1 - (1+2ika)e^{-2ika}\right] \qquad \text{--- (3.6.8)}$$

From (2.2.23) with $S(0) = S_{(PO)}(0)$ we get for the backscattering cross section :

$$\sigma_{(PO)} = \frac{\pi b^4}{a^2}\left[1 - \frac{1}{ka}\sin 2ka + \frac{1}{2k^2a^2}(1-\cos 2ka)\right] \qquad \text{--- (3.6.9)}$$

From (3.5.1) we have $\sigma_0 = \pi b^4/a^2$,

$$\therefore\ \sigma_{(PO)}/\sigma_0 = \left[1 - \frac{1}{ka}\sin 2ka + \frac{1}{2k^2a^2}(1-\cos 2ka)\right] \qquad \text{--- (3.6.10)}$$

From (3.6.10) it follows that $\lim_{k\to\infty} \sigma_{(PO)}/\sigma_0 = 1$, and that the normalized backscattering cross section according to physical optics cannot distinguish between spheroids of differing eccentricity. In Fig. (3.10) $\sigma_{(PO)}/\sigma_0$ is shown plotted as a function of D = ka for $10 \le D \le 80$ with $\sigma_{(sc)}/\sigma_0$ for a:b = 5. $\sigma_{(PO)}/\sigma_0$ was computed by means of subroutine PHYSOP (p. A25).

A significant high frequency scattering theory is J.B. Keller's geometric theory of diffraction [Keller (1958)]. This theory was applied by Levy and Keller (1959) to

smooth objects, and these results were specialized for spheroids by the same authors [Levy and Keller (1960)].

The geometric theory of diffraction is a generalization of geometrical optics in the sense that Fermat's Principle is extended to apply to "diffracted rays", in addition to reflected and refracted rays.

If Fermat's Principle is applied to optical paths which must pass through two fixed points, it is found that these extremals obey the eiconal equation. This equation may also be obtained by applying Maxwell's equation in integral form to the discontinuity across the wave front of a propagating electromagnetic disturbance. The rays of optics are the extremals of Fermat's Principle as well as the orthogonal trajectories of the wave fronts of an electromagnetic field. If Fermat's Principle is applied to two fixed points on the same side of a surface of discontinuity with the additional restriction that the optical paths must touch the surface of discontinuity, it is found that, in addition to the eiconal, the rays must obey Snell's laws of reflection at the point of incidence on the surface. Thus an incident ray gives rise to a ray of reflection. This method however breaks down if (i) a normal to the surface cannot be defined - hence at edges and vertices, and (ii) if the incident ray strikes the surface at a tangent. By postulating the creation of "diffracted" rays in such cases of incidence and applying Fermat's theorem to them, Keller succeeded in generalizing geometrical optics and also extending its range of applicability to lower frequencies.

As the spheroid is a smooth body, diffracted rays can only be produced by tangentially incident rays. A tangentially incident ray gives rise to a surface ray which travels around the body, continuously shedding

diffracted rays and becoming progressively attenuated. The rate at which diffracted rays are shed at a particular point is determined by the incident field, the material properties of the surface and the curvature of the surface at the point. The phases and amplitudes of the diffracted rays at the surface are found by matching them with those of the surface rays, using the boundary conditions. The phases and amplitudes of the surface rays are found by calculating optical path lengths from the point of incidence and applying energy conservation, taking continuous attenuation into account.

The exterior field at a given point is found by adding together the fields of each reflected and diffracted ray passing through the point. The amplitude and phase of the field associated with each ray is determined by applying energy conservation to bundles of rays and calculating optical path lengths from the given point to the point on the surface which gave rise to the rays.

If the point at which the exterior field is to be calculated is situated on a caustic of the diffracted rays, the field becomes infinite at the particular point. By a modification Levy and Keller however succeeded in obtaining a finite field on caustics (Levy and Keller (1959), pp. 186 - 187). In the particular case of the backscattered field for axial incidence, the axis of symmetry is a caustic of the diffracted rays.

From Levy and Keller (1960), equation (16), we have for the total backscattered far field from a hard prolate spheroid for an axially incident plane wave:

$$S_{(GTD)}(0) = \frac{ka(b/a)^2}{2}\left[e^{-2ika} - \frac{2\pi^2(ka)^{1/3}}{9A^2 6^{1/3}(b/a)^{4/3}} e^{2ika + i\frac{\pi}{3} + 2i\tau(ka)^{1/3}F}\right]$$

--- (3.6.11)

In (3.6.11):

$$F = \frac{(b/a)^{2/3}}{(1-(b/a)^2)^{1/2}} \int_0^{\pi/2} \frac{d\eta}{\left(\frac{(b/a)^2}{1-(b/a)^2} + \sin^2\eta\right)}$$

$$q = 1,469354$$

$$A = 1,16680$$

$$T = \frac{q}{6^{1/3}} e^{i\pi/3}$$

--- (3.6.12)

In (3.6.11) $\frac{ka}{2}(b/a)^2 e^{-2ika} = \frac{kb^2}{2a} e^{-2ika}$ is the contribution of the geometrical optics field. The notation used here differs from that of Levy and Keller. The spherical coordinates used by them are defined by the equations:

$$x = h \cosh\xi \cos\eta$$
$$y = h \sinh\xi \sin\eta \cos\phi$$
$$z = h \sinh\xi \sin\eta \sin\phi$$

In addition, a few corrections have been made, mainly printing errors. The factor in front of the square brackets in (3.6.11) is erroneous in Levy and Keller - they give the factor appropriate for an oblate spheroid.

The integrand of the elliptic integral in (3.6.12) is computed by subroutine ELLIP, p. A26. The elliptic integral is computed by means of subroutine GREER (p. A27), using Simpson's 1/3-rule. The output of subroutine AMPLI (p. A28) is the real and imaginary parts of the far field as functions of D = ka and b/a. The main program calls on AMPLI and computes the normalized backscattering cross section $\sigma_{(GTD)}/\sigma_0$ according to (3.5.3).

In Fig. (3.10) $\sigma_{(GTD)}/\sigma_0$ is shown for the 2:1 hard

prolate spheroid plotted as a function $D = ka$, $10 \leq D \leq 80$. $\sigma_{(GTD)}/\sigma_0$ for the 5:1 and 10:1 spheroids are not shown, as the results were poor. For the 5:1 spheroid values of $\sigma_{(GTD)}/\sigma_0$ were found which were of the order of 20, while for the 10:1 spheroid values of the order of a few hundred were found. This is in agreement with the finding of Kazarinoff and Ritt (1959) that Keller's theory is applicable only when the wavelength is small relative to the radius of curvature at the tip of the spheroid, i.e. for fat spheroids in the high frequency range.

To compute $\sigma_{(sc)}/\sigma_0$ for $10 \leq D \leq 80$ the same subroutines were used as for the range $0 \leq D \leq 10$. For the 5:1 and 10:1 spheroids the computations were terminated respectively at $ka = 75$ and $ka = 55$. Owing to the increasingly oscillatory nature of HR and HI in (3.5.10) with increasing ka and eccentricity, the computations became excessively laborious. For instance a:b = 10 at $ka = 60$ the integral in (3.5.9) had not converged sufficiently after 2^{15} divisions of the interval, which took 30 min. CPU time on the Univac 1106. This is also the reason for the relatively few values of $\sigma_{(sc)}/\sigma_0$ computed for the thinner spheroids.

The range of values of ka for which $\sigma_{(sc)}/\sigma_0$ was computed is well within the range of values of $k\rho$ for which BESJ (pp. A6 - A8) accurately computes the spherical Bessel functions. For instance, for a:b = 5 at $ka = 80$, $20 \leq k\rho \leq 40$.

Looking at the curve of $\sigma_{(sc)}/\sigma_0$ for the 2:1 spheroid, the oscillations become progressively damped with increasing ka, and the end of the resonance region is reached at $ka \approx 60$, when the curve is practically level. For a:b = 2:1, $\sigma_{(sc)}/\sigma_0 \sim 2{,}4$ for $ka = 80$ can be inferred from the graph. This is a failing of the method of spherical currents but is about the same as the maximum

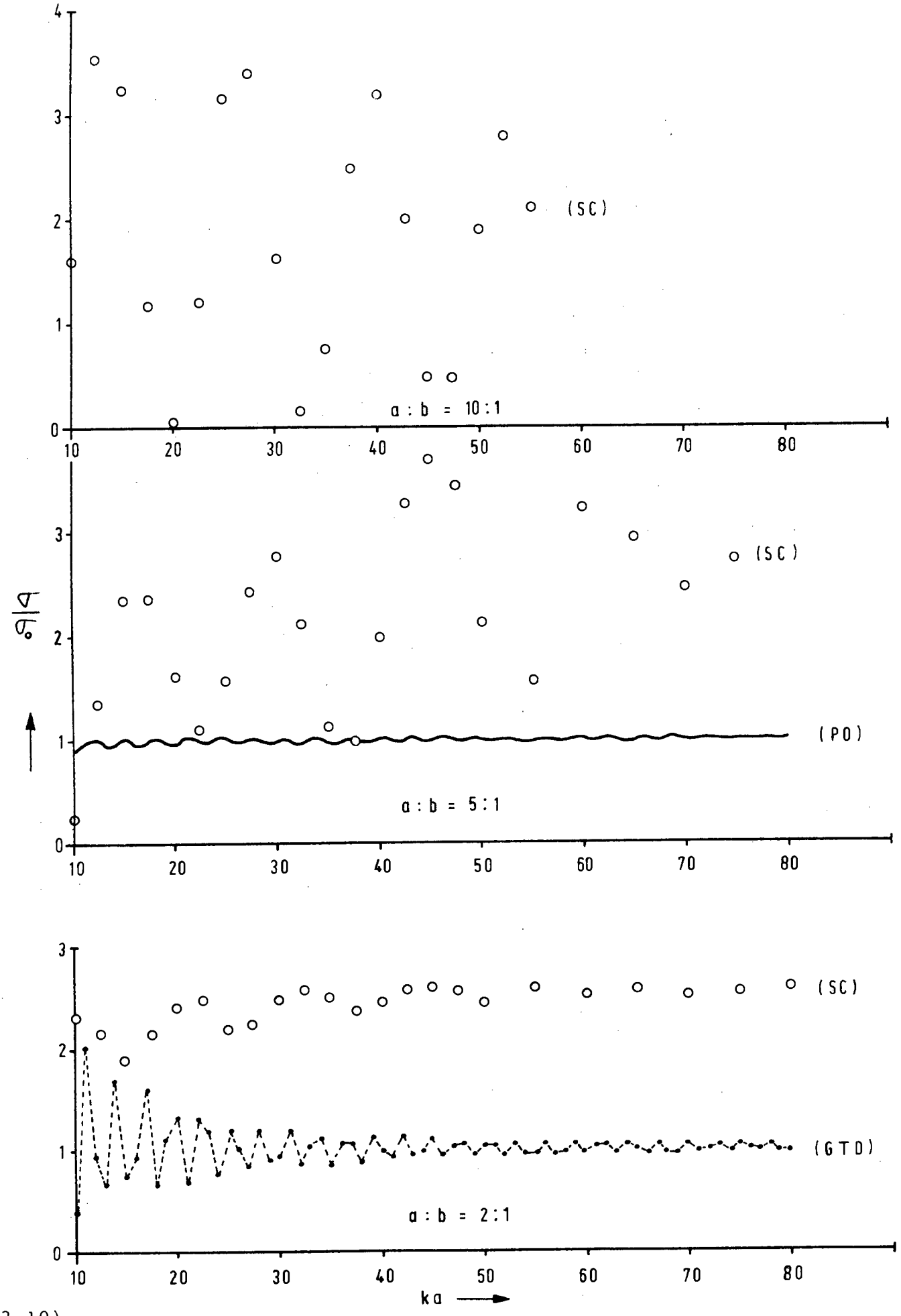

ig. (3.10)

Normalized backscattering cross sections
Method of spherical currents (ooo)
Geometrical theory of diffraction (---)
Physical optics (——)

amplitude ratios measured in section (3.5).

As the eccentricity increases the minima tend to increase at a slower rate and the oscillations retain their regularity for larger values of ka. This is consistent with the model of two individual, interfering sources of scattering situated on the axis which produces regular oscillations and becomes more applicable with increasing a:b

CHAPTER IV

AXIAL BACKSCATTERING FROM HARD FINITE CONES.

(4.1) Rayleigh scattering - Siegel's empirical formulae for hard flatbacked cones and cone spheres.

Consider a finite, closed, acoustically hard body, surface S, illuminated by a plane wave

$$\Phi^{(i)}(x_i) = e^{ikU_i x_i} \qquad \text{--- (4.1.1)}$$

The incident field may be expanded as a power series in k.

$$\therefore \Phi^{(i)}(x_i) = \sum_{m=0}^{\infty} (ik)^m \Phi_m^{(i)}(x_i) \qquad \text{--- (4.1.2)}$$

In (4.1.2) $\Phi_0^{(i)} = 1$, $\Phi_1^{(i)} = n_i x_i$, etc.

A similar expansion can be made for the scattered field (see Kleinman (1965), pp. 848 - 849).

$$\Phi^{(s)}(x_i) = \sum_{m=0}^{\infty} (ik)^m \Phi_m^{(s)}(x_i) \qquad \text{--- (4.1.3)}$$

This series has a finite radius of convergence as a function of k. The total field $\Phi^{(t)} = \Phi^{(i)} + \Phi^{(s)}$ may now also be represented by a power series expansion.

$$\Phi^{(t)}(x_i) = \sum_{m=0}^{\infty} (ik)^m \Phi_m^{(t)}(x_i) \qquad \text{--- (4.1.4)}$$

For a sound hard obstacle the boundary condition is:

$$\left.\frac{\partial \Phi^{(t)}}{\partial n}\right|_S = 0 \qquad \text{--- (4.1.5)}$$

The Rayleigh series (4.1.3) is essentially a near field result. In order to determine the far field the problem resolves itself into two parts: firstly the determination of the near field terms, and secondly their extension to the far field. Here we merely wish to prove one of Rayleigh's scattering laws, i.e. that the scattered field varies inversely with the square of the wave length. The procedure is due to Senior (1973).

On substituting the expansions (4.1.3) and (4.1.4) into the Helmholtz equation and equating like powers of k it is found that $\Phi_0^{(s)}$, $\Phi_1^{(s)}$, $\Phi_0^{(t)}$ and $\Phi_1^{(t)}$ satisfy Laplace's equation. From (4.1.5) it follows that

$$\left.\frac{\partial \Phi_m^{(t)}}{\partial n}\right|_S = 0,$$

and it is easily shown that $\Phi_0^{(s)}$ is zero everywhere, hence $\Phi_0^{(t)} = 1$.

The coefficient of the next term of (4.1.4) is found by utilizing the integral equation (2.1.20h) for the surface field on a hard object. In this equation the fields and e^{ikR}/R are expanded in powers of k, and like powers of k are equated. For the terms in k we get:

$$\Phi_1^{(t)}(\xi_i) = 2u_i\xi_i + \frac{1}{2\pi}\oint_S \Phi_1^{(t)}(\eta_i)\frac{\partial}{\partial n}\left(\frac{1}{R}\right)d\varphi \qquad \text{--- (4.1.6),}$$

where $\partial/\partial n = n_i\,\partial/\partial\eta_i$ and $R = |x_i - \eta_i|$.

The extension to the far zone is achieved with the aid of the integral representation (2.1.18h) for the scattered field. If, in this equation, we use (4.1.5), the expansion (4.1.3) and the asymptotic expansion (2.6.2), we get:

$$\Phi^{(s)}(x_i) \sim \frac{e^{ikr}}{4\pi r}\left\{-k^2\oint_S [\hat{e}_i\eta_i - \Phi_1^{(t)}(\eta_i)]n_j\hat{e}_j\,d\mathcal{S} + \text{higher order terms in } k\right\} \quad \text{--- (4.1.7)}$$

The far field amplitude $S(\theta,\phi)$ is defined by the equation $\Phi^{(s)} = e^{ikr}S/kr$. From the preceding it therefore follows that S will have a power series expansion

$$S = k^3\sum_{m=0}^{\infty} k^m f_m \quad \text{--- (4.1.8)},$$

where the coefficients f_m are functions of the angular variables θ and ϕ, the body parameters and the incident field. Since S is a dimensionless function the coefficient of each power of k must be proportional to a like power of a body dimension.

For sufficiently small values of k S may be approximated by the leading term, and it follows from (2.2.23) that the so-called Rayleigh cross section is then given by

$$\sigma = 4\pi k^4 |f_0|^2. \quad \text{--- (4.1.9)}$$

For axially symmetric bodies with axial incidence Siegel (1959) devised a method for the estimation of $|f_0|$ in the backscattered direction. At wavelengths large compared with the greatest linear dimension of the obstacle, the obstacle appears as a singularity to the wave and shape factors appear as essentially second order corrections in $|f_0|$. It follows from (4.1.8) that f_0 must have the dimensions of volume, and consequently $|f_0|$ is taken as proportional to the volume of the obstacle in (4.1.9).

$$\therefore \sigma = C k^4 (VF)^2 \qquad \text{--- (4.1.10)}$$

In (4.1.10) C is a pure proportionality constant, V is the volume and F a dimensionless correction factor that takes into account the dependence of the cross section on the shape. The shape correction factor F for elongated bodies is now determined by examining its form for the spheroid, of which the exact result for f_0 is known [Rayleigh (1897)]. As the flatness of the scatterer increases the approximation is expected to get worse as an infinitely flat body like a disc has a zero volume but a non-zero cross section. It turns out that for the spheroid

$$F = 1 + e^{-y}/\pi y \qquad \text{--- (4.1.11),}$$

and $$C = 1/\pi \qquad \text{--- (4.1.12)}$$

In (4.1.11) y = b/a, the ratio of the semi-minor axis to the semi-major axis. In the electromagnetic case $C = 4/\pi$ owing to the presence of a magnetic dipole in addition to the electric dipole. Hence, for a hard prolate spheroid, the Rayleigh backscattering cross section is given by

$$\sigma = \frac{1}{\pi} k^4 \left(\frac{4}{3}\pi a b^2\right)^2 \left[1 + e^{-b/a}/\pi b/a\right]^2$$

--- (4.1.13)

With a = b we get for the sphere

$$\sigma = 1{,}248 \frac{k^4}{\pi} \left(\frac{4}{3}\pi a^3\right)^2 ,$$

compared with the exact result obtainable from (2.2.21h), (2.2.8) and (2.2.23):

$$\sigma = \frac{25}{16} \cdot \frac{k^4}{\pi} \left(\frac{4}{3}\pi a^3\right)^2$$

$$= 1{,}563\, k^4 V^2/\pi$$

Siegel now assumes that (4.1.10) with $C = 1/\pi$ (for hard obstacles) and F defined by (4.1.11) is a valid approximation of the Rayleigh cross section in the backscattered direction where y is a constant times a length-to-width ratio, where length is associated with the maximum dimensions of the body in the direction of propagation of the incident wave and width is associated with maximum dimensions of the body in a direction perpendicular to that previously mentioned.

Hence for the on-axis excitation of bodies of revolution

$$\sigma = \frac{k^4}{\pi} V^2 \left[1 + e^{-y}/\pi y\right]^2$$

--- (4.1.14)

Consider the case of the right circular cone (flat-backed) of hight h and base radius a. From (4.1.14):

$$\sigma_{cone} = \frac{k^4}{\pi}\left(\frac{1}{3}\pi a^2 h\right)^2 \left[1 + \frac{e^{-rh/2a}}{\pi rh/2a}\right]^2$$

--- (4.1.15)

To compensate for the loss of accuracy as the body becomes flatter, Siegel requires that

$$\lim_{h \to 0} \sigma_{cone} = \sigma_{disc} = \frac{1}{\pi} k^4 \left(\frac{4}{3} a^3\right)^2$$

--- (4.1.16),

the backscattering cross section of a hard circular

disc of radius a. This enables us to calculate r and we find r = ½. Hence from (4.1.15)

$$\sigma_{cone} = \frac{k^4}{\pi}\left(\frac{\pi}{3}a^2h\right)^2\left[1 + \frac{e^{-h/4a}}{\pi h/4a}\right]^2$$

--- (4.1.17)

On putting a/h = tanβ we have from (4.1.17)

$$\frac{\sigma_{cone}}{\pi a^2} = \frac{(ka)^4}{9\tan^2\beta}\left[1 + \frac{4}{\pi}\tan\beta\, e^{-1/4\tan\beta}\right]^2$$

--- (4.1.18)

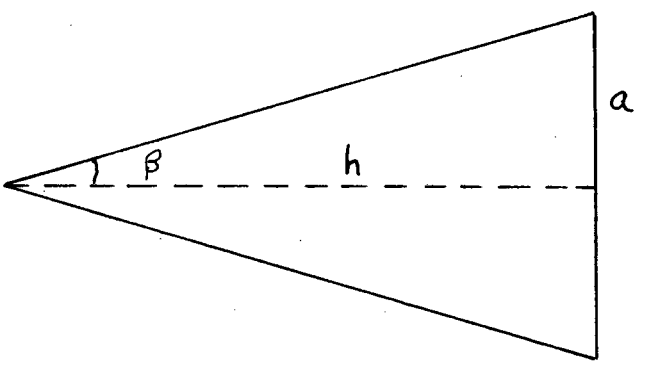

$\sigma_{cone}/\pi a^2$ was computed using program SIEG1 (p. A29) and is shown as a function of ka for β = 12°, 45° and 60° in Fig. (4.1).

For the cone sphere the Rayleigh backscattering cross section was derived by Siegel (1963). Here the hemispherically capped cone is used to calculate the cross section of the cone sphere on the grounds that in the long wavelength limit the matching of the first derivatives at the join of the hemisphere and the cone has no bearing on the first term in the Rayleigh series in view of the consideration that the body as a whole appears as a singularity to the wave.

It should be noted however that the difference in volumes between hemispherically capped cones and cone spheres with the same base radii and total lengths increases with decreasing length.

Firstly Siegel calculates the Rayleigh cross section for the hemispheroid, semi-major axis b and semi-minor axis a.

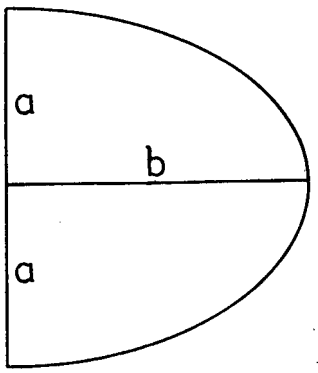

From (4.1.14) we have for the hemispheroid

$$\sigma = \frac{k^4}{\pi}\left(\frac{2}{3}\pi a^2 b\right)^2 \left(1 + \bar{e}^{y}/y\pi\right)^2, \quad y = \frac{r\,b}{2a}$$

The factor r can be found by requiring that $\lim_{b\to 0} \sigma = \sigma_{disc}$. It follows (using 4.1.16) that $r = 1$.

Hence, for the hemispheroid

$$\sigma = \frac{k^4}{\pi}\left(\frac{2}{3}\pi a^2 b\right)^2 \left(1 + \frac{\bar{e}^{\,b/2a}}{\pi b/2a}\right)^2$$

Next, the Rayleigh cross section is found for the cone spheroid.

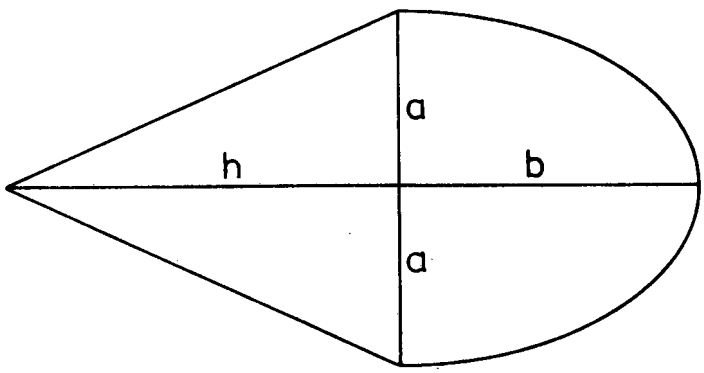

From (4.1.14)

$$\sigma = \frac{k^4}{\pi}\left(\frac{1}{3}\pi a^2 h + \frac{2}{3}\pi a^2 b\right)^2 \left(1 + e^{-y}/y\right)^2$$

--- (4.1.19)

In this case however y is not found by putting it equal to r.(b + h)/2a and then requiring that in the limit as h → 0 and b → 0 the cross section must equal that of the disc of radius a. Rather it is noted that with y = (h + 2b)/4a in (4.1.19) the cross section of the flatbacked cone is found with b = 0 and that of the hemispheroid is found with h = 0.

The cross section of the cone sphere (hemispherically capped cone) is obtained from (4.1.19) by putting b = a with y = (h + 2b)/4a.

$$\sigma_{\text{cone sphere}} = \frac{\pi}{9}(ka)^4 (h+2a)^2 \left[1 + \frac{4a}{\pi(h+2a)} e^{-(h+2a)/4a}\right]^2$$

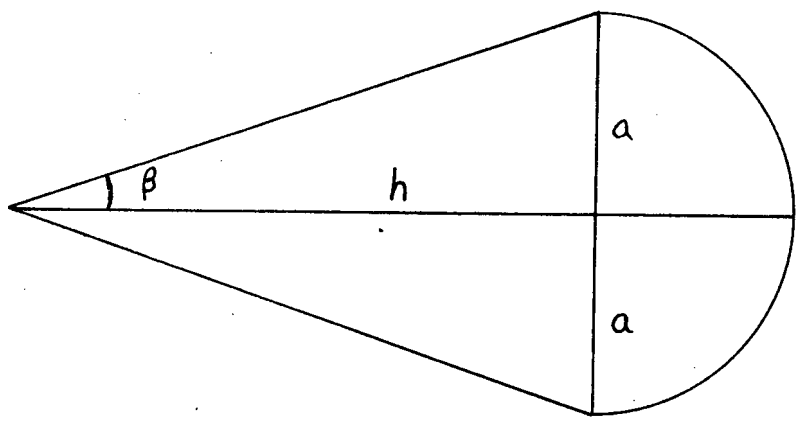

With a/h = tanβ we have

$$\frac{\sigma_{\text{cone sphere}}}{\pi a^2} = \frac{(ka)^4}{9}(2 + 1/\tan\beta)^2 \left[1 + \frac{4}{\pi(2+1/\tan\beta)} e^{-(2+1/\tan\beta)/4}\right]^2$$

--- (4.1.20)

$\sigma_{\text{cone sphere}}/\pi a^2$ was computed using program SIEG2 (p. A30) and is shown as a function of ka for $\beta = 12^\circ$, 45° and 60° in Fig. (4.1).

(4.2) Scattering by a hard flatbacked cone - the method of spherical currents.

Consider a right circular cone of base radius a and altitude h. Choose a Cartesian system of axes with 3-axis coinciding with the axis of symmetry of the cone, origin at the apex and the base intersecting with the 3-axis at $x_3 = -h$. Let η, θ', ϕ' be the spherical polar coordinates of a point on the cone. The equation of the cone in these coordinates is given by

$$\theta' = \theta_0 = \pi - \beta \qquad \text{--- (4.2.1)}$$

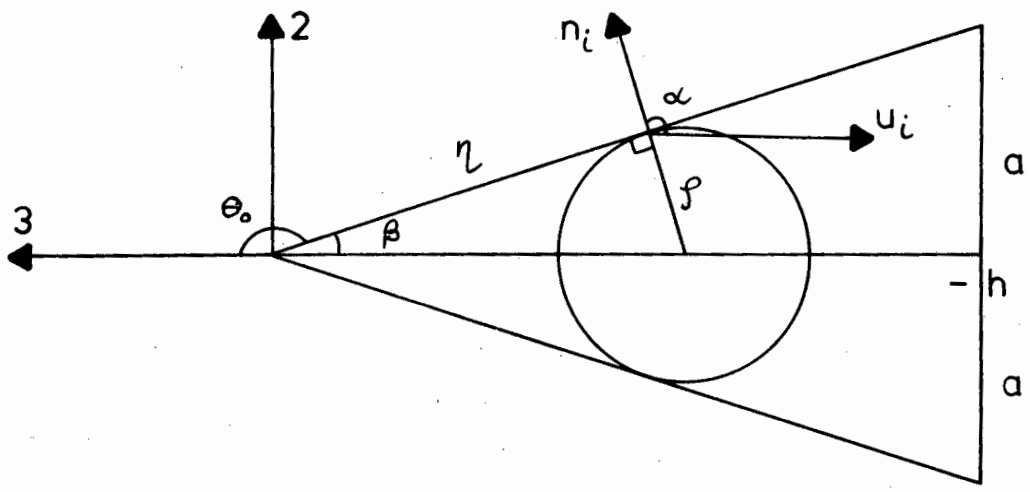

Let the cone be sound hard and illuminated by an on-axis incident plane wave e^{-ikx_3}, then the far field amplitude is given by the equation

$$S_{(sc)}(\theta, \phi) = C(\theta, \phi) + D(\theta, \phi)$$

--- (4.2.2),

where $C(\theta,\phi)$ is the contribution of the conical part and $D(\theta,\phi)$ is the contribution of the flat disc of radius a. The contribution $C(\theta,\phi)$ cannot be calculated by means of (2.6.4h) as in this case η is not a function of θ'. However, (2.6.3h) may be used with θ' replaced by η.

$$\therefore\ C(\theta,\phi) = \frac{-ik^2}{4\pi}\int_a^{\sqrt{a^2+h^2}}\int_0^{2\pi} n_i \hat{e}_c^r e^{-ik\eta_i \hat{e}_c^r} F(\eta)\left|\varepsilon_{ijk}\frac{\partial\eta_j}{\partial\eta}\frac{\partial\eta_k}{\partial\phi'}\right| d\eta\, d\phi'$$

--- (4.2.3)

In (4.2.3)

$$\left.\begin{aligned}\eta_1 &= \eta \sin\theta_0 \cos\phi' \\ \eta_2 &= \eta \sin\theta_0 \sin\phi' \\ \eta_3 &= \eta \cos\theta_0\end{aligned}\right\} \qquad \text{--- (4.2.4)}$$

and $n_i = \varepsilon_{ijk}\frac{\partial\eta_j}{\partial\eta}\frac{\partial\eta_k}{\partial\phi'} \Big/ \left|\varepsilon_{ijk}\frac{\partial\eta_j}{\partial\eta}\frac{\partial\eta_k}{\partial\phi'}\right|$ is

the unit outward normal to the conical part. $F(\eta)$ is the surface field on the conical portion and is defined by (2.4.8). In this case we have for the radius ρ of the representative sphere

$$\rho = \eta \tan(\pi-\theta_0) = \eta \tan\beta$$

--- (4.2.5)

This follows from (2.4.21) or directly from the geometry of the cone. Here the angle between the normal n_i and the direction of propagation of the incident wave

is $3\pi/2 - \theta_o$. Hence, from (2.4.8):

$$F(\eta) = \frac{i}{k^2\eta^2\tan^2\theta_o} \sum_{n=0}^{\infty} \frac{(2n+1)i^n P_n(-\sin\theta_o)}{h_n^{(1)\prime}(-k\eta\tan\theta_o)}$$

--- (4.2.6)

With the choice of coordinates (4.2.4) it follows that C is independent of ϕ and (4.2.3) becomes:

$$C(\theta) = \frac{-ik^2}{4\pi} \int_0^{\sqrt{a^2+h^2}} e^{ik\eta\cos\theta\cos\theta_o} \left[\cos\theta\sin\theta_o I_1 - \sin\theta\cos\theta_o I_2\right] F(\eta)\sin\theta_o \eta\, d\eta$$

--- (4.2.7),

where

$$I_1 = \int_0^{2\pi} e^{-ik\eta\sin\theta\sin\theta_o\cos(\phi-\phi')} d\phi' = -2\pi \sum_{n=1}^{\infty} \frac{(-1)^n}{((n-1)!)^2} \left(\frac{k\eta}{2}\sin\theta\sin\theta_o\right)^{2n-2}$$

and

$$I_2 = \int_0^{2\pi} \cos(\phi-\phi') e^{-ik\eta\sin\theta\sin\theta_o\cos(\phi-\phi')} d\phi' = 2\pi i \sum_{n=1}^{\infty} \frac{(-1)^n}{n!(n-1)!} \left(\frac{k\eta}{2}\sin\theta\sin\theta_o\right)^{2n-1}$$

as shown in Appendix B.

In the backscattered direction ($\theta = 0$) we get from (4.2.7):

$$C(0) = -\frac{ik^2}{2}\sin^2\theta_0 \int_0^{\sqrt{a^2+h^2}} e^{-ik\eta\cos\theta_0}\, F(\eta)\,\eta\, d\eta$$

--- (4.2.8),

where F(η) is defined by (4.2.6).

The contribution D(θ,φ) of the circular base of the cone can be obtained from (2.6.4h) with

$$\eta = -h/\cos\theta' \qquad \text{--- (4.2.9)}$$

and $$F(\theta') = 2\, e^{ikh} \qquad \text{--- (4.2.10)},$$

from (2.4.6). It follows that D is independent of φ and is given by:

$$D(\theta) = \frac{ik^2h}{2\pi}\cos\theta\, e^{ikh(1+\cos\theta)} \int_{\theta_0}^{\pi} \eta \frac{\sin\theta'}{\cos^2\theta'} I_1\, d\theta'$$

--- (4.2.11),

where I_1 is defined in Appendix B.

Integration w.r.t. θ' is easily carried out by introducing the variable r = -h tanθ'. We get

$$D(\theta) = -\frac{ik^2a^2}{2}\cos\theta\, e^{ikh(1+\cos\theta)} \sum_{n=1}^{\infty} \frac{(-1)^n}{n\,((n-1)!)^2}\left(\frac{ka}{2}\sin\theta\right)^{2n-2}$$

--- (4.2.12)

In the backscattered direction

$$D(0) = \frac{ik^2a^2}{2}\, e^{2ikh} \qquad \text{--- (4.2.13)}$$

Hence, from (4.2.2), (4.2.8) and (4.2.13), the following expression for the far field amplitude of a flatbacked cone is obtained:

$$S_{(sc)}(0) = -\frac{ik^2}{2}\sin^2\theta_0 \int_0^{\sqrt{a^2+h^2}} e^{-ik\eta\cos\theta_0} F(\eta)\eta\, d\eta + \frac{ik^2a^2}{2} e^{2ikh}$$

--- (4.2.14)

For computational purposes the variables β and z were introduced to the expression for $C(0)$ defined in (4.2.8), where

$$\beta = \pi - \theta_0 \quad \text{and} \quad z = k\eta.$$

$$\therefore C(0) = -\frac{i\sin^2\beta}{2} \int_0^{ka/\sin\beta} e^{iz\cos\beta} G(z) z\, dz, \quad G(z) = F(\eta)$$

With $ka = D$, (4.2.14) now becomes:

$$S_{(sc)}(0) = -\frac{i\sin^2\beta}{2} \int_0^{D/\sin\beta} e^{iz\cos\beta} G(z) z\, dz + \frac{iD^2}{2} e^{2iD/\tan\beta}$$

--- (4.2.15),

where, from (4.2.6)

$$G(z) = \frac{i}{(z\tan\beta)^2} \sum_{n=0}^{\infty} \frac{(2n+1) i^n P_n(-\sin\beta)}{h_n^{(1)\prime}(z\tan\beta)}$$

--- (4.2.16).

The integrand of the integral in (4.2.15) was computed by means of subroutine GRAND, p. A31, source module name CONEF1. This subroutine calls on POTAS (p. A10)

to produce the real and imaginary parts of G(z) after supplying POTAS with $-\sin\beta$ and $z\tan\beta$ as input. G(z) is then multiplied by $-(i/2)\sin^2\beta\, e^{iz\cos\beta}$ to give FR and FI, the real and imaginary parts resp. of the integrand, as output of GRAND, source module name CONEF1. The integral in (4.2.15) is computed by subroutine GREAT, p. A32, which calls on GRAND (p. A31) to provide FR and FI as input and has as its output TR and TI, resp. the real and imaginary parts of the integral.

The main program, MAIN2, p. A33, computes $\sigma_{(sc)}/\pi a^2$, where $\sigma_{(sc)}$ is the backscattering cross section of a hard flatbacked cone for axial incidence according to the method of spherical currents.

From (2.2.23) we have

hence $$\sigma_{(sc)}/\pi a^2 = \frac{4}{D^2}\,|S(0)|^2 \qquad \text{--- (4.2.17),}$$

with $D = ka$ and $S(0)$ defined by (4.2.14). MAIN2 calls on GREAT (p. A32) to provide the real and imaginary parts TR and TI of $C(0)$, adds to this resp. UR and UI, the real and imaginary parts of $D(0) = \frac{iD^2}{2}\, e^{2iD/\tan\beta}$ and computes $\sigma_{(sc)}/\pi a^2$ according to (4.2.17).

In Fig. (4.1) $\sigma_{(sc)}/\pi a^2$ is shown as a function of $D = ka$ for $\beta = 12^\circ, 45^\circ, 60^\circ$. For $0 \le ka \le 1$ the graph is a straight line, as it should be in the Rayleigh region, and the slope is approximately 3, i.e. 1 less than 4 predicted by the fourth power law of the Rayleigh cross section. Apart from this difference in slope the cross section predicted by the method of spherical currents is considerably larger than the Raleigh cross section. With increasing β there is a shift to the right of the graphs, that is for fixed ka, $\sigma/\pi a^2$ decreases with

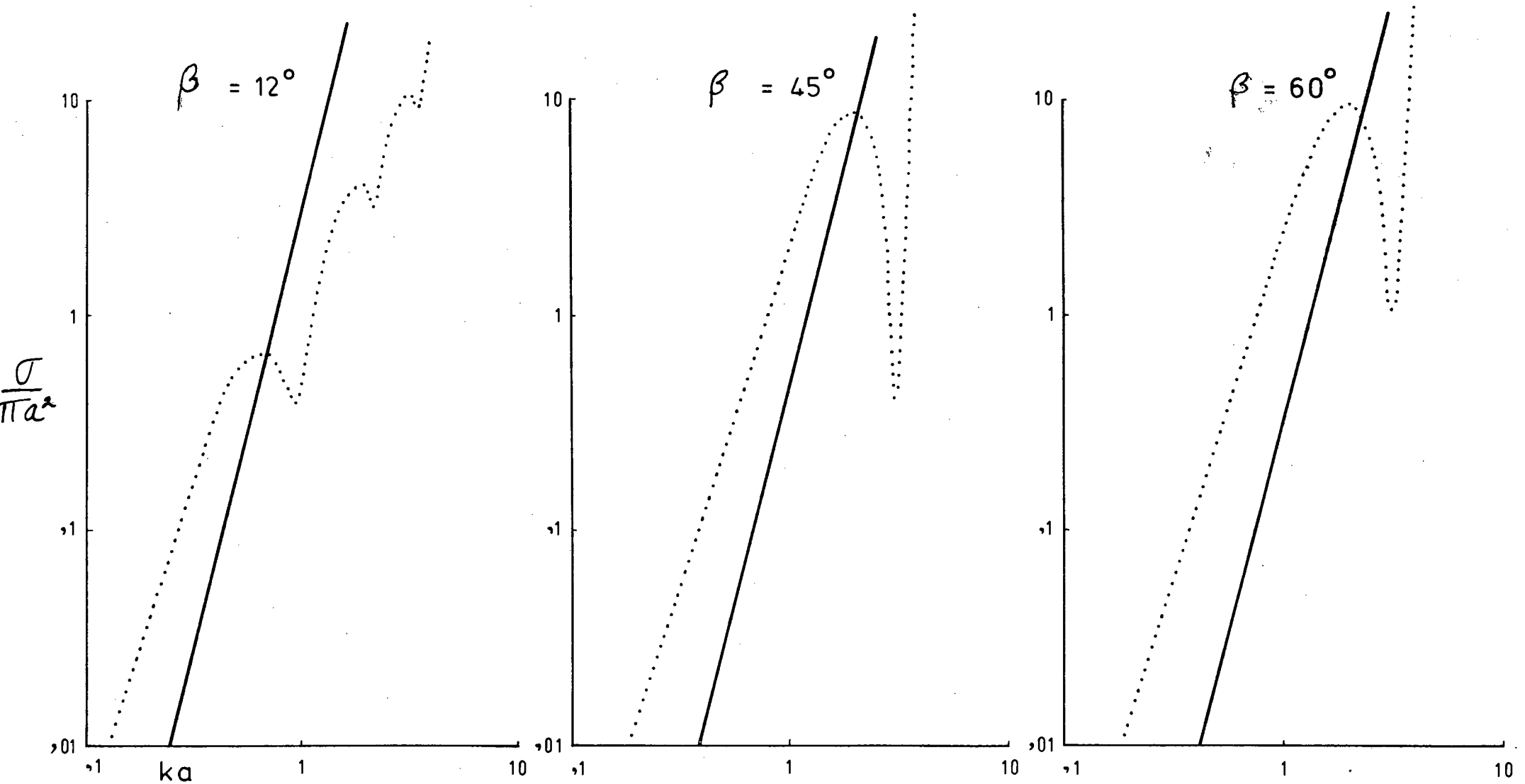

ig. (4.1) Nose-on backscattering from hard flatbacked cones
Siegel (——)
Method of spherical currents (···)

increasing β. Hence the two methods discriminate between the different cones in qualitatively the same way. There is therefore a reasonable correspondence between Rayleigh theory and the method of spherical currents in the range $0 \leq ka < 1$.

For $ka > 1$ the method of spherical currents gives results which deviate from Rayleigh theory in a correct way. The curves of $\sigma_{(sc)}/\pi a^2$ begin to oscillate, indicating the low frequency end of a resonance region.

(4.3) Scattering by a hard cone sphere - the method of spherical currents.

Consider a cone sphere of semi-vertex angle β and base radius a. A system of axes is chosen with origin at the centre of the spherical base and 3-axis coinciding with the axis of symmetry such that the vertex points in the positive direction.

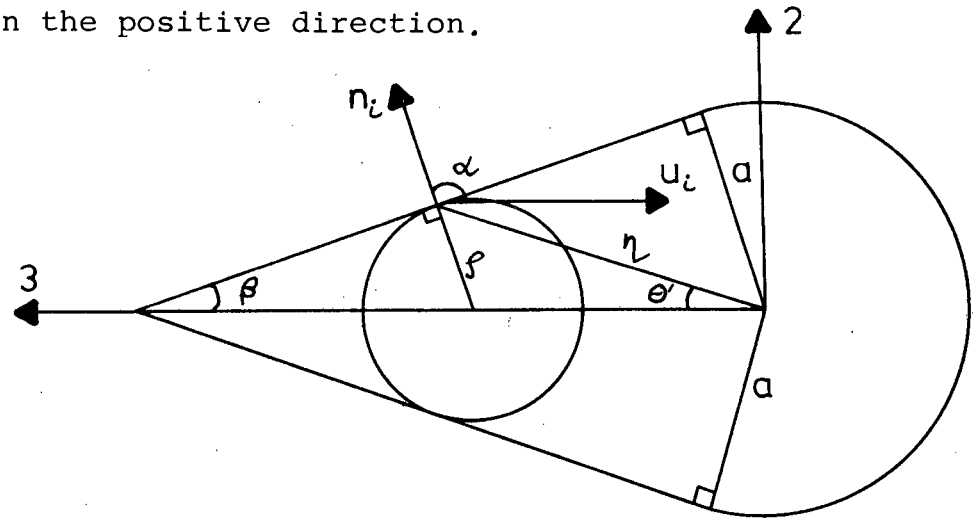

We now calculate the far field for a hard cone sphere in the backscattered direction for nose-on incidence of a plane wave. Let $S_{(sc)}(\theta)$ be the far field amplitude, then

$$S_{(sc)}(\theta) = C(\theta) + B(\theta) \qquad \text{--- (4.3.1),}$$

where $C(\theta)$ is the contribution of the conical part $(0 \leq \theta' \leq \pi/2 - \beta)$ and $B(\theta)$ is the contribution of the spherical part $(\pi/2 - \beta \leq \theta' \leq \pi)$.

The parametric equations of the conical part are

$$\eta_1 = \eta(\theta') \sin\theta' \cos\phi'$$
$$\eta_2 = \eta(\theta') \sin\theta' \sin\phi'$$
$$\eta_3 = \eta(\theta') \cos\theta'$$

with $\eta = a \operatorname{Cosec}(\theta' + \beta)$ --- (4.3.2)

On using these equations in (2.6.4h) we get:

$$C(\theta) = \frac{-ik^2}{4\pi a} \int_0^{\pi/2-\beta} \{ I_1 \cos\theta \sin\beta + I_2 \sin\theta \cos\beta \} e^{-ik\eta \cos\theta \cos\theta'} F(\theta') \eta^3 \sin\theta' d\theta'$$

--- (4.3.3),

with I_1 and I_2 defined by (2.6.5) and (2.6.6). The total surface field $F(\theta')$ is defined by (2.4.8) in which ρ and $\cos\alpha$ have to be expressed as functions of θ'.

From (2.4.18) and (4.3.2), or by direct inspection, we have:

$$\cos\alpha = -\sin\beta$$ --- (4.3.4)

The radius of the representative sphere may be obtained from (2.4.21), or can be obtained directly from the figure above. We find

$$\rho = \eta \sin\theta' / \cos\beta$$ --- (4.3.5),

where η is given by (4.3.2).

Hence (2.4.8) becomes:

$$F(\theta') = \frac{i}{k^2\rho^2} \sum_{n=0}^{\infty} \frac{(2n+1)\, i^n\, P_n(-\sin\beta)}{h_n^{(1)\prime}(k\rho)}$$

--- (4.3.6),

where ρ is defined by (4.3.5).

In the backscattered direction ($\theta = 0$) we have from (4.3.3):

$$C(0) = -\frac{ik^2 \sin\beta}{2a} \int_0^{\pi/2-\beta} e^{-ik\eta\cos\theta'} F(\theta')\, \eta^3 \sin\theta'\, d\theta'$$

--- (4.3.7)

The contribution $B(\theta)$ of the spherical part of the cone sphere is given by (2.6.4h) with $\eta = a$. Hence

$$B(\theta) = -\frac{ik^2a^2}{4\pi} \int_{\pi/2-\beta}^{\pi} \{I_1 \cos\theta\cos\theta' + I_2 \sin\theta \sin\theta'\} F(\theta') e^{-ika\cos\theta\cos\theta'} \sin\theta'\, d\theta'$$

--- (4.3.8).

In (4.3.8)

$$F(\theta') = \frac{i}{k^2a^2} \sum_{n=0}^{\infty} \frac{(2n+1)\, i^n\, P_n(-\cos\theta')}{h_n^{(1)\prime}(ka)}$$

--- (4.3.9)

This result follows from (2.4.8) with $\rho = a$ and $\cos\alpha = -\cos\theta'$.

In the backscattered direction we have from (4.3.8)

$$B(0) = -\frac{ik^2a^2}{2}\int_{\pi/2-\beta}^{\pi} e^{-ika\cos\theta'} F(\theta')\cos\theta'\sin\theta' d\theta'$$

--- (4.3.10)

From (4.3.1), (4.3.7) and (4.3.10) we get the following expression for the far field amplitude in the back-scattered direction with $\cos\theta' = z$:

$$S_{(sc)}(0) = C(0) + B(0) = -\frac{i\sin\beta}{2ka}\int_{\sin\beta}^{1} e^{-ik\eta z} G(z)(k\eta)^3 dz$$

$$- \frac{ik^2a^2}{2}\int_{-1}^{\sin\beta} e^{-ikaz} G(z) z\, dz$$

--- (4.3.11)

In (4.3.11) $G(z) = F(\theta')$ where $F(\theta')$ is defined by (4.3.6) for $0 \le \theta' \le \pi/2 - \beta$ and by (4.3.9) for $\pi/2 - \beta < \theta' \le \pi$.

With the input integer JJ = 1 subroutine GRAND, p. A35, source module name CONES, computes the real and imaginary parts of the integrand of the first integral in (4.3.11). GRAND calls on STRAL, p. A34, to provide $k\rho$ and $k\eta$ as functions of the variable z and the parameters D = ka and β. With $\cos\alpha = -\sin\beta$ the necessary input for POTAS, p. A10, is provided, and GRAND calls on POTAS for the real and imaginary parts of G(z). G(z) is then multiplied by $-\frac{i\sin\beta}{2ka} e^{-ik\eta z}(k\eta)^3$ to give FR and FI, the real and imaginary parts of the integrand. The first integral in (4.3.11) is then computed by subroutine GREAT, p. A32. GREAT, with

input integer JJ = 1, calls on GRAND to provide the real and imaginary parts of the integrand as input.

The integrand of the second integral in (4.3.11) is also computed by means of subroutine GRAND, p. A35, source module name CONES, by putting input integer JJ = 2. With $k\rho = ka$ and $\cos\alpha = -z$ GRAND calls on POTAS (p. A10) to provide the real and imaginary parts of G(z). Multiplication of G(z) by $-ik^2a^2ze^{ikaz}/2$ gives the real and imaginary parts of the integrand as output of GRAND with JJ = 2. The second integral in (4.3.11) is also computed by subroutine GREAT by setting JJ = 2.

By consecutively putting JJ = 1 and 2 the main program, MAIN3 (p. A36), calls on GREAT to give the real and imaginary parts of the contribution to the far field in the backscattered direction of respectively the conical and spherical parts of the cone sphere. These are then added together and (4.2.16) is used to compute $\sigma_{(sc)}/\pi a^2$.

In Fig. (4.2) $\sigma_{(sc)}/\pi a^2$ for the hard cone sphere is shown as a function of D = ka for $\beta = 12^\circ$, 45° and 60°. For $0 \leq ka < 1$ the graph is a straight line very closely adhering to the fourth power law. Moreover the values of the cross sections calculated by means of the two methods are much closer than in the case of the hard flatbacked cone, the greatest difference being the case $\beta = 12^\circ$. As ka approaches unity $\sigma_{(sc)}/\pi a^2$ deviates from the Rayleigh law in the desired direction and begins to oscillate for ka > 1, indicating the low frequency end of a resonance region.

As in the case of flatbacked cones, the Rayleigh law discriminates between cones of different β in that the cross section for fixed ka decreases with increasing β. This is also evident from the graphs of $\sigma_{(sc)}/\pi a^2$

against ka in the Rayleigh region, but to a less marked degree than in the case of flatbacked cones.

Using Rayleigh theory and in particular Siegel's results as a criterion it is clear that the method of spherical currents gives a better prediction of the behaviour of cone spheres than of flatbacked cones. From the viewpoint of the method of spherical currents the main difference between the flatbacked cone and the cone sphere for nose-on incidence is the surface fields used on the surface in the shadow region. As the edge of the flatbacked cone has a negligible effect at long wavelengths, this could imply that the method used to assign the surface field at points at which both principal radii of curvature tend to infinity is unsatisfactory irrespective of the position of the point on the surface. On the other hand it may point to the surface on the shadow side as being the critical one as far as assigning boundary values according to the method of spherical currents is concerned.

Finally it should be pointed out that the Rayleigh cross sections are the same for both nose-on and base-on incidence. This result has been experimentally verified for radar cross sections in the low-frequency range.

For the hard cone sphere for $\beta = 12^{\circ}$, 45° and 60°, $0 \leq ka < 1$, the graph of $\sigma_{(sc)}/\pi a^2$ for base-on incidence is virtually coincident with the graph of $\sigma_{(sc)}/\pi a^2$ for nose-on incidence. Only for $ka > 1$ does the difference between the two graphs become apparent.

In the case of hard flatbacked cones however the graphs of $\sigma_{(sc)}/\pi a^2$ for nose-on and base-on incidence do differ in the range $0 < ka < 1$. In the range $0 < ka < 1$ $\sigma_{(sc)}/\pi a^2$ for base-on incidence is actually numerically closer to the Rayleigh cross section $\sigma/\pi a^2$, and the best agreement between the three graphs of $\sigma/\pi a^2$, $\sigma_{(sc)}/\pi a^2$

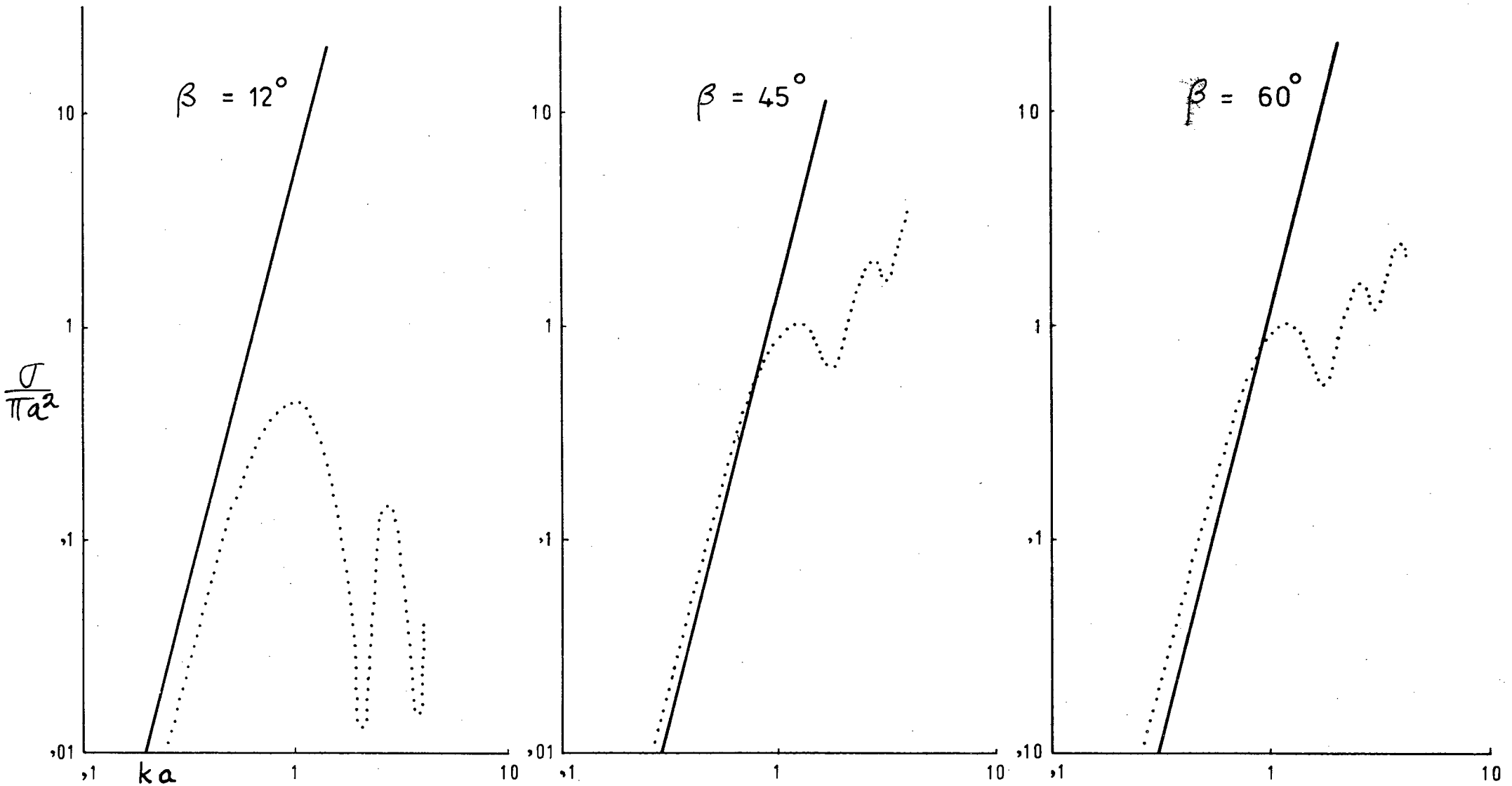

Fig. (4.2) Nose-on backscattering from hard cone spheres
Siegel (——)
Method of spherical currents (···)

for nose-on incidence and $\sigma_{(sc)}/\pi a^2$ for base-on incidence in the range $0 < ka < 1$ is found for $\beta = 12^{o}$. Now the ratio of the areas of the flat part of the flatbacked cone to the conical part is equal to $\sin\beta$, hence in the case of $\beta = 12^{o}$ the approximation of the surface field as twice the incident field is used over the smallest part of the total surface.

The good numerical results obtained for the hard cone sphere for both nose-on and base-on incidence indicate that the position of the point at which the approximation is made (i.e. whether the point is in the illuminated region or shadow region) is of negligible importance in the Rayleigh region. The poorer results for the flatbacked cone indicate that the method of approximation at points where both principal radii of curvature tend to infinity is unsatisfactory, at least in the Rayleigh region.

CHAPTER V

THE SCATTERING OF ELECTROMAGNETIC WAVES BY AN IDEALLY CONDUCTIVE CONVEX BODY ACCORDING TO THE METHOD OF SPHERICAL CURRENTS.

(5.1) The integral representation of the field at points exterior to an ideal conductor.

The fundamental equations of electromagnetic theory are Maxwell's equations. In differential form for stationary media they are:

$$\varepsilon_{ijk}\,\partial_j H_k = \frac{\partial D_i}{\partial t} + j_i \qquad \text{--- (5.1.1)}$$

$$\varepsilon_{ijk}\,\partial_j E_k = -\frac{\partial B_i}{\partial t} \qquad \text{--- (5.1.2)}$$

where the symbols have their usual meaning.

On using the equation of continuity

$$\partial_i j_i + \frac{\partial \rho}{\partial t} = 0 \qquad \text{--- (5.1.3)}$$

we get from (5.1.1) and (5.1.2)

$$\partial_i D_i = \rho \qquad \text{--- (5.1.4)}$$

$$\partial_i B_i = 0 \qquad \text{--- (5.1.5)}$$

With a given current density j_i the two vector differential equations do not form a soluble system - they must be amplified by the material equations which for homogeneous isotropic media have the form

$$D_i = \epsilon E_i \qquad \text{--- (5.1.6)}$$

$$B_i = \mu H_i \qquad \text{--- (5.1.7)}$$

Here ϵ is the dielectric constant and μ the permeability of the medium. In the case of a conducting medium we have in addition to (5.1.6) and (5.1.7) $j_i = \sigma E_i$, where σ is the conductivity.

If a time dependence of exp(-iωt) is assumed and then eliminated, (5.1.1) and (5.1.2) become:

$$\varepsilon_{ijk}\,\partial_j H_k = -i\omega D_i + j_i \qquad \text{--- (5.1.8)}$$

$$\varepsilon_{ijk}\,\partial_j E_k = i\omega B_i \qquad \text{--- (5.1.9)}$$

The field vectors in (5.1.8) and (5.1.9) are now independent of the time.

Let S be a closed surface interior to which the current and charge densities are zero, then the field at points x_i interior to S may be represented i.t.o. their values on S by the following equations:

$$E_i(x_i) = -\frac{1}{4\pi}\oint_S \left[\varepsilon_{kjq} E_q \varepsilon_{ikp}\partial_p G + E_j \partial_i G + i\omega G \varepsilon_{ijk} B_k\right] df_j$$

--- (5.1.10)

$$H_i(x_i) = -\frac{1}{4\pi}\oint_S \left[\varepsilon_{kjq} H_q \varepsilon_{ikp}\partial_p G + H_j \partial_i G - i\omega G \varepsilon_{ijk} D_k\right] df_j$$

--- (5.1.11)

In (5.1.10) and (5.1.11) df_j is the vectorial surface element, $\therefore$ $df_i = n_i df$ where n_i is the unit normal pointing away from the interior of S.

$$G = \frac{e^{ik|x_i-\eta_i|}}{|x_i-\eta_i|} \quad \text{and} \quad \partial_i = \frac{\partial}{\partial \eta_i} \quad \text{, where}$$

η_i is a point on S.

Equations (5.1.10) and (5.1.11) may be derived by using (5.1.8) and (5.1.9) with $j_i = 0$ and a vector analogue of Green's Theorem, or see Jones (1964), pp. 43 - 55.

We now apply (5.1.10) and (5.1.11) to the region exterior to S but interior to the closed surface Σ.

Let

$$A_{ij} = \varepsilon_{kjq} E_q \varepsilon_{ikp} \partial_p G + E_j \partial_i G + i\omega G \varepsilon_{ijk} B_k$$

$$B_{ij} = \varepsilon_{kjq} H_q \varepsilon_{ikp} \partial_p G + H_j \partial_i G - i\omega G \varepsilon_{ijk} D_k$$

--- (5.1.12),

then

$$E_i(x_i) = \frac{1}{4\pi} \oint_S A_{ij} \, df_j - \frac{1}{4\pi} \oint_\Sigma A_{ij} \, df_j \qquad \text{--- (5.1.13)}$$

$$H_i(x_i) = \frac{1}{4\pi} \oint_S B_{ij} \, df_j - \frac{1}{4\pi} \oint_\Sigma B_{ij} \, df_j \qquad \text{--- (5.1.14)}$$

The normal to S points away from the interior of S, and the normal to Σ away from the interior of Σ.

If S is the surface of a scattering object and the field in (5.1.13) and (5.1.14) is the scattered field, then the radiation conditions (Jones (1964), p. 57) apply:

$$|R E_i| < K, \quad |R B_i| < K \qquad \text{--- (5.1.15)}$$

$$\left.\begin{aligned} R(\omega \varepsilon_{ijk} e_j^R B_k + k E_i) &\to 0 \\ R(k \varepsilon_{ijk} e_j^R E_k - \omega B_i) &\to 0 \end{aligned}\right\} \qquad \text{--- (5.1.16)}$$

uniformly w.r.t. direction as $R \to \infty$.

Here Σ is chosen to be a sphere of radius R, R_i is the position vector of a point on Σ w.r.t. its centre and $e_i^R = R_i/R$.

Let $R \to \infty$ in (5.1.13) and (5.1.14), then the integrals over Σ tend to zero, and these equations become for the scattered fields $E_i^{(s)}$ and $H_i^{(s)}$:

$$E_i^{(s)}(x_i) = \frac{1}{4\pi}\oint_S A_{ij}^{(s)}\, d\mathcal{f}_j \qquad \text{--- (5.1.17)}$$

$$H_i^{(s)}(x_i) = \frac{1}{4\pi}\oint_S B_{ij}^{(s)}\, d\mathcal{f}_j \qquad \text{--- (5.1.18)}$$

We now apply (5.1.13) and 5.1.14) to the field incident on the surface S of the scatterer. This field is chosen to be a plane electromagnetic disturbance propagated in the direction u_i with electric vector defined by

$$E_i = t_i e^{ik u_i x_i}$$
$$u_i t_i = 0 \qquad \text{--- (5.1.19)}$$

The magnetic vector is then defined by

$$H_i = \sqrt{\frac{\epsilon}{\mu}}\, \varepsilon_{ijk} u_j E_k \qquad \text{--- (5.1.20)}$$

The vectors E_i, H_i and u_i form an orthogonal triad.

The plane wave does not satisfy the radiation conditions (5.1.15) and (5.1.16), and consequently the integrals over Σ in (5.1.13) and (5.1.14) do not vanish as $R\to\infty$.

However $\oint_S A_{ij}^{(i)}\, d\mathcal{f}_j = \oint_S B_{ij}^{(i)}\, d\mathcal{f}_j = 0$ for the plane incident wave as this wave satisfies Maxwells equations in the region interior to S, and G has no singularity in this region - x_i in (5.1.13) and (5.1.14) is exterior to S. Hence the volume integrals vanish to which these surfaces integrals relate via the vector analogue of Green's Theorem. For the plane field (5.1.13) and (5.1.14) become:

$$E_i^{(i)}(x_i) = -\frac{1}{4\pi}\oint_\Sigma A_{ij}^{(i)}\, d\mathcal{f}_j \qquad \text{--- (5.1.21)}$$

$$H_i^{(i)}(x_i) = -\frac{1}{4\pi}\oint_\Sigma B_{ij}^{(i)}\, d\mathcal{f}_j \qquad \text{--- (5.1.22)}$$

Equations (5.1.21) and (5.1.22) may also be verified directly by integrating over the sphere Σ.

The total field exterior to the obstacle is defined by

$$\left.\begin{aligned} E_i^{(t)} &= E_i^{(i)} + E_i^{(s)} \\ H_i^{(t)} &= H_i^{(i)} + H_i^{(s)} \end{aligned}\right\} \qquad \text{--- (5.1.23)}$$

For the total field equations (5.1.13) and (5.1.14) become:

$$\left.\begin{aligned} E_i^{(t)}(x_i) &= E_i^{(i)}(x_i) + \frac{1}{4\pi}\oint_S A_{ij}^{(t)}\, df_j \\ H_i^{(t)}(x_i) &= H_i^{(i)}(x_i) + \frac{1}{4\pi}\oint_S B_{ij}^{(t)}\, df_j \end{aligned}\right\} \qquad \text{--- (5.1.24),}$$

where we have used (5.1.17), (5.1.18) and the fact that the radiation conditions apply to the scattered field.

The scattered field outside S can now be defined in terms of the boundary values of the total field. From (5.1.23), (5.1.24) and (5.1.12) we have with $df_j = n_j df$:

$$E_i^{(s)}(x_i) = \frac{1}{4\pi}\oint_S \left[\varepsilon_{kjq} n_j E_q^{(t)} \varepsilon_{ikp}\partial_p G + n_j E_j^{(t)} \partial_i G + i\omega G \varepsilon_{ijk} n_j B_k^{(t)}\right] df$$

--- (5.1.25)

$$H_i^{(s)}(x_i) = \frac{1}{4\pi}\oint_S \left[\varepsilon_{kjq} n_j H_q^{(t)} \varepsilon_{ikp}\partial_p G + n_j H_j^{(t)} \partial_i G - i\omega G \varepsilon_{ijk} n_j D_k^{(t)}\right] df$$

--- (5.1.26)

Let S now be the surface of a perfect conductor, i.e. a body for which the total electric field tangential to the surface vanishes.

$$\therefore \quad \varepsilon_{ijk} n_j E_k^{(t)}(\eta_i) = 0 \qquad \text{--- (5.1.27)}$$

For a perfect conductor it can be shown (Stratton (1941) pp. 483 - 484) that:

$$n_i B_i(\eta_i) = 0 \qquad \text{--- (5.1.28)}$$

The surface current S_i is defined as follows:

$$S_i = \varepsilon_{ijk} n_j H_k^{(t)} \qquad \text{--- (5.1.29)}$$

Using (5.1.27), (5.1.28), (5.1.29) and the material equations (5.1.6) and (5.1.7) in (5.1.25) and (5.1.26), the following expressions for the scattered field of an ideal conductor are found:

$$E_i^{(s)}(x_i) = \frac{1}{4\pi} \oint_S [n_j E_j^{(t)} \partial_i G + i\omega\mu G S_i] \, df \qquad \text{--- (5.1.30)}$$

$$H_i^{(s)}(x_i) = \frac{1}{4\pi} \oint_S \varepsilon_{ijk} S_j \partial_k G \, df \qquad \text{--- (5.1.31)}$$

By multiplying (5.1.31) vectorially by n_i and then taking the limit $x_i \to \xi_i$ where ξ_i is a point on S, a vector Fredholm equation is obtained which may in principle be solved for the surface current S_i. This solution may then be substituted into (5.1.30) which, after scalar multiplication by n_i and taking the limit $x_i \to \xi_i$, will yield an integral equation in $n_i E_i = \sigma/\varepsilon$, where σ is the surface charge density. Substitution of the surface fields into (5.1.30) and (5.1.31) will

yield the field vectors E_i and H_i at exterior points. To find E_i and H_i at exterior points it is however sufficient to know S_i alone. If S_i is known, H_i is given by (5.1.31). The electric field may then be found from (5.1.8) with $j_i = 0$.

(5.2) The surface current according to the method of spherical currents.

We now calculate the surface current $S_i = \varepsilon_{ijk} n_j H_k^{(t)}$ at the point P on the surface S of the convex ideal conductor according to the method of spherical currents. As in the scalar case, section (2.4), a representative sphere of radius ρ is constructed passing through P. The centre of the sphere is situated on the normal to the surface at P and ρ is the least of the principal radii of curvature. A Cartesian coordinate system $\bar{S}$ is chosen with origin at the centre of the representative sphere such that the incident plane wave has the following orientation w.r.t. $\bar{S}$:

$$\left.\begin{aligned} (\bar{E}_i^{(i)}) &= (e^{ik\bar{x}_3}, 0, 0) \\ (\bar{H}_i^{(i)}) &= (0, \sqrt{\tfrac{\epsilon}{\mu}}\, e^{ik\bar{x}_3}, 0) \end{aligned}\right\} \quad \text{--- (5.2.1)}$$

W.r.t. $\bar{S}$ the direction of propagation is defined by the unit vector $\bar{u}_i$,

$$(\bar{u}_i) = (0, 0, 1) \quad \text{--- (5.2.2)}$$

The direction of propagation is therefore along the positive $\bar{3}$-axis.

Let $\bar{\eta}_i$ be the Cartesian coordinates of an arbitrary point on the representative sphere, and in particular those of P, w.r.t. $\bar{S}$. Spherical polar coordinates ρ, $\bar{\theta}$, $\bar{\phi}$ are now introduced by the following equations:

$$\left.\begin{aligned}\bar{\eta}_1 &= \rho \sin\bar{\theta}\cos\bar{\phi}\\ \bar{\eta}_2 &= \rho \sin\bar{\theta}\sin\bar{\phi}\\ \bar{\eta}_3 &= \rho\cos\bar{\theta}\end{aligned}\right\} \qquad \text{--- (5.2.3)}$$

Let $\bar{S}_i$ be the surface current on a perfectly conducting sphere such as described above. Then

$$\bar{S}_i = \bar{e}^{\bar{\theta}}_i S_{\bar{\theta}} + \bar{e}^{\bar{\phi}}_i S_{\bar{\phi}} \qquad \text{--- (5.2.4)}$$

$$\left.\begin{aligned}(\bar{e}^{\bar{\theta}}_i) &= (\cos\bar{\theta}\cos\bar{\phi}, \cos\bar{\theta}\sin\bar{\phi}, -\sin\bar{\theta})\\ (\bar{e}^{\bar{\phi}}_i) &= (-\sin\bar{\phi}, \cos\bar{\phi}, 0)\end{aligned}\right\} \qquad \text{--- (5.2.5)}$$

$S_{\bar{\theta}}$ is the component of the surface current in the direction of the parametric line $\bar{\phi}$ = const, and $S_{\bar{\phi}}$ is the component of the surface current in the direction of the parametric line $\bar{\theta}$ = const.

According to Hönl, Maue and Westpfahl (1961), p. 559, eq. 154.1, these components of the surface current on an ideally conducting sphere of radius ρ illuminated by a plane incident wave travelling along the positive $\bar{3}$-axis are defined by the equations:

$$S_{\bar{\theta}} = \sqrt{\frac{\epsilon}{\mu}}\,\frac{\cos\bar{\phi}}{k\rho}\sum_{n=1}^{\infty}\frac{(2n+1)}{n(n+1)}\,i^n\left\{\frac{i\tau_n(\cos\bar{\theta})}{[k\rho\, h_n^{(1)}(k\rho)]'} - \frac{\pi_n(\cos\bar{\theta})}{k\rho\, h_n^{(1)}(k\rho)}\right\}$$

$$S_{\bar{\phi}} = -\sqrt{\frac{\epsilon}{\mu}}\,\frac{\sin\bar{\phi}}{k\rho}\sum_{n=1}^{\infty}\frac{(2n+1)}{n(n+1)}\,i^n\left\{\frac{i\pi_n(\cos\bar{\theta})}{[k\rho\, h_n^{(1)}(k\rho)]'} - \frac{\tau_n(\cos\bar{\theta})}{k\rho\, h_n^{(1)}(k\rho)}\right\}$$

--- (5.2.6)

In (5.2.6) the prime indicates differentiation w.r.t. $k\rho$ and

$$\left.\begin{aligned} \tau_n(\cos\bar\theta) &= -\frac{d}{d\bar\theta}P_n^1(\cos\bar\theta) = -\frac{d^2P_n(\cos\bar\theta)}{d\bar\theta^2} \\ \pi_n(\cos\bar\theta) &= -\frac{1}{\sin\bar\theta}P_n^1(\cos\bar\theta) = -\frac{1}{\sin\bar\theta}\frac{d}{d\bar\theta}P_n(\cos\bar\theta) \end{aligned}\right\} \quad (5.2.7)$$

Let S be a Cartesian system of arbitrary orientation with origin in the region interior to the obstacle, and let points on the surface of the obstacle, in particular P, have coordinates η_i w.r.t. S. Spherical polar coordinates are introduced in S by means of the equations

$$\begin{aligned} \eta_1 &= \eta\sin\theta\cos\phi \\ \eta_2 &= \eta\sin\theta\sin\phi \\ \eta_3 &= \eta\cos\theta \end{aligned} \quad \text{--- (5.2.8)}$$

On the surface of the scatterer $\eta = \eta(\theta,\phi)$. A point Q with coordinates x_i w.r.t. S has coordinates $\bar x_i$ w.r.t. $\bar S$ and these sets of coordinates are related by means of the orthogonal transformation

$$x_i = a_{ij}\bar x_j + b_i \quad \text{--- (5.2.9)}$$

In (5.2.9) a_{ij} is the cosine of the angle less than π between the positive i-axis of S and the positive j-axis of $\bar S$. The nine matrix elements are not independent - they satisfy the orthogonality relations

$$a_{ij}a_{jk} = \delta_{jk} \quad \text{--- (5.2.10)}$$

In (5.2.9) b_i is the position vector of the origin of the representative sphere w.r.t. S.

The surface current at P on the scatterer is now defined by (5.2.6) and (5.2.4) as a vector function of ρ, $\bar\theta$ and $\bar\phi$. We wish to find the coordinates S_i of the surface current, expressed as functions of θ and ϕ.

From (5.2.9) it follows that S_i and $\bar{S}_i$ are connected by the transformations

$$S_i = a_{ij}\,\bar{S}_j(\rho, \bar{\theta}, \bar{\phi}) \qquad \text{--- (5.2.11)}$$

Hence, from (5.2.4)

$$S_i = a_{ij}\left(\bar{e}^{\bar{\theta}}_j S_{\bar{\theta}}(\rho, \bar{\theta}, \bar{\phi}) + \bar{e}^{\bar{\phi}}_j S_{\bar{\phi}}(\rho, \bar{\theta}, \bar{\phi})\right)$$

--- (5.2.12),

where the unit vectors $e^{\bar{\theta}}_i$ and $e^{\bar{\phi}}_i$ are defined by (5.2.5). In (5.2.12) ρ, $\bar{\theta}$ and $\bar{\phi}$ must now be expressed as functions of θ and ϕ. The least principal radius of curvature is found as a function of θ and ϕ as described in section (2.4), and is defined by (2.4.21). The angles $\bar{\theta}$ and $\bar{\phi}$ may be found as functions of θ and ϕ from (5.2.3), (5.2.8) and (5.2.9), but it is simpler to proceed as follows. From (5.2.12), (5.2.5) and (5.2.6) it follows that S_i depends on $\bar{\theta}$ and $\bar{\phi}$ through the functions $\cos\bar{\theta}$, $\sin\bar{\theta}$, $\cos\bar{\phi}$ and $\sin\bar{\phi}$.

W.r.t. $\bar{S}$ the outward unit normal has coordinates $\bar{n}_i$ defined by:

$$\left.\begin{aligned} \bar{n}_1 &= \sin\bar{\theta}\cos\bar{\phi} \\ \bar{n}_2 &= \sin\bar{\theta}\sin\bar{\phi} \\ \bar{n}_3 &= \cos\bar{\theta} \end{aligned}\right\} \qquad \text{--- (5.2.13)}$$

W.r.t. S the unit normal has coordinates n_i defined by (2.4.14), i.e.

$$n_i = N_i/N \qquad \text{--- (5.2.14)},$$

where $$N_i = \varepsilon_{ijk}\frac{\partial y_j}{\partial\theta}\frac{\partial y_k}{\partial\phi} \qquad \text{--- (2.4.13)}$$

and $$N = |N_i|.$$

From (5.2.9) it follows that the coordinates of the unit normal in the two systems are related by the transformation equations $n_i = a_{ij}\bar{n}_j$, or, making use of the orthogonality relations (5.2.10),

$$\bar{n}_i = a_{ji}\, n_j \qquad \text{--- (5.2.15)}$$

From (5.2.13), (5.2.14) and (5.2.15) we find:

$$\cos\bar{\theta} = \bar{n}_3 = a_{i3} N_i / N$$

$$\sin\bar{\theta} = (1-\cos^2\bar{\theta})^{1/2} = (N^2 - (a_{i3}N_i)^2)^{1/2}/N$$

$$\cos\bar{\phi} = \frac{\bar{n}_1}{\sin\bar{\theta}} = \frac{a_{i1}N_i}{\sin\bar{\theta}\,N} = \frac{a_{i1}N_i}{(N^2-(a_{3i}N_i)^2)^{1/2}}$$

$$\sin\bar{\phi} = \frac{\bar{n}_2}{\sin\bar{\theta}} = \frac{a_{i2}N_i}{\sin\bar{\theta}\,N} = \frac{a_{i2}N_i}{(N^2-(a_{3i}N_i)^2)^{1/2}}$$

--- (5.2.16)

In $S_{\bar{\theta}}$ and $S_{\bar{\phi}}$ (5.2.6), we substitute for $\cos\bar{\theta}$, $\cos\bar{\phi}$ and $\sin\bar{\phi}$ according to (5.2.16), and from (5.2.5) and (5.2.16) we get:

$$(\bar{e}_j) = \frac{1}{N(N^2-(a_{i3}N_i)^2)^{1/2}}\left(a_{i3}N_i a_{j1}N_j,\ a_{i3}N_i a_{j2}N_j,\ -N^2+(a_{i3}N_i)^2\right)$$

$$(\bar{\phi}_i) = \frac{1}{(N^2-(a_{i3}N_i)^2)^{1/2}}\left(-a_{i2}N_i,\ a_{i1}N_i,\ 0\right)$$

--- (5.2.17)

It now remains to relate the coefficients a_{ij} to the directions of propagation and polarization of the incident wave.

Let the direction of propagation w.r.t. S be defined by the unit vector

$$u_i = \cos\gamma_i \qquad \text{--- (5.2.18).}$$

If the 3-axis is rotated through γ_3 about an axis perpendicular to the plane spanned by the vectors $(e_i^3) = (0,0,1)$ and $(u_i) = (\cos\gamma_1, \cos\gamma_2, \cos\gamma_3)$, then the 3-axis has the same direction and orientation as the $\bar{3}$-axis. The unit vector in the direction of the axis of rotation is

$$e_i = \varepsilon_{ijk} e_j^3 u_k / |\varepsilon_{ijk} e_j^3 u_k| \qquad \text{--- (5.2.19)}$$

Now $(\varepsilon_{ijk} e_j^3 u_k) = (-\cos\gamma_2, \cos\gamma_1, 0)$,

$\therefore\ |\varepsilon_{ijk} e_j^3 u_k| = \sin\gamma_3$, and

$$(e_i) = \frac{1}{\sin\gamma_3}(-\cos\gamma_2, \cos\gamma_1, 0) \qquad \text{--- (5.2.20)}$$

The rotation tensor $D_{ij}(e_i, \gamma_3)$ mapping e_i^3 onto u_i is given by the equation (see Duschek and Hochrainer 1960, pp. 87 - 89)

$$D_{ij}(e_i,\gamma_3) = e_i e_j (1-\cos\gamma_3) + \delta_{ij}\cos\gamma_3 - \sin\gamma_3 \varepsilon_{ijk} e_k \qquad \text{--- (5.2.21)}$$

u_i and e_i^3 are related through

$$u_i = D_{ij} e_j^3 \qquad \text{--- (5.2.22)}$$

From (5.2.20) and (5.2.21) we have:

$$[D_{ij}] = \begin{bmatrix} \cos\gamma_3 + \frac{\cos^2\gamma_2}{1+\cos\gamma_3} & -\frac{\cos\gamma_1\cos\gamma_2}{1+\cos\gamma_3} & \cos\gamma_1 \\ -\frac{\cos\gamma_1\cos\gamma_2}{1+\cos\gamma_3} & \cos\gamma_3 + \frac{\cos^2\gamma_1}{1+\cos\gamma_3} & \cos\gamma_2 \\ -\cos\gamma_1 & -\cos\gamma_2 & \cos\gamma_3 \end{bmatrix}$$

--- (5.2.23)

This rotation tensor may be used as an orthogonal transformation matrix to define a new Cartesian system S' related to S by the orthogonal transformations

$$x_i = D_{ij} x'_j \qquad \text{--- (5.2.24),}$$

where x'_i are the coordinates of a point w.r.t. S'. Should S' share the origin with $\bar{S}$, then (5.2.24) has the form

$$x_i = D_{ij} x'_j + b_i .$$

The 3-axes of S' and $\bar{S}$ have the same direction and orientation. Assume that the angle less than π between the positive directions of their 1-axes is α, then the incident electric vector includes the angle α with the 1-axis of S'. The axes of S' and $\bar{S}$ can be made to coincide by a rotation through α about the 3-axis of S'. Let this be achieved by the rotation tensor $d_{ij}(e_i^{3'}, \alpha)$ where

$$d_{ij}(e_c^{3'}, \alpha) = e_c^{3'} e_j^{3'} (1 - \cos\alpha) + \delta_{ij}\cos\alpha - \sin\alpha\, \varepsilon_{ijk} e_k^{3'}$$

--- (5.2.25)

The tensor d_{ij} maps $(e_i^{1'}) = (1,0,0)$ onto $(t_i') = (\text{Cos}\alpha, \text{Sin}\alpha, 0)$. Here t_i' is the unit vector defining the direction of polarization of the incident electric vector - w.r.t. $\bar{S}$ it is $(\bar{t}_i) = (1,0,0)$ and w.r.t. S it has coordinates t_i [see (5.1.19)].

$$\therefore \quad t_i' = d_{ij} e_j' \qquad \text{--- (5.2.26)}$$

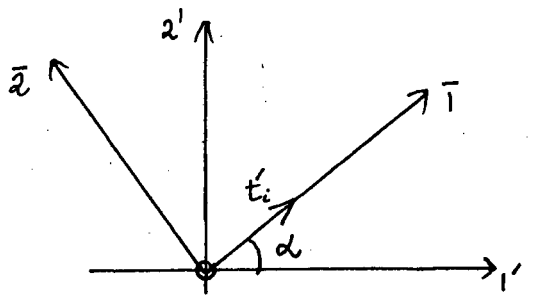

Hence, from (5.2.25) or by inspection from the figure:

$$[d_{ij}] = \begin{bmatrix} \text{Cos}\alpha & -\text{Sin}\alpha & 0 \\ \text{Sin}\alpha & \text{Cos}\alpha & 0 \\ 0 & 0 & 1 \end{bmatrix} \qquad \text{--- (5.2.27)}$$

The equations connecting the coordinates of a point in S' and $\bar{S}$ are now given by

$$x_i' = d_{ij} \bar{x}_j \qquad \text{--- (5.2.28)},$$

where it has been assumed that S' and $\bar{S}$ share a common origin.

From (5.2.24) and (5.2.29) it follows that

$$x_i = D_{ij} d_{jk} \bar{x}_k + b_i \qquad \text{--- (5.2.29)}$$

Comparison of (5.2.29) with (5.2.9) yields

$$a_{ik} = D_{ij} d_{jk} \qquad \text{--- (5.2.30)}$$

The equations (5.2.30) define the a_{ij}'s in (5.2.12), (5.2.16) and (5.2.17) as functions of the γ_i and α. Explicitly we have, using (5.2.30), (5.2.27) and (5.2.23):

$$a_{11} = \cos\alpha\left(\cos\gamma_3 + \frac{\cos^2\gamma_2}{1+\cos\gamma_3}\right) - \frac{\sin\alpha\cos\gamma_1\cos\gamma_2}{1+\cos\gamma_3}$$

$$a_{12} = -\sin\alpha\left(\cos\gamma_3 + \frac{\cos^2\gamma_2}{1+\cos\gamma_3}\right) + \frac{\cos\alpha\cos\gamma_1\cos\gamma_2}{1+\cos\gamma_3}$$

$$a_{13} = \cos\gamma_1$$

$$a_{21} = -\frac{\cos\alpha\cos\gamma_1\cos\gamma_2}{1+\cos\gamma_3} + \sin\alpha\left(\cos\gamma_3 + \frac{\cos^2\gamma_1}{1+\cos\gamma_3}\right)$$

$$a_{22} = -\frac{\sin\alpha\cos\gamma_1\cos\gamma_2}{1+\cos\gamma_3} + \cos\alpha\left(\cos\gamma_3 + \frac{\cos^2\gamma_1}{1+\cos\gamma_3}\right)$$

$$a_{23} = \cos\gamma_2$$

$$a_{31} = -\cos\alpha\cos\gamma_1 - \sin\alpha\cos\gamma_2$$

$$a_{32} = \sin\alpha\cos\gamma_1 - \cos\alpha\cos\gamma_2$$

$$a_{33} = \cos\gamma_3$$

--- (5.2.31)

The surface current (5.2.12), expressed as a function of θ, ϕ, γ_i and α is defined as the surface current of the perfectly conducting scatterer and denoted by $S_i^{(sc)}$.

The unit vector t_i in (5.1.19) defining the polarization of the electric vector may now be expressed in terms of the γ_i and α. From (5.2.9)

$$t_i = a_{ij} \bar{t}_j \qquad \text{--- (5.2.32)}$$

where $\bar{t}_j = \bar{e}_j$, $(\bar{e}_i) = (1, 0, 0)$

and the a_{ij}'s are given by (5.2.31)

$$\therefore t_1 = a_{11}, \quad t_2 = a_{21} \quad \text{and} \quad t_3 = a_{31}$$

or $$t_i = a_{i1} \qquad \text{--- (5.2.33).}$$

The results obtained above are now specialized for an axi-symmetric perfect conductor for axial incidence. The system of axes are chosen such that η in (5.2.8) is a function solely of θ [see section (2.4)]. Furthermore, the 3-axis is taken with positive direction in the direction of propagation of the incident wave and the incident electric vector is polarized in the direction of the 1-axis.

Hence $\gamma_1 = \gamma_2 = \frac{\pi}{2}$, $\gamma_3 = 0$ and $\alpha = 0$, and (5.2.31) becomes

$$a_{ij} = \delta_{ij} \qquad \text{--- (5.2.34)}$$

Equations (5.2.17) and (5.2.16) now become:

$$(\bar{e}_i^{\theta}) = \frac{1}{N(N^2 - N_3^2)^{1/2}} (N_1 N_3, \; N_2 N_3, \; N_3^2 - N^2)$$

$$(\bar{e}_i^{\phi}) = \frac{1}{(N^2 - N_3^2)^{1/2}} (-N_2, \; N_1, \; 0)$$

$$\text{--- (5.2.35)}$$

$$\cos\bar{\theta} = N_3/N\,,\quad \sin\bar{\theta} = (N^2 - N_3^2)^{1/2}/N$$

$$\cos\bar{\phi} = N_1/(N^2 - N_3^2)^{1/2}\,,\quad \sin\bar{\phi} = N_2/(N^2 - N_3^2)^{1/2}$$

--- (5.2.36)

N_i and $N = |N_i|$ are defined respectively by (2.5.9) and (2.5.10):

$$(N_i) = \eta\sin\theta\left(-\frac{d}{d\theta}(\eta\cos\theta)\cos\bar{\phi}\,,\ -\frac{d}{d\theta}(\eta\cos\theta)\sin\phi\,,\ \frac{d}{d\theta}(\eta\sin\theta)\right)$$

$$N = \eta\sin\theta\,(\eta^2 + \eta'^2)^{1/2}$$

Using these expressions for N_i and N in (5.2.35) and (5.2.36) we find:

$$(\bar{e}_\theta) = \frac{1}{(\eta^2+\eta'^2)^{1/2}}\left(\frac{d}{d\theta}(\eta\sin\theta)\cos\phi\,,\ \frac{d}{d\theta}(\eta\sin\theta)\sin\phi\,,\ \frac{d}{d\theta}(\eta\cos\theta)\right),$$

$$(\bar{e}_\phi) = (-\sin\phi\,,\ \cos\phi\,,\ 0)$$

--- (5.2.37),

and

$$\cos\bar{\theta} = \frac{d(\eta\sin\theta)/d\theta}{(\eta^2+\eta'^2)^{1/2}}\,,\quad \sin\bar{\theta} = -\frac{d(\eta\cos\theta)/d\theta}{(\eta^2+\eta'^2)^{1/2}}$$

$$\cos\bar{\phi} = \cos\phi\,,\quad \sin\bar{\phi} = \sin\phi$$

--- (5.2.38)

From (5.2.12) and (5.2.33) the surface current $S_i^{(sc)}$ is now defined by

$$S_i^{(sc)} = \bar{e}_i^{\bar{\theta}} S_{\bar{\theta}} + \bar{e}_i^{\bar{\phi}} S_{\bar{\phi}} \qquad \text{--- (5.2.39),}$$

where $e_i^{\bar{\theta}}$ and $e_i^{\bar{\phi}}$ are given by (5.2.37), $S_{\bar{\theta}}$ and $S_{\bar{\phi}}$ by (5.2.6) and the trigonometric functions by (5.2.38).

(5.3) <u>The far field in the backscattered direction for an axially symmetric perfect conductor</u>.

Denote the magnetic field vector of the scattered field according to the method of spherical currents by H_i, then it follows from (5.1.31) that

$$H_i(x_i) = \frac{1}{4\pi} \oint_S \varepsilon_{ijk} S_j^{(sc)}(\eta_i) \frac{\partial G(x_i, \eta_i)}{\partial \eta_k} \, df$$

--- (5.3.1),

where $(x_i) = (r\cos\phi,\ r\sin\theta\ \sin\phi,\ r\cos\theta)$ is a point exterior to S and

$$(\eta_i) = (\eta(\theta')\sin\theta'\cos\phi',\ \eta(\theta')\sin\theta'\sin\phi',\ \eta(\theta')\cos\theta')$$

is a point on S.

The surface current $S_i^{(sc)}$ is defined by (5.2.39) as a function of θ' and ϕ',

$$G = \frac{e^{ik|x_i - \eta_i|}}{|x_i - \eta_i|}$$

, and from (2.5.10)

for the axi-symmetric obstacle we have

$$df = \left|\varepsilon_{ijk} \frac{\partial \eta_j}{\partial \theta'} \frac{\partial \eta_k}{\partial \phi'}\right| d\theta' d\phi' = |N_i| \, d\theta' d\phi' = \eta \sin\theta' \left(\eta^2 + \left(\frac{\partial \eta}{\partial \theta'}\right)^2\right)^{1/2} d\theta' d\phi'$$

Hence (5.3.1) becomes:

$$H_i(x_i) = \frac{1}{4\pi} \int_0^{\pi} \int_0^{2\pi} \varepsilon_{ijk} S_j^{(sc)}(\eta_i) \frac{\partial G(x_i, \eta_i)}{\partial \eta_k} \left(\eta^2 + \left(\frac{d\eta}{d\theta'}\right)^2\right)^{1/2} \eta \sin\theta' \, d\theta' \, d\phi'$$

--- (5.3.2)

For $r >> \eta$

$$\frac{\partial G}{\partial \eta_i} \sim -ik \frac{e^{ikr}}{r} \cdot e^{-ik\eta_i e_i^r} e_i^r$$

--- (5.3.3)

In the backscattered direction ($\theta = \pi$),

$$(e_i^r) = (0, 0, -1).$$

$$\therefore \left(\frac{\partial G}{\partial \eta_i}\right)_{\theta=\pi} = ik \frac{e^{ikr}}{r} \cdot e^{ik\eta\cos\theta'} (0, 0, 1)$$

--- (5.3.4)

Denote the magnetic far field in the backscattered direction vector by $\mathcal{H}_i$, then it follows from (5.3.2), (5.3.4), (5.2.39), (5.2.6) and (5.2.37) that

$$\mathcal{H}_1 = 0$$

$$\mathcal{H}_2 = \frac{e^{ikr}}{kr} \cdot \left(\frac{-ik^2}{4}\right) \int_0^{\pi} U(\theta') e^{ik\eta\cos\theta'} (\eta^2 + \eta'^2)^{1/2} \eta \sin\theta' \, d\theta'$$

$$\mathcal{H}_3 = 0$$

--- (5.3.5),

where

$$U(\theta) = \sqrt{\frac{\epsilon}{\mu}} \frac{\cos\bar{\theta}}{k\rho} \sum_{n=1}^{\infty} \frac{(2n+1)}{n(n+1)} \left\{ \frac{i T_n(\cos\bar{\theta})}{[k\rho h_n^{(1)}(k\rho)]'} - \frac{\Pi_n(\cos\bar{\theta})}{k\rho h_n^{(1)}(k\rho)} \right\}$$

$$+ \sqrt{\frac{\epsilon}{\mu}} \frac{1}{k\rho} \sum_{n=1}^{\infty} \frac{(2n+1)}{n(n+1)} \left\{ \frac{i \Pi_n(\cos\bar{\theta})}{[k\rho h_n^{(1)}(k\rho)]'} - \frac{T_n(\cos\bar{\theta})}{k\rho h_n^{(1)}(k\rho)} \right\}$$

--- (5.3.6)

and

$$\cos\bar{\theta} = \frac{d(\eta \sin\theta')/d\theta'}{\left(\eta^2 + \left(\frac{d\eta}{d\theta'}\right)^2\right)^{1/2}} \qquad \text{--- (5.3.7)}$$

From (5.3.2) and (5.3.3) it follows that

$$H_i(x_i) \sim A_i \frac{e^{ikr}}{r} \qquad \text{--- (5.3.8)}$$

where

$$A_i = \frac{-ik}{4\pi} \int_0^{\pi} \int_0^{2\pi} \epsilon_{ijk} S_j^{(s)}(\eta_i) \hat{e}_k^r e^{-ik\eta_i \hat{e}_i^r} \left(\eta^2 + \left(\frac{d\eta}{d\theta'}\right)^2\right)^{1/2} \eta \sin\theta' \, d\theta \, d\phi' .$$

In spherical polar coordinates r, θ, ϕ

$$\partial_i = \frac{\partial}{\partial x_i} = \hat{e}_i^r \frac{\partial}{\partial r} + \frac{\hat{e}_i^{\theta}}{r} \frac{\partial}{\partial \theta} + \frac{\hat{e}_i^{\phi}}{r \sin\theta} \frac{\partial}{\partial \phi}$$

where the unit vectors are defined in (2.5.12). Hence it follows from (5.3.8) that

$$\partial_j H_k(x_i) \sim \hat{e}_j^r A_k \frac{\partial}{\partial r}\left(\frac{e^{ikr}}{r}\right) \sim ik \hat{e}_j^r H_k \qquad \text{--- (5.3.9)}$$

From the Maxwell equation (5.1.8) with $j_i = 0$ we have that

$$E_i = \frac{i}{\omega\epsilon}\,\varepsilon_{ijk}\,\partial_j H_k$$

hence, using (5.3.9)

$$E_i \sim -\frac{k}{\omega\epsilon}\,\varepsilon_{ijk}\,\hat{e}^r_j\,H_k \qquad \text{--- (5.3.10)}$$

$\therefore$

$$\left.\begin{aligned} \mathcal{E}_1 &= -\frac{k}{\omega\epsilon}\mathcal{H}_2 = -\sqrt{\frac{\mu}{\epsilon}}\,\mathcal{H}_2 \\ \mathcal{E}_2 &= 0 \\ \mathcal{E}_3 &= 0 \end{aligned}\right\} \qquad \text{--- (5.3.11)}$$

where $\mathcal{E}_i$ is the far field electric vector in the backscattered direction.

The radar cross section is also defined by (2.2.22):

$$\therefore\ \sigma = \lim_{r\to\infty} 4\pi r^2\,\frac{|W^{(s)}|}{|W^{(i)}|},$$

but here the power flux densities for the harmonic electromagnetic field are given by the time average of the Poynting vector $\frac{1}{2}R(\varepsilon_{ijk}E_jH_k^*)$, where R means take the real part and the asterisk denotes the complex conjugate. Denote the radar cross section according to the method of spherical currents by $\sigma^{(sc)}$, then

$$\sigma^{(sc)} = \lim_{r\to\infty} 4\pi r^2\,\frac{|R\,\varepsilon_{ijk}\,\mathcal{E}_j\,\mathcal{H}_k^*|}{|R\,\varepsilon_{ijk}\,E_j^{(i)}\,H_k^{(i)*}|} \qquad \text{--- (5.3.12)}$$

Here $\mathcal{E}_i$ and $\mathcal{H}_i$ are defined by (5.3.5) and (5.3.11), and $E_i^{(i)}$ and $H_i^{(i)}$ are the incident electric and magnetic field vectors.

From (5.2.1) in the backscattered direction, with directions of propagation and polarization as chosen above,

$$(E_i^{(i)}) = (e^{-ikr}, 0, 0)$$

$$(H_i^{(i)}) = (0, \sqrt{\frac{\epsilon}{\mu}} e^{-ikr}, 0)$$

--- (5.3.13)

By using these expressions for the scattered and incident fields in (5.3.12) we get

$$\sigma^{(sc)} = \frac{4\pi}{k^2} |S(\pi)|^2$$

--- (5.3.14)

where

$$S(\pi) = i\sqrt{\frac{\mu}{\epsilon}} \frac{k^2}{4} \int_0^{\pi} U(\theta') e^{ik\eta \cos\theta'} (\eta^2 + \eta'^2)^{1/2} \eta \sin\theta' d\theta'$$

--- (5.3.15)

and $U(\theta')$ is given by (5.3.6).

parameters characterizing the surface of the obstacle. In the electromagnetic case it is also possible to complete the integration w.r.t. one of the variables for axial incidence on bodies of revolution, and it is shown that in such cases the far field in the backscattered direction has the same polarization as the incident field.

It is a disadvantage of the method that it was not always possible to complete analytically the integration referred to above. This makes the physical interpretation of the results more difficult as the contribution of various scattering centres such as specular points, shadow boundaries, edges and vertices are not separately displayed.

An advantage of the method is that it is not highly body specific. Apart from the outward unit normal, the least principal radius of curvature and the distance from the origin to the surface, which have to be found as functions of the surface parameters, the formulae for the fields referred to above are the same for all convex bodies.

Another advantage of the method is that the integrands of the integrals in terms of which the exterior fields are expressed, always involve Legendre polynomials, spherical Bessel functions and the derivatives of spherical Bessel functions. This is a natural consequence of the method, being based on the solution for the sphere. This leads to a standardization of computational techniques and subroutines. In addition methods of computation for these functions exist over a wide range of argument which in turn makes it possible to calculate the surface and scattered fields over a wide range of ka. At large values of ka ($ka > 10$) the integrands of the scattered field integrals oscillate very rapidly and consequently the integration becomes very time consuming. This may possibly be avoided if numerical techniques specifically designed to cope with

rapidly oscillating integrands are employed.

(6.2) Numerical results of surface- and backscattered fields from spheroids and cones.

The numerical results obtained for the surface fields on hard spheroids according to the method of spherical currents compare well with those of exact theory. For the 2:1 hard spheroid at c = 5 (ka = 5,77) there is a close agreement in the surface field amplitudes on the illuminated side calculated by the exact method and the method of spherical currents. The largest differences are found in middle portion of the shadow region. With increasing eccentricity the surface field activity according to the method of spherical currents drops more rapidly than in the case of exact theory, but on the whole the surface fields compare reasonably well for the thinner bodies.

It should be borne in mind that the good correllation between the method of spherical currents and exact theory in the prediction of surface fields at c = 5 could be fortuitous. In section (3.5) it is pointed out that at c = 5 the normalized backscattering cross sections according to the method of spherical currents are relatively close to the values of exact theory. At other values of c the surface fields according to the two methods could differ far more than at c = 5.

From the graphs of the surface field amplitudes it is apparent that the main difference in a qualitative sense between the surface fields according to exact theory and the method of spherical currents is that in the latter case there is a relatively greater activity on the shadow side. This observation is best seen in the case of the 2:1 spheroid.

The results obtained for the scattering patterns of hard

spheroids in section (3.4) tend to reinforce the conclusion drawn above. The best correspondence between the scattering patterns according to exact theory and those calculated by means of the method of spherical currents are obtained on the illuminated side of the scatterer for the lowest frequency. In addition it is found that on the whole, for all frequencies, there is stronger scattering in the forward directions according to the method of spherical currents than according to exact theory.

The frequency response of soft and hard spheroids according to the method of spherical currents are shown and compared with the results of exact theory in section (3.5). Although the numerical discrepancy between the normalized backscattering coefficients calculated according to the two methods is large over the full range $0 \leq ka \leq 10$ for soft spheroids, the method of spherical currents discriminates between soft spheroids of differing eccentricity in qualitatively the same way as exact theory. For a given eccentricity the normalized cross sections have a maximum at $ka = 0$ which decreases rapidly with increasing ka, and the separation of their maxima became more constant as ka increases. With increasing eccentricity the oscillations become more pronounced.

As far as hard spheroids are concerned, both normalized backscattering coefficients $\sigma_{(sc)}/\sigma_0$ and σ/σ_0 tend to zero as $ka \to 0$, and their numerical difference in the range $0 \leq ka \leq 1$ is relatively small - this difference also decreases with decreasing eccentricity and ka. In contrast with soft spheroids, the method of spherical currents gives a relatively good account of the backscattering behaviour of hard spheroids in the Rayleigh region.

For $1 \leq ka \leq 10$ the numerical discrepancy between $\sigma_{(sc)}/\sigma_0$ and σ/σ_0 is large, and increases with increasing

eccentricity. However, as described in section (3.5), the method of spherical currents gives qualitatively the same description of the frequency response as exact theory for a given hard spheroid, and also discriminates between hard spheroids of differing eccentricity in qualitatively the same way.

It should be noted however that, especially in the case of the thinner bodies, the separation distance in ka between successive maxima for $\sigma_{(sc)}/\sigma_0$ is very nearly double that of σ/σ_0. This fact is also discernible in the acoustically soft case. Extensive checks were made so as to exclude the possibility of residual manipulative or computational errors. The surface fields of hard spheres were compared with known results, and the backscattering cross sections for soft and hard spheroids were computed with b = a. These results compared excellently with those obtained using the exact expressions for the backscattering cross sections of spheres. Furthermore, by considering spheroids close to the spherical shape, the results for such spheroids merge continuously with those obtained for spheres.

A possible explanation for the abovementioned discrepancy is that for a given ka, where a is the semi-major axis of the spheroid, $ka > k\rho$, where ρ is the least of the principal radii of curvature of the spheroid at an arbitrary point. Now ρ is the radius of the representative sphere of which the surface field is used to represent the surface field of the spheroid, and consequently relative to ka a lower frequency behaviour of spheres is used to describe the surface field on the given body by means of the method of spherical currents.

The higher average values of $\sigma_{(sc)}/\sigma_0$ than those of σ/σ_0 could be attributed to the relatively more intense surface activity on the shadow side predicted by the method of spherical currents. This could be caused by

the fact that the point on the representative sphere at which the surface field is taken to represent that of the given body is closer to the shadow boundary of the representative sphere than the shadow boundary of the given body as measured along their respective surfaces. If creeping wave theory is used to explain the surface excitation on the shadow side, this implies that the surface field on the shadow side according to the method of spherical currents is relatively less attenuated than is the actual case.

In section (3.6) the frequency response of hard prolate spheroids for axial incidence at high frequencies is discussed. Here the graphs of $\sigma_{(sc)}/\sigma_0$ plotted as functions of ka ($10 \leq ka \leq 80$) show in a correct way the dampening of the oscillations as ka increases for the 2:1 body. The end of a resonance region is displayed, but an incorrect high frequency limit is indicated - more than double that of the correct value of 1 for the normalized backscattering cross section. As the eccentricity increases, the method of spherical currents correctly shows that the oscillations retain their regularity over an increasing frequency range.

At high frequencies the method of spherical currents using $\sigma_{(sc)}/\sigma_0$, discriminates between spheroids of different eccentricity which physical optics, using $\sigma_{(PO)}/\sigma_0$, fails to do. The method of spherical currents also provides a better description of the backscattering behaviour of hard spheroids, in particular for the thinner bodies, than the geometric theory of diffraction.

In sections (4.2) and (4.3) the frequency response of resp. flatbacked cones and cone spheres according to the method of spherical currents in the Rayleigh region is compared with Siegel's low frequency method.

In both cases the method of spherical currents discriminates

between cones of different semi-vertex angles in a manner similar to that of Siegel's method, and the curves of $\sigma_{(sc)}/\pi a^2$ deviate from the Rayleigh results at about $ka = 1$ in the correct way, indicating the low frequency end of a resonance region.

The results obtained for the cone sphere are considerably better than those obtained for the flatbacked cone. For the cone sphere the method of spherical currents displays the fourth power law and for $0 < ka < 1$ there is very little difference between nose-on and base-on incidence - these results agree with those predicted by the Rayleigh cross sections according to Siegel's method. For the flatbacked cone $\sigma_{(sc)}/\pi a^2$ varies proportionally to about $(1/\lambda)^3$ for $0 < ka < 1$, and there is reasonable agreement between base-on and nose-on backscattering only at very long wavelengths.

From the low frequency results for finite cones we conclude that the method of approximation of the surface field on flat surfaces is unsatisfactory, and that the better results for cone spheres is due to the spherical termination of the body.

Combining the results obtained for spheroids and finite cones, one concludes that the best results according to the method of spherical currents will be obtained for those bodies over which the ratio of the principal radii of curvature remain fairly close to one. This conclusion is nearly self-evident, considering the nature of the method of approximation. It is also likely that the method of spherical currents gives a better description of the scattered field in the low frequency range.

Numerical results are however obtainable over a wide range of frequencies, and even for relatively elongated bodies a qualitative insight into the behaviour of

scattered fields is obtainable by means of the method of spherical currents.

(6.3) Conjectures on possible improvements of the method.

In the light of the results given and the conclusions drawn in the previous section, a few ways suggest themselves by means of which the method of spherical currents may be improved.

In spite of the fact that the choice of least principal radius of curvature for the representative sphere leads to a good approximation of the surface fields on hard spheroids for $c = 5$, the frequency response may improve if a larger quantity (such as the Guassian curvature) is used as radius for the representative sphere. This would incorporate more of the higher frequency behaviour of spheres into the surface field of the body, and could possibly lead to a relatively less excited shadow region as creeping waves would suffer more attenuation on larger spheres.

At those points on the obstacle at which one of the principal radii of curvature becomes infinite, the surface field on an infinite circular cylinder might be used in a way analogous to that used for spheres in the method of spherical currents. The theoretical results of Wait (1955) for the scattered fields of infinite cylinders for oblique incidence can be used as a basis for this method.

Another method, which could be considered a generalization of the method of spherical currents, would be to use spheroids to approximate the surface field of a convex body at all points at which both principal radii of curvature are different but finite. Such a method is however more complex, and would also be computationally more laborious than the method of spherical currents, owing to the presence of spheroidal wave functions.

A much better insight into the method of spherical currents can be obtained if its results could be compared with other theoretical and also experimental results of a wider choice of bodies and fequency ranges. In this study for instance no conclusions regarding the effect of an edge could be drawn by using the method of spherical currents, as results for the flatbacked cone were interpreted only in the Rayleigh region.

A much more comprehensive test of this approximation method can be carried out by using equations (5.3.14) and (5.3.15) to calculate the radar cross sections in the backscattered direction for axial incidence for a variety of shapes for perfect conductors. Theoretical and experimental results are available for perfectly conducting spheroids, flatbacked cones, cone spheres, ogives, double-backed cones and double-rounded cones over a wide frequency range.

Recent exact theoretical results on the electromagnetic scattering of spheroids are those of Sinha and MacPhie (1975) and Asano and Yamamoto (1975). Many results concerning scattering from prolate spheroids are contained in the report of Sleator (1964), and Moffatt and Kennaugh (1965) have applied the method of impulse analysis to obtain the frequency response in the backscattered direction of a perfectly conducting prolate spheroid.

For the cone sphere shape results on the backscattering radar cross section have been published by Senior (1965a), and Moffatt and Kennaugh (1962), have applied impulse analysis to the cone sphere.

The report by Kleinman and Senior (1963) is a comprehensive survey of results, both theoretical and experimental, on the scattering behaviour of a variety of cone shapes.

Bechtel (1965) evaluated the ability of the geometrical theory of diffraction to predict the radar cross section of a perfectly conducting flatbacked cone by comparing computed results with measured values, and Hong and Borison (1968) published experimental measurements of short-pulse scattering by a slightly blunted flat-backed cone.

Experimental measurements of the nose-on backscattering radar cross sections of ogives, double-backed cones, double-rounded cones and cone spheres were made by Blore (1964), and compared with Rayleigh theory, impulse analysis and Adachi's extension of physical optics.

The reviews of Crispin and Maffett on radar cross section estimation also contain many results with which the method of spherical currents may be usefully compared.

A better evaluation of the limits of applicability of the method of spherical currents is possible by comparing its predictions on radar cross sections with the results mentioned above.

A,Y)

SLEG DATE 062476 PAGE 26

```
@ELT,L DIFF.SLEG
ELTOT7 RLI870 06/24-09:49:22-(0.)
000001       000           FUNCTION PLEG(N,Y)
000002       000           P1=1.
000003       000           P2=Y
000004       000           IF(N-2)3,4,5
000005       000         3 PLEG=P1
000006       000           RETURN
000007       000         4 PLEG=P2
000008       000           RETURN
000009       000         5 DO 7 L=3,N
000010       000           XL=1./(L-1)
000011       000           P3=XL*((2*L-3)*Y*P2-(L-2)*P1)
000012       000           P1=P2
000013       000         7 P2=P3
000014       000           PLEG=P3
000015       000           RETURN
000016       000           END

END ELT.


@HDG SMAIN
```

```
@ELT,L DIFF.SPSI
ELTOT7 RLIB70 06/24-09:49:30-(0,)
000001       000          FUNCTION PSI(N,X)
000002       000          T1=1.
000003       000          SUM=T1
000004       000          DO 11 L=1,200
000005       000          L2=2*L
000006       000          T2=-T1*X*X/(L2*(2*N+L2-1))
000007       000          SUM=SUM+T2
000008       000          E=(ABS(T1)+ABS(T2))/ABS(SUM)
000009       000          IF(E.LE.1.E-6) GO TO 12
000010       000          T1=T2
000011       000       11 CONTINUE
000012       000       12 SER=SUM
000013       000          P=SER/X
000014       000          DO 13 L=1,N
000015       000          P=P*X/(2*L-1)
000016       000          IF(ABS(P).GT.1.E-30) GO TO 13
000017       000          P=SIGN(1.E-30,P)
000018       000          GO TO 15
000019       000       13 CONTINUE
000020       000       15 PSI=P
000021       000          RETURN
000022       000          END

END ELT.


@HDG SPUT
```

```
@ELT,L DIFF.SZETA
ELTOT7 RLI870 06/24-09:49:38-(0.)
000001       000          FUNCTION ZETA(N,X)
000002       000          T1=1.
000003       000          SUM=T1
000004       000          DO 11 L=1,200
000005       000          L2=2*L
000006       000          T2=-T1*X*X/(L2*(L2-2*N+1))
000007       000          SUM=SUM+T2
000008       000          E=(ABS(T1)+ABS(T2))/ABS(SUM)
000009       000          IF(E.LE.1.E-6) GO TO 12
000010       000          T1=T2
000011       000       11 CONTINUE
000012       000       12 SER=SUM
000013       000          P=SER
000014       000          DO 13 L=1,N
000015       000          P=P*(2*L-3)/X
000016       000          IF(ABS(P).LT.1.E30) GO TO 13
000017       000          P=SIGN(1.E30,P)
000018       000          GO TO 15
000019       000       13 CONTINUE
000020       000       15 ZETA=P
000021       000          RETURN
000022       000          END

END ELT.


@HDG         DIFF.
```

```
@ELT,L DIFF.SDPSI
ELTDT7 RLI370 06/24-09:49:15-(0,)
000001      000          FUNCTION DPSI(N,X)
000002      000          IF(N-1)4,4,5
000003      000        4 DPSI=-PSI(2,X)
000004      000          GO TO 8
000005      000        5 DPSI=PSI(N-1,X)-N/X*PSI(N,X)
000006      000        8 RETURN
000007      000          END

END ELT.


@HDG SDZETA
```

```
@ELT,L DIFF.SDZETA
ELTOT7 RL1870 06/24-09:49:16-(0.)
000001      000           FUNCTION DZETA(N,X)
000002      000           IF(N-1)4,4,5
000003      000         4 DZETA=-ZETA(2,X)
000004      000           GO TO 8
000005      000         5 DZETA=ZETA(N-1,X)-N/X*ZETA(N,X)
000006      000         8 RETURN
000007      000           END

END ELT.


@HDG SFAR
```

```
@ELT,L DIFF.SBESJ
ELTOT7 RLIB7J 06/24-09:49:10-(J,)
000001      JOJ          SUBROUTINE BESJ(X,FNU,N,F)                                    BESJ
000002      JOJ     C---------------------------------------------------------------------
000003      JOJ     C     REGULAR BESSEL FUNCTIONS OF REAL ARGUMENT.
000004      JOJ     C---------------------------------------------------------------------
000005      JOJ     C     ARGUMENT DEFINITION
000006      JOJ     C        X     IS THE ARGUMENT OF THE BESSEL FUNCTION.
000007      JOJ     C        FNU   IS THE FRACTIONAL PART OF TH+ ORDER.
000008      JOJ     C        N     IS THE INTEGRAL PART OF THE HIGHEST ORDER TO BE
000009      JOJ     C              COMPUTED.
000010      JOJ     C        F     IS THE OUTPUT ARRAY OF BESSEL FUNCTIONS.
000011      JOJ     C---------------------------------------------------------------------
000012      JOJ     C     REFERENCES
000013      JOJ     C        M. GOLDSTEIN AND R.M. THALER, RECURRENCE TECHNIQUES FOR THE
000014      JOJ     C              CALCULATION OF BESSEL FUNCTIONS, MTAC, 1959.
000015      JOJ     C        M. GOLDSTEIN AND R. M. THALER, BESSEL FUNCTIONS FOR LARGE
000016      JOJ     C              ARGUMENTS, MTAC. 1959.
000017      JOJ     C        G.N. WATSON, A TREATISE ON THE THEORY OF BESSEL FUNCTIONS.
000018      JOJ     C              CAMBRIDGE UNIVERSITY PRESS, 1948.
000019      JOJ     C---------------------------------------------------------------------
000020      JOJ          DIMENSION F(1),C(5)                                           BESJ
000021      JOJ          DATA PI2/1.57079632/                                          BESJ
000022      JOJ          F(1)=1.0
000023      JOJ          DO 100 I=1,N
000024      JOJ      100 F(I+1)=0
000025      JOJ          NN=IABS(N)
000026      JOJ          CX=2./X                                                       BESJ
000027      JOJ          IF(FNU.GT.1.5)GO TO 1                                         BESJ
000028      JOJ          IY=1                                                          BESJ
000029      JOJ          GO TO 2                                                       BESJ
000030      JOJ        1  FNU=FNU-2.                                                   BESJ
000031      JOJ          IY=2                                                          BESJ
000032      JOJ        2 CXNU=CX*FNU                                                   BESJ
000033      JOJ          IF (X.GT.88.) GO TO 12
000034      JOJ          KK=X+20.                                                      BESJ
000035      JOJ          M=MAXO(KK,NN+10)                                              BESJ
000036      JOJ          IF(X.LT.1.)GO TO 3                                            BESJ
000037      JOJ          KK=39.*X**.333333333                                          BESJ
000038      JOJ          GO TO 4                                                       BESJ
000039      JOJ        3 KK=172.69388/(3.5888795-ALOG(X))                              BESJ
000040      JOJ        4 M=MINO(M,KK)/2
000041      JOJ          K=M+M+1
000042      JOJ          F(K+1)=1.E-37                                                 BESJ
000043      JOJ          F(K+2)=0.                                                     BESJ
000044      JOJ          KK=K+1                                                        BESJ
000045      JOJ          TT=FNU+KK
000046      JOJ          DO 5 I=1,K
000047      JOJ          J=K-I                                                         BESJ
000048      JOJ          TT=TT-1.                                                      BESJ
000049      JOJ        5 F(J)=CX*TT*F(J+1)-F(J+2)
000050      JOJ          IF(X.GT.10.)GO TO 12
000051      JOJ          PHI=FNU+2.
000052      JOJ          ALFA=F(1)+F(3)*PHI                                            BESJ
000053      JOJ          T1=FNU-1.                                                     BESJ
000054      JOJ          T2=T1-1.                                                      BESJ
000055      JOJ          TT=1.                                                         BESJ
```

```
000056      000         DO 6 I=2,M                                                    BESJ
000057      000         TT=TT+1.                                                      BESJ
000058      000         PHI=PHI*(FNU+TT+TT)*(T1+TT)/(TT*(T2+TT+TT))                   BESJ
000059      000       6 ALFA=PHI*F(2*I+1)+ALFA                                        BESJ
000060      000         CALL GAMMA(1.+FNJ,TT,$50,$50)                                 BESJ
000061      000         ALFA=CX**FNU*ALFA*TT                                          BESJ
000062      000         I1=1                                                          BESJ
000063      000       7 DO 8 I=I1,K                                                   BESJ
000064      000       8 F(I)=F(I)/ALFA                                                BESJ
000065      000         IF(N.GE.0)GO TO 11                                            BESJ
000066      000       9 IF (IY.EQ.2) GO TO 49                                         BESJ
000067      000         F(2)=CXNU*F(1)-F(2)                                           BESJ
000068      000         IF(NN.LE.1)RETURN
000069      000         TT=FNU                                                        BESJ
000070      000         DO 10 I=2,NN                                                  BESJ
000071      000         TT=TT-1.                                                      BESJ
000072      000      10 F(I+1)=CX*TT*F(I)-F(I-1)                                      BESJ
000073      000      11 IF(IY.EQ.1)RETURN
000074      000      49 N=M                                                           BESJ
000075      000         X=Y1                                                          BESJ
000076      000         FNJ=Y2                                                        BESJ
000077      000      50 RETURN
000078      000    C.....ASYMPTOTIC EXPANSION......                                  BESJ
000079      000      12 KK=1                                                          BESJ
000080      000         FU=FNU                                                        BESJ
000081      000         XXX=1./X                                                      BESJ
000082      000         XX=XXX*XXX                                                    BESJ
000083      000         TT=1./SQRT(PI2*X)                                             BESJ
000084      000      13 A=FU**2-.25                                                   BESJ
000085      000         C(5)=.25                                                      BESJ
000086      000         C(4)=.15625*A-.375                                            BESJ
000087      000         C(3)=(.1171875*A-1.15625)*A+1.375                             BESJ
000088      000         C(2)=((.09521484375*A-2.38671875)*A+14.2265625)*A-19.6875     BESJ
000089      000         C(1)=(((.08093261719*A-4.10585937)*A+58.224609375)*A-277.875)*A+ BESJ
000090      000        1354.375                                                       BESJ
000091      000         P=C(1)                                                        BESJ
000092      000         DO 14 I=2,5                                                   BESJ
000093      000      14 P=P*XX+C(I)                                                   BESJ
000094      000         BT=(P*A*XX+1.)*TT                                             BESJ
000095      000         C(5)=.5                                                       BESJ
000096      000         C(4)=.04166666*A-.25                                          BESJ
000097      000         C(3)=(.0125*A-.35)*A+.75                                      BESJ
000098      000         C(2)=((.00055035718*A-.42410714286)*A+3.60267857)*A-5.625     BESJ
000099      000         C(1)=(((.00303319444*A-.486111)*A+10.28645833)*A-58.)*A+78.75 BESJ
000100      000         P=C(1)                                                        BESJ
000101      000         DO 15 I=2,5                                                   BESJ
000102      000      15 P=P*XX+C(I)                                                   BESJ
000103      000         PHI=X+XXX*P*A-(FU+.5)*PI2                                     BESJ
000104      000         IF(KK.EQ.2)GO TO 16                                           BESJ
000105      000         F1=BT*COS(PHI)                                                BESJ
000106      000         Y1=BT*SIN(PHI)                                                BESJ
000107      000         FU=FNU+1.                                                     BESJ
000108      000         KK=2                                                          BESJ
000109      000         GO TO 13                                                      BESJ
000110      000      16 F2=BT*COS(PHI)                                                BESJ
000111      000         Y2=BT*SIN(PHI)                                                BESJ
000112      000         IF (X.GT.88.) GO TO 17
```

```
000113      000          IF(ABS (F1).LT.ABS(F2))GO TO 20                    BESJ
000114      000          ALFA=F(1)/F1                                       BESJ
000115      000          GO TO 22                                           BESJ
000116      000       17 F(1)=F1                                            BESJ
000117      000          F(2)=F2                                            BESJ
000118      000          IF(N)9,11,18                                       BESJ
000119      000       18 IF(N.LE.1)GO TO 11                                 BESJ
000120      000          TT=FNU                                             BESJ
000121      000          DO 19 I=2,NN                                       BESJ
000122      000          TT=TT+1.                                           BESJ
000123      000       19 F(I+1)=CX*TT*F(I)-F(I-1)                           BESJ
000124      000          GO TO 11                                           BESJ
000125      000       20 ALFA=F(2)/F2                                       BESJ
000126      000       22 F(1)=F1                                            BESJ
000127      000          F(2)=F2                                            BESJ
000128      000          I1=3                                               BESJ
000129      000          GO TO 7                                            BESJ
000130      000          END                                                BESJ

END ELT.


@HDG SBOSS
```

```
@ELT,L DIFF.SDBES
ELTOT7 RLI870 06/24-09:49:15-(0,)
000001       000          SUBROUTINE DBES (KODE,N,X,F,G,DPSI,DZETA)
000002       000          DIMENSION F(N),G(N),DPSI(N),DZETA(N)
000003       000          B=SQRT(1.5707963/X)
000004       000          IF(KODE.LT.0) GO TO 2
000005       000          DPSI(1)=-B*F(2)
000006       000          DO 1 I=2,N
000007       000        1 DPSI(I)=B*(F(I-1)-I/X*F(I))
000008       000          IF(KODE.GT.0) RETURN
000009       000        2 DZETA(1)=-B*G(3)
000010       000          IT=-1
000011       000          DO 3 I=2,N
000012       000          DZETA(I)=IT*B*(G(I)+I/X*G(I+1))
000013       000        3 IT=-IT
000014       000          RETURN
000015       000          END

END ELT.


@HDG SDPSI
```

```
@ELT,C DIFF.SPSTAS
ELTOT7 RLI870 06/24-09:49:28-(0.)
000001       003          SUBROUTINE POTAS(X,Y,QR,QI)
000002       003          DIMENSION F(200),G(200),DPSI(200),DZETA(200)
000003       003          IF(X.GT.0.31) GO TO 40
000004       003          QR=1+(.5-.555556*PLEG(3,Y))*X*X+(.125-.25*PLEG(2,Y)
000005       003         $-.030864*PLEG(3,Y)+.017143*PLEG(5,Y))*X**4
000006       003          QI=1.5*PLEG(2,Y)*X-(.333333+.116667*PLEG(4,Y))*X**3
000007       003          RETURN
000008       003       40 NN=INT((9*X+120)/7)
000009       003          CALL BESJ(X,.5,NN,F)
000010       003          CALL BESJ(X,.5,-NN,G)
000011       003          CALL OBES (0,NN,X,F,G,DPSI,DZETA)
000012       003          SR=0.
000013       003          SI=0.
000014       003          DO 43 N=1,NN
000015       003          A=(2*N-1)*PLEG(N,Y)
000016       003          U=DPSI(N)
000017       003          V=DZETA(N)
000018       003          R=1/(U*U+V*V)
000019       003          WU=U*R
000020       003          WV=V*R
000021       003          K=MOD(N,4)+1
000022       003          GO TO (44,45,46,47),K
000023       003       44 FR=WU
000024       003          FI=-WV
000025       003          GO TO 48
000026       003       45 FR=WV
000027       003          FI=WU
000028       003          GO TO 48
000029       003       46 FR=-WU
000030       003          FI=WV
000031       003          GO TO 48
000032       003       47 FR=-WV
000033       003          FI=-WU
000034       003       48 TR1=A*FR
000035       003          TI1=A*FI
000036       003          SR=SR+TR1
000037       003          SI=SI+TI1
000038       003          IF(N.EQ.1) GO TO 50
000039       003          ER=(ABS(TR1)+ABS(TR2))/ABS(SR)
000040       003          EI=(ABS(TI1)+ABS(TI2))/ABS(SI)
000041       003          IF(ER.LE.1.E-5.AND.EI.LE.1.E-5) GO TO 42
000042       003       50 TR2=TR1
000043       003          TI2=TI1
000044       003       43 CONTINUE
000045       003       42 B=1/(X*X)
000046       003          QR=B*SR
000047       003          QI=B*SI
000048       003          RETURN
000049       003          END

END ELT.
```

```
@ELT,L DIFF.SPUT
ELTOT7 RLIB7J 06/24-09:49:32-(J,)
000001      00J          SUBROUTINE PUT (X,Y,QR,QI)
000002      00J          SR=0.
000003      00J          SI=0.
000004      00J          DO 43 N=1,20J
000005      00J          A=(2*N-1)*PLEG(N,Y)
000006      00J          U=PSI(N,X)
000007      00J          V=ZETA(N,X)
000008      00J          WU=0.
000009      00J          WV=1/V
000010      00J          VU=(V/U)**2
000011      00J          CALL OVERFL(M)
000012      00J          IF(M.EQ.1) GO TO 90
000013      00J          WU=1/(U+VU*U)
000014      00J          WV=1/(V+V/VU)
000015      00J       90 K=MOD(N,4)+1
000016      00J          GO TO (44,45,46,47),K
000017      00J       44 FR=WU
000018      00J          FI=-WV
000019      00J          GO TO 48
000020      00J       45 FR=WV
000021      00J          FI=WU
000022      00J          GO TO 48
000023      00J       46 FR=-WU
000024      00J          FI=WV
000025      00J          GO TO 48
000026      00J       47 FR=-WV
000027      00J          FI=-WU
000028      00J       48 TR1=A*FR
000029      00J          TI1=A*FI
000030      00J          SR=SR+TR1
000031      00J          SI=SI+TI1
000032      00J          IF(N.EQ.1) GO TO 50
000033      00J          ER=(ABS(TR1)+ABS(TR2))/ABS(SR)
000034      00J          EI=(ABS(TI1)+ABS(TI2))/ABS(SI)
000035      00J          IF(ER.LE.1.E-5.AND.EI.LE.1.E-5) GO TO 42
000036      00J       50 TR2=TR1
000037      00J          TI2=TI1
000038      00J       43 CONTINUE
000039      00J       42 QR=SR/X
000040      00J          QI=SI/X
000041      00J          RETURN
000042      00J          END

END ELT.


@HDG SRAD
```

BLK	REC	CONTROL	COMMAND	OPERAND	RECORD	TYPE	NAME	DATE	TIME
001398	123					SOR	SPS	04/14/76	15.15
001398	181				SUBROUTINE SPS(X,Y,PR,PI)			03000310	
001398	220				SR=0.			03000320	
001399	005				SI=0.			03000330	
001399	024				DO 43 N=1,200			03000340	
001399	051				A=(2*N-1)*PLEG(N,Y)			03000350	
001399	084				U=PSI(N,X)			03000360	
001399	108				V=ZETA(N,X)			03000370	
001399	133				FR=0.			03000380	
001399	152				FI=0.			03000390	
001399	171				VU=(V/U)**2			03000400	
001399	196				CALL OVERFL(M)			03000410	
001400	005				IF(M.EQ.1) GO TO 90			03000420	
001400	038				FR=(V/U)/(1+VU)			03000430	
001400	067				FI=1/(1+VU)			03000440	
001400	092		90		TR1=A*FR			03000450	
001400	117				TI1=A*FI			03000460	
001400	139				SR=SR+TR1			03000470	
001400	162				SI=SI+TI1			03000480	
001400	185				IF(N.EQ.1) GO TO 50			03000490	
001401	005				ER=(ABS(TR1)+ABS(TR2))/ABS(SR)			03000500	
001401	049				EI=(ABS(TI1)+ABS(TI2))/ABS(SI)			03000510	
001401	093				IF(ER.LE.1.E-5.AND.EI.LE.1.E-5) GO TO 42			03000520	
001401	147		50		TR2=TR1			03000530	
001401	171				TI2=TI1			03000540	
001401	192		43		CONTINUE			03000550	
001401	217		42		PR=SR			03000560	
001402	005				PI=SI			03000570	
001402	024				RETURN			03000580	
001402	044				END			03000590	

BLK	REC	CONTROL	COMMAND	OPERAND	RECORD	TYPE	NAME	DATE	TIME
000324	133					SOR	RAG	12/18/75	12.36
000324	191				SUBROUTINE RAG(C,BA,E,I,RHO,ETA,CAN)			00000010	
000325	005				RECRO=1/SQRT(1-BA*BA)			00000020	
000325	043				Z=RECRO*E/SQRT(RECRO*RECRO-1+E*E)			00000030	
000325	087				ENU=1+(BA**4-1)*Z*Z			00000040	
000325	123				DEN=1+(BA*BA-1)*Z*Z			00000050	
000325	153				BRAK=ENU/DEN			00000060	
000325	179				GO TO (32,33,31),I			00000070	
000325	211			31	RHO=C*RECRO/BA*SQRT(BRAK**3)			00000080	
000326	005				GO TO 36			00000090	
000326	027			32	RHO=C*RECRO*BA*SQRT(BRAK)			00000100	
000326	069				GO TO 36			00000110	
000326	091			33	RHO=C*RECRO*BRAK			00000120	
000326	124			36	ETA=C*BA*RECRO/SQRT(DEN)			00000130	
000326	165				CAN=(1/SQRT(ENU))*(-BA*BA*Z)			00000140	
000326	207				RETURN			00000150	
000326	227				END			00000160	

```
@ELT,L DIFF.SRAD
ELTOT7 RLIB7O 06/24-09:49:34-(0.)
000001      OOO          SUBROUTINE RAD (D,BA,Z,RHO,ETA,CAN)
000002      OOO          ENU = 1. + (BA**4 - 1.)*Z**2
000003      OOO          DEN = 1. + (BA**2 - 1.)*Z**2
000004      OOO          BRAK = ENU/DEN
000005      OOO          RHO = D*BA*SQRT(BRAK)
000006      OOO          ETA = D*BA/SQRT(DEN)
000007      OOO          CAN = (1./SQRT(ENU))*(-BA**2*Z)
000008      OOO          RETURN
000009      OOO          END

END ELT.


@HDG SSCAPA
```

```
@ELT,L DIFF.SMASH
ELTOT7 RLIB70 06/24-09:49:27-(0,)
000001      000          SUBROUTINE HASH(D,BA,Z,THE,HR,HI)
000002      000          CALL RAD(D,BA,Z,RHO,Y,CAN)
000003      000          DD=.01745329*THE
000004      000          A1=SQRT(1-Z*Z)*SIN(DD)
000005      000          B1=Z*COS(DD)
000006      000          A=Y*A1/2
000007      000          B=Y*B1
000008      000          IF(B1.NE.0.) GO TO 21
000009      000          ALP=0.
000010      000          GO TO 51
000011      000       21 S1=-1.
000012      000          SS=S1
000013      000          DO 41 N=1,100
000014      000          S1=-S1*A*A/(N*N)
000015      000          SS=SS+S1
000016      000          IF(SS.EQ.0.) GO TO 41
000017      000          E=ABS(S1/SS)
000018      000          IF(E.LE.1.E-5) GO TO 11
000019      000       41 CONTINUE
000020      000       11 ALP=-B1*SS
000021      000       51 IF(A1.NE.0.) GO TO 13
000022      000          BET=0.
000023      000          GO TO 14
000024      000       13 S1=-A
000025      000          SS=S1
000026      000          DO 42 N=1,100
000027      000          S1=-S1*A*A/(N*N+N)
000028      000          SS=SS+S1
000029      000          IF(SS.EQ.0.) GO TO 42
000030      000          E=ABS(S1/SS)
000031      000          IF(E.LE.1.E-5) GO TO 12
000032      000       42 CONTINUE
000033      000       12 BET=A1*SS/(BA*BA)
000034      000       14 COE=Y**4/(2*D*D)
000035      000          CB=COS(B)
000036      000          SB=SIN(B)
000037      000          HR=COE*(BET*CB-ALP*SB)
000038      000          HI=-COE*(ALP*CB+BET*SB)
000039      000          RETURN
000040      000          END

END ELT.


@HOS SPOTAS
```

```
PAGE  0001   DATE 76/07/07
      SUBROUTINE GREAT(D,BA,THE,A,B,S)
      EVR=0.
      ODR=0.
      EVI=0.
      ODI=0.
      CALL GRIND(D,BA,A,THE,AFR,AFI)
      CALL GRIND(D,BA,B,THE,BFR,BFI)
      N=1
      DO 41 I=1,20
      M=N
      N=2*N
      EVR=ODR+EVR
      EVI=ODI+EVI
      C=(B-A)/N
      ODR=0.
      ODI=0.
      DO 61 J=1,M
      Z=A+C*(2*J-1)
      CALL GRIND(D,BA,Z,THE,XR,XI)
      ODR=ODR+XR
   61 ODI=ODI+XI
      TR1=C*(AFR+BFR+2*EVR+4*ODR)/3
      TI1=C*(AFI+BFI+2*EVI+4*ODI)/3
      SS1=TR1*TR1+TI1*TI1
      WRITE(5,1) N,TR1,TI1,SS1
    1 FORMAT(1X,'N=',I9,' TR1=',E12.6,' TI1=',E12.6,' SS1=',E12.5)
      IF(I.EQ.1) GO TO 41
      IF(ABS(SS1/SS2-1).LE.1.E-3) GO TO 51
   41 SS2=SS1
   51 S=SS1
      RETURN
      END
```

BLK	REC	CONTROL	COMMAND	OPERAND	RECORD	TYPE	NAME	DATE	TIME
000056	084					SOR	PUT	10/28/75	18.50 C
000056	142				SUBROUTINE PUT (X,Y,QR,QI)				03000010
000056	182				SR=0.				03000020
000056	201				SI=0.				03000030
000056	220				DO 43 N=1,200				03000040
000057	005				A=(2*N-1)*PLEG(N,Y)				03000050
000057	038				U=PSI(N,X)				03000060
000057	062				V=ZETA(N,X)				03000070
000057	087				WU=0.				03000080
000057	106				WV=1/V				03000090
000057	126				VU=(V/U)**2				03000100
000057	151				CALL OVERFL(M)				03000110
000057	179				IF(M.EQ.1) GO TO 90				03000120
000057	212				WU=1/(U+VU*U)				03000130
000058	005				WV=1/(V+V/VU)				03000140
000058	032			90	K=MOD(N,4)+1				03000150
000058	061				GO TO (44,45,46,47),K				03000160
000058	096			44	FR=WU				03000170
000058	118				FI=-WV				03000180
000058	138				GO TO 48				03000190
000058	160			45	FR=WV				03000200
000058	182				FI=WU				03000210
000058	201				GO TO 48				03000220
000058	223			46	FR=-WU				03000230
000059	005				FI=WV				03000240
000059	024				GO TO 48				03000250
000059	046			47	FR=-WV				03000260
000059	069				FI=-WU				03000270
000059	089			48	TR1=A*FR				03000280
000059	114				TI1=A*FI				03000290
000059	136				SR=SR+TR1				03000300
000059	159				SI=SI+TI1				03000310
000059	182				IF(N.EQ.1) GO TO 50				03000320
000060	005				ER=(ABS(TR1)+ABS(TR2))/ABS(SR)				03000330
000060	049				EI=(ABS(TI1)+ABS(TI2))/ABS(SI)				03000340
000060	093				IF(ER.LE.1.E-5.AND.EI.LE.1.E-5) GO TO 42				03000350
000060	147			50	TR2=TR1				03000380
000060	171				TI2=TI1				03000390
000060	192			43	CONTINUE				03000400
000060	217			42	QR=SR/X				03000410
000061	005				QI=SI/X				03000420
000061	025				RETURN				03000430
000061	046				END				03000440

```
@ELT,L DIFF.SHURI
ELTOT7 RLI87J J6/24-J9:49:21-(J,)
000001      JOJ          SUBROUTINE HURI(D,BA,Z,HR,HI)
000002      JOJ          CALL RAD(D,BA,Z,RHO,Y,CAN)
000003      JOJ          A=Y**3/(2*D*D*BA*BA)
000004      JOJ          S=Y*Z
000005      OOJ          HR=A*COS(S)
000006      OOJ          HI=-A*SIN(S)
000007      JOJ          RETURN
000008      OOJ          END

END ELT.


@HDG SLEG
```

```
@ELT,L DIFF.SFAR
ELTOT7 RLI870 06/24-09:49:16-(),)
000001       000           SUBROUTINE ASH(D,BA,Z,HR,HI)
000002       000           CALL RAD(D,BA,Z,RHO,Y,CAN)
000003       000           A=-Y**4*Z/(2*D*D)
000004       000           S=Y*Z
000005       000           HR=A*SIN(S)
000006       000           HI=A*COS(S)
000007       000           RETURN
000008       000           END

END ELT.


@HDG SGRAND
```

```
@ELT,L DIFF.SGRAND
ELTOT7 RLIB7J 06/24-09:49:17-(J,)
000001       00J          SUBROUTINE GRAND (D,BA,Z,FR,FI)
000002       00J          CALL RAD (D,BA,Z,X,ETA,Y)
000003       00J          CALL POTAS(X,Y,QR,QI)
000004       00J          CALL ASH(D,BA,Z,AR,AI)
000005       00J          FR=QR*AR-QI*AI
000006       00J          FI=QR*AI+QI*AR
000007       00J          RETURN
000008       00J          END

END ELT.


@HDG SGRATE
```

```
HO,Y,CAN)
```



```
@ELT,L DIFF.SGRATE,.SGRATE
ELTGT7 RLI370 06/24-09:49:18-(1,0)
000001      000          SUBROUTINE GRATE(D,BA,A,B,S)
000002      000          EVR=0.
000003      000          ODR=0.
000004      000          EVI=0.
000005      000          ODI=0.
000006      000          CALL GRAND (D,BA,A,AFR,AFI)
000007      000          CALL GRAND (D,BA,B,BFR,BFI)
000008      000          N=1
000009      000          DO 41 I=1,20
000010      000          M=N
000011      000          N=2*N
000012      000          EVR=ODR+EVR
000013      000          EVI=ODI+EVI
000014      000          C=(B-A)/N
000015      000          ODR=0.
000016      000          ODI=0.
000017      000          DO 61 J=1,M
000018      000          Z=A+C*(2*J-1)
000019      000          CALL GRAND (D,BA,Z,XR,XI)
000020      000          ODR=ODR+XR
000021      000       61 ODI=ODI+XI
000022      000          TR1=C*(AFR+BFR+2*EVR+4*ODR)/3
000023      000          TI1=C*(AFI+BFI+2*EVI+4*ODI)/3
000024      000          WRITE(5,1) N,TR1,TI1,SS1
000025      000        1 FORMAT(1X,'N=',I9,' TR1=',E12.6,' TI1=',E12.6,' SS1=',E12.6)
000026      000          SS1=TR1*TR1+TI1*TI1
000027      000          IF(I.EQ.1) GO TO 41
000028      000          IF(ABS(SS1/SS2-1).LE.1.E-3) GO TO 51
000029      000       41 SS2=SS1
000030      000       51 S=SS1
000031      000          RETURN
000032      000          END

END ELT.

@HDG SGREAT
```

BLK	REC	CONTROL	COMMAND	OPERAND	RECORD	TYPE	NAME	DATE	TIME
000688	005					SOR	PHYSOP	01/06/76	12.46 C
000689	063				PROGRAM PHYSOP			00000010	
000688	091				WRITE(3,2)			00000020	
000688	115				2 FORMAT('0',3X,'D',10X,'CROSS',7X,'LOGCROSS')			00000030	
000688	175				DO 41 J=1,71			00000040	
000688	201				D=9.+J			00000050	
000688	221				S=SIN(2*D)			00000060	
000689	005				F=1-S/D+S*S/(D*D)			00000070	
000689	035				G=ALOG10(F)			00000080	
000689	061				WRITE(3,4) D,F,G			00000090	
000689	091				4 FORMAT(1X,F5.2,2E15.6)			00000100	
000689	129				41 CONTINUE			00000110	
000689	154				STOP			00000120	
000689	172				END			00000130	

BLK	REC	CONTROL	COMMAND	OPERAND	RECORD	TYPE	NAME	DATE	TIME
000943	139					SOR	ELLIP	03/23/76	16.51 C
000943	197				SUBROUTINE ELLIP(I,Z,BA,EL)			03000010	
000944	305				S=SIN(Z)			03000020	
000944	327				B2=BA*BA			03000030	
000944	349				EL=SQRT(B2/(1-B2)+S*S)			03000040	
000944	385				RETURN			03000050	
000944	105				END			03000060	

BLK	REC	CONTROL	COMMAND	OPERAND	RECORD	TYPE	NAME	DATE	TIME	
000783	005									
000783	063				FUNCTION GREER(I,A,B,BA)	SOR	GREER	03/12/76	12.35	0
000783	101				EVR=0.					03000010
000783	121				ODR=0.					03000020
000783	141				CALL ELLIP(I,A,BA,AFR)					03000030
000783	177				CALL ELLIP(I,B,BA,BFR)					03000040
000783	213				N=1					03000050
000784	005				DO 41 KK=1,11					03000060
000784	032				M=N					03000070
000784	049				N=2*N					03000080
000784	068				EVR=ODR+EVR					03000090
000784	093				C=(B-A)/N					03000100
000784	116				ODR=0.					03000110
000784	136				DO 61 J=1,M					03000120
000784	161				Z=A+C*(2*J-1)					03000130
000784	188				CALL ELLIP(I,Z,BA,XR)					03000140
000784	223			61	ODR=ODR+XR					03000150
000785	005				TR1=C*(AFR+BFR+2*EVR+4*ODR)/3					03000160
000785	048				IF (KK.EQ.1) GO TO 41					03000170
000785	083				IF(TR2.EQ.0.) GO TO 41					03000180
000785	119				DR=ABS(TR1/TR2-1)					03000190
000785	150				IF(DR.LE.1.E-4) GO TO 51					03000200
000785	188			41	TR2=TR1					03000210
000785	212			51	GREER=TR1					03000220
000786	005				RETURN					03000230
000786	025				END					03000240
										03000250

BLK	REC	CONTROL	COMMAND	OPERAND	RECORD	TYPE	NAME	DATE	TIME
000786	042								
000786	100				SUBROUTINE AMPLI(D,BA,SR,SI)	SOR	AMPLI	03/24/76	12.30 C
000786	142				A=0.			00000010	
000786	160				B=1.570795			00000020	
000786	184				I=1			00000030	
000786	201				F1=GREER(I,A,B,BA)			00000040	
000786	233				BA2=BA*BA			00000050	
000787	005				A1=SQRT(1-BA2)			00000060	
000787	033				A2=CBRT(D)			00000070	
000787	057				C=A2*CBRT(BA2)*F1/A1			00000080	
000787	091				C1=EXP(-1.40057*C)			00000090	
000787	123				C2=2*D+1.047198+.808617*C			00000100	
000787	162				C3=5.430336*A2/CBRT(BA2*BA2)			00000110	
000787	204				C4=.5*D*BA2			00000120	
000787	229				C5=C1*C3*C4			00000130	
000788	005				SR=C4*COS(2*D)-C5*COS(C2)			00000140	
000788	044				SI=-C4*SIN(2*D)-C5*SIN(C2)			00000150	
000788	084				RETURN			00000160	
000788	104				END			00000170	
								00000180	

BLK	REC	CONTROL	COMMAND	OPERAND	RECORD	TYPE	NAME	DATE	TIME
001635	178					SOR	SIE31	04/15/76	09.30 C
001636	005				PROGRAM SIE31			00000010	
001636	032				READ(1,1) SVA			00000020	
001636	059			1	FORMAT(F10.0)			00000030	
001636	088				WRITE(3,2) SVA			00000040	
001636	115			2	FORMAT(26X,' SVA =',F6.2)			00000050	
001636	157				WRITE(3,3)			00000060	
001636	181			3	FORMAT('0',13X,'D',10X,'SS',10X,'DL',11X,'SSL')			00000070	
001637	005				T=.017453*SVA			00000080	
001637	032				TA=TAN(T)			00000090	
001637	055				F=(1+4*TA*EXP(-1/(4*TA))/3.14159)/(3*TA)			00000100	
001637	109				FF=F*F			00000110	
001637	129				DO 4 I=1,40			00000120	
001637	154				D=.025*I			00000130	
001637	176				SS=FF*D**4			00000140	
001637	200				DL=ALOG10(D)			00000150	
001637	226				SSL=ALOG10(SS)			00000160	
001638	005				WRITE(3,5) D,SS,DL,SSL			00000170	
001638	041			5	FORMAT(10X,F6.2,2X,E12.6,2X,F10.6,2X,E12.6)			00000180	
001638	100			4	CONTINUE			00000190	
001638	124				STOP			00000200	
001638	142				END			00000210	

BLK	REC	CONTROL	COMMAND	OPERAND	RECORD	TYPE	NAME	DATE	TIME
001638	159					SOR	SIE32	04/15/76	09.32 C
001638	217				PROGRAM SIE32			03000010	
001639	005				READ(1,1) SVA			03000020	
001639	032			1	FORMAT(F10.3)			03000030	
001639	061				WRITE(3,2) SVA			03000040	
001639	089			2	FORMAT(26X,' SVA =',F6.2)			03000050	
001639	130				WRITE(3,3)			03000060	
001639	154			3	FORMAT('0',13X,'D',10X,'SS',10X,'DL',11X,'SSL')			03000070	
001639	217				T=.017453*SVA			03000080	
001640	005				TB=TAN(T)			03000090	
001640	028				TA=TB/(1+2*TB)			03000100	
001640	056				F=(1+4*TA*EXP(-1/(4*TA))/3.14159)/(3*TA)			03000110	
001640	110				FF=F*F			03000120	
001640	130				DO 4 I=1,40			03000130	
001640	155				D=.025*I			03000140	
001640	177				SS=FF*D**4			03000150	
001640	201				DL=ALOG10(D)			03000160	
001640	227				SSL=ALOG10(SS)			03000170	
001641	005				WRITE(3,5) D,SS,DL,SSL			03000180	
001641	041			5	FORMAT(10X,F6.2,2X,E12.6,2X,F10.6,2X,E12.6)			03000190	
001641	100			4	CONTINUE			03000200	
001641	124				STOP			03000210	
001641	142				END			03000220	

```
@ELT,L DIFF.SCONEF1,,SCONEF1
ELTOT7 RLIB70 07/26-14:57:21-(3,0)
000001      000          SUBROUTINE GRAND(JJ,D,SVA,Z,FR,FI)
000002      000          X=TAN(SVA)*Z
000003      000          Y=-SIN(SVA)
000004      000          CALL POTAS(X,Y,QR,QI)
000005      000          A=Z*COS(SVA)
000006      000          AA=.5*Z*Y*Y
000007      000          HR=AA*SIN(A)
000008      000          HI=-AA*COS(A)
000009      000          FR=QR*HR-QI*HI
000010      000          FI=QI*HR+QR*HI
000011      000          RETURN
000012      000          END

END ELT.


@HDG SCONES
```

```
@ELT,L DIFF.SGREAT,.SGREAT
ELTOT7 RLIB70 07/26-14:57:36-(1,0)
000001      000          SUBROUTINE GREAT(JJ,D,SVA,A,B,TR,TI)
000002      000          EVR=0.
000003      000          ODR=0.
000004      000          EVI=0.
000005      000          ODI=0.
000006      000          CALL GRAND(JJ,D,SVA,A,AFR,AFI)
000007      000          CALL GRAND(JJ,D,SVA,B,BFR,BFI)
000008      000          N=1
000009      000          DO 41 I=1,20
000010      000          M=N
000011      000          N=2*N
000012      000          EVR=ODR+EVR
000013      000          EVI=ODI+EVI
000014      000          C=(B-A)/N
000015      000          ODR=0.
000016      000          ODI=0.
000017      000          DO 61 J=1,M
000018      000          Z=A+C*(2*J-1)
000019      000          CALL GRAND(JJ,D,SVA,Z,XR,XI)
000020      000          ODR=ODR+XR
000021      000       61 ODI=ODI+XI
000022      000          TR1=C*(AFR+BFR+2*EVR+4*ODR)/3
000023      000          TI1=C*(AFI+BFI+2*EVI+4*ODI)/3
000024      000          SS1=TR1*TR1+TI1*TI1
000025      000          WRITE(5,1) N,TR1,TI1,SS1
000026      000        1 FORMAT(1X,'N=',I9,' TR1=',E12.6,' TI1=',E12.6,' SS1=',E12.6)
000027      000          IF(I.EQ.1) GO TO 41
000028      000          IF(ABS(SS1/SS2-1).LE.1.E-3) GO TO 51
000029      000       41 SS2=SS1
000030      000       51 TR=TR1
000031      000          TI=TI1
000032      000          RETURN
000033      000          END

END ELT.

@HDG SGRIND
```

```
@ELT,L DIFF.SMAIN2,.SMAIN2
ELTOT7 RLIB70 07/26-14:57:48-(3,0)
000001      000          READ(8,1) SVA
000002      000        1 FORMAT(F10.0)
000003      000          WRITE(5,2) SVA
000004      000        2 FORMAT(26X,' SVA =',F6.2)
000005      000          WRITE(5,3)
000006      000        3 FORMAT('0',13X,'D',10X,'SS',10X,'DL',11X,'SSL')
000007      000          T=.0174533*SVA
000008      000          SN=SIN(T)
000009      000          DO 4 I=1,15
000010      000          D=1+.2*I
000011      000          A=0.
000012      000          B=D/SN
000013      000          CALL GREAT(JJ,E,T,A,B,TR,TI)
000014      000          A1=D*D/2
000015      000          A2=2*D/TAN(T)
000016      000          UR=-A1*SIN(A2)
000017      000          UI=A1*COS(A2)
000018      000          SR=TR+UR
000019      000          SI=TI+UI
000020      000          SS=4*(SR*SR+SI*SI)/(D*D)
000021      000          DL=ALOG10(D)
000022      000          SSL=ALOG10(SS)
000023      000          WRITE(5,5) D,SS,DL,SSL
000024      000        5 FORMAT(10X,F6.2,2X,E12.6,2X,F10.6,2X,E12.6)
000025      000        4 CONTINUE
000026      000          STOP
000027      000          END

END ELT.


@HDG SMAIN3
```

```
000086.3)   000          WRITE(5,2)
```



```
@ELT,L DIFF.SSTRAL
ELTOT7 RLIB70 07/26-14:58:00-(0,)
000001      000          SUBROUTINE STRAL(D,SVA,Z,RHO,ETA)
000002      000          S=SIN(SVA)
000003      000          C=COS(SVA)
000004      000          SZ=SQRT(1-Z*Z)
000005      000          ETA=D/(Z*S+SZ*C)
000006      000          RHO=SZ*ETA/C
000007      000          RETURN
000008      000          END

END ELT.


@HDG SSYMINT
```

```
@ELT,L DIFF.SCONES,.SCONES
ELTOT7 RLIB70 08/09-17:10:07-(1,0)
000001       000          SUBROUTINE GRAND(JJ,D,SVA,Z,FR,FI)
000002       000          IF(JJ.GT.1) GO TO 1
000003       000          CALL STRAL(D,SVA,Z,RHO,ETA)
000004       000          S=SIN(SVA)
000005       000          AA=.5*S*ETA**3/D
000006       000          AR=-AA*SIN(Z*ETA)
000007       000          AI=-AA*COS(Z*ETA)
000008       000          CALL POTAS(RHO,-S,QR,QI)
000009       000          GO TO 2
000010       000        1 CALL POTAS(D,-Z,QR,QI)
000011       000          DZ=D*Z
000012       000          ODZ=-.5*D*DZ
000013       000          AR=ODZ*SIN(DZ)
000014       000          AI=ODZ*COS(DZ)
000015       000        2 FR=QR*AR-QI*AI
000016       000          FI=QR*AI+QI*AR
000017       000          RETURN
000018       000          END

END ELT.


@HDG SDBES
```

```
@ELT,L DIFF.SMAIN3,.SMAIN3
ELTOT7 RLIB70 07/26-14:57:51-(3,0)
000001       000          READ(8,1) SVA
000002       000        1 FORMAT(F10.0)
000003       000          WRITE(5,2) SVA
000004       000        2 FORMAT(26X,' SVA =',F6.2)
000005       000          WRITE(5,3)
000006       000        3 FORMAT('0',13X,'D',10X,'SS',10X,'DL',11X,'SSL')
000007       000          T=.0174533*SVA
000008       000          SI=SIN(T)
000009       000          DO 4 I=1,15
000010       000          D=1+.2*I
000011       000          CALL GREAT(1,D,T,SI,1.,TR,TI)
000012       000          CALL GREAT(2,D,T,-1.,SI,UR,UI)
000013       000          VR=TR*UR
000014       000          VI=TI*UI
000015       000          SS=4*(VR*VR+VI*VI)/(D*D)
000016       000          DL=ALOG10(D)
000017       000          SSL=ALOG10(SS)
000018       000          WRITE(5,5) D,SS,DL,SSL
000019       000        5 FORMAT(10X,F6.2,2X,E12.6,2X,F10.6,2X,E12.6)
000020       000        4 CONTINUE
000021       000          STOP
000022       000          END

END ELT.


@HDG SMASH
```

APPENDIX B

From section (2.6) we have

$$I_1 = \int_0^{2\pi} e^{-iA\cos(\phi-\phi')}\, d\phi' \qquad \text{--- (1)}$$

$$I_2 = \int_0^{2\pi} \cos(\phi-\phi')\, e^{-iA\cos(\phi-\phi')}\, d\phi' \qquad \text{--- (2)}$$

where $A = k\eta \sin\theta \sin\theta'$ --- (3)

Now $$\frac{\partial I_1}{\partial A} = -i \int_0^{2\pi} \cos(\phi-\phi')\, e^{-iA\cos(\phi-\phi')}\, d\phi'$$

$$= -i I_2$$

$$\therefore \quad I_2 = i\, \partial I_1 / \partial A \qquad \text{--- (4)}$$

By putting $\alpha = \phi' - \phi$ and using the periodicity of the trig. functions it can be shown that

$$I_1 = \int_0^{2\pi} e^{iA\cos\phi'}\, d\phi' \qquad \text{--- (5)}$$

Now $$I_1 = \int_0^{\pi} e^{-iA\cos\phi'} d\phi' + \int_{\pi}^{2\pi} e^{iA\cos\phi'} d\phi'$$

$$= \int_0^{\pi} \left(e^{-iA\cos\phi'} + e^{iA\cos\phi'}\right) d\phi',$$

$$\therefore I_1 = 2\int_0^{\pi} \cos(A\cos\phi')\, d\phi' \qquad \text{--- (6)}$$

In (6) we use $$\cos x = \sum_{n=0}^{\infty} \frac{(-1)^n x^{2n}}{(2n)!},$$

and interchange the order of the integration and the summation.

(6) becomes

$$I_1 = 2\sum_{n=0}^{\infty} \frac{(-1)^n A^{2n}}{(2n)!} \int_0^{\pi} (\cos\phi')^{2n}\, d\phi' \qquad \text{--- (7)}$$

In (7) put $J_m = \int_0^{\pi} (\cos\phi')^m d\phi'.$

On integrating by parts this gives

$$J_m = \int_0^{\pi} (m-1)\cos\phi'^{\,m-2} \sin^2\phi' d\phi'$$

$$= (m-1)\int_0^{\pi} \cos\phi'^{\,m-2} d\phi' - (m-1)\int_0^{\pi} \cos^m\phi' d\phi'$$

$$\therefore J_m = (m-1) J_{m-2} - (m-1) J_m$$

or $$J_{m+2} = \frac{m+1}{m+2} \cdot J_m .$$

As $J_1 = 0$, $J_m = 0$ for m odd.

$$\therefore J_{2n+2} = \frac{2n+1}{2n+2} \cdot J_{2n} \qquad \text{--- (8)}$$

using $J_0 = \pi$, we get

$$J_{2n} = \frac{(2n)!}{2^{2n}(n!)^2} \cdot \pi \qquad \text{--- (9)}$$

$\therefore$ from (7) and (9)

$$I_1(\theta,\theta') = 2\pi \sum_{n=0}^{\infty} \frac{(-1)^n}{(n!)^2}\left(\frac{A}{2}\right)^{2n} = -2\pi \sum_{n=1}^{\infty} \frac{(-1)^n}{((n-1)!)^2}\left(\frac{A}{2}\right)^{2n-2}$$

--- (10)

From (4) and (9) we have

$$I_2(\theta,\theta') = 2\pi i \sum_{n=1}^{\infty} \frac{(-1)^n}{n!(n-1)!}\left(\frac{A}{2}\right)^{2n-1}$$

--- (11)

BIBLIOGRAPHY

Abramowitz, M. and I.A. Stegun (1965) "Handbook of Mathematical Functions", Dover Publications.

Adachi, S. (1960) "The Nose-on Echo Area of Axially Symmetric Thin Bodies having sharp Apices", Ohio State University, Columbus, Ohio, Research Foundation Rept. No. 925-1, AD 240851.

Ahner, J.F. (1975) "The Exterior Dirichlet Problem for the Helmholtz Equation", J. Math. Anal. and Appl., Vol. 52, 415 - 429.

Asano, S and G. Yamamoto (1975) "Light Scattering by a Spheroidal Particle", Applied Optics, Vol. 14, No. 1, 29 - 49.

Bechtel, M.E. (1965) "Application of Geometric Diffraction Theory to Scattering from Cones and Disks", Proc. IEEE, Vol. 53, 877 - 882.

Blore, W.E. (1964) "The Radar Cross Section of Ogives, Double-backed Cones, Double-rounded Cones and Cone-spheres", IEEE Trans. Antennas Propagat. Vol. AP-12, 582 - 590.

British Association for the Advancement of Science Mathematical Tables, Part Volume A: Legendre Polynomials, Cambridge Univ. Press (1946).

Burnside, W.D., C.L. Yu and R.J. Marhefka (1975) "A Technique to Combine the Geometrical Theory of Diffraction and the Moment Method", IEEE Trans. Antennas Propagat, Vol. AP-23, 551 - 558.

Burton, A.J. and G.F. Miller (1971) "The Application of Integral Equation Methods to the Numerical Solution of some Exterior Boundary Value Problems", Proc. Roy. Soc. Ser. A, Vol. 323, 201 - 210.

Crispin, J.W. and A.L. Maffett (1965) "Radar Cross-Section Estimation for Simple Shapes", Proc. IEEE, Vol. 53, 833.

Crispin, J.W. and A.L. Maffett (1965) "Radar Cross-Section Estimation for Complex Shapes", Proc. IEEE, Vol. 53, 972.

Dawson, T.W.G. and W.R. Turner (1960) "Calculation of Radar Echoing Areas by the Cylindrical Current Method", Royal Aircraft Establishment, Farnborough, England, Tech. Note RAD 788

Duschek, A and A. Hochrainer (1960) "Tensorrechnung in Analytischer Darstellung, I Tensoralgebra", Springer-Verlag.

Duschek, A. and A. Hochrainer (1961) "Tensorrechnung in Analytischer Darstellung, II Tensoranalysis", Springer-Verlag.

Flammer, C. (1957) "Spheroidal Wave Functions", Stanford Univ. Press, Stanford Calif.

Fock, V. (1946) J. Phys. Moscow, Vol. 10, 130.

Franz, W. (1954), Z. Naturforsch. Vol. 9a, 705.

Goldstein, M. and R.M. Thaler (1958) "Bessel Functions for Large Arguments", MTAC, Vol. XII, 18 - 26.

Goldstein, M. and R.M. Thaler (1959) "Recurrence Techniques for the Calculation of Bessel Functions", MTAC, Vol. XIII, 102 - 108.

Harrington, R.F. (1968) "Field Computation by Moment Methods", MacMillan (New York).

Hong, S. and S.L. Borison (1968) "Short-pulse Scattering by a Cone - Direct and Inverse", IEEE Trans. Antennas Propagat., Vol. AP-16, 98 - 102.

Hönl, H., A.W. Maue and K. Westpfahl (1961) "Theorie der Beugung", Encyclopaedia of Physics, Vol. XXV/1, Springer-Verlag.

Imai, I. (1954) Z. Physik, Vol. 137, 31.

Jones, D.S. (1957) "High-frequency Scattering of Electromagnetic Waves", Proc. Roy. Soc., A, Vol. 240, 206 - 213.

Jones, D.S. (1964) "The Theory of Electromagnetism", Pergamon Press.

Kazarinoff, N.D. and R.K. Ritt (1959) "On the Theory of Scalar Diffraction and its Application to the Prolate Spheroid", Annals of Physics, Vol. 6, No. 3, 277 - 299.

Keller, J.B. (1958) "A geometrical theory of Diffraction" in "Calculus of Variations and its Applications", Proc. Symp. Appl. Math., Vol. 8, McGraw-Hill.

Keller, J.B., R.E. Kleinman and T.B.A. Senior (1972) "Dipole Moments in Rayleigh Scattering", J. Inst. Math. Appl., Vol. 9, 14 - 22.

Keller, J.B., R.M. Lewis and B.D. Seckler (1956) "Asymptotic Solution of some Diffraction Problems", Commun. Pure Appl. Math., Vol. IX, 207 - 265.

Kellogg, O.D. (1929) "Foundations of Potential Theory", Dover Publications Inc. (1953). Reissue of the first edition of 1929.

Kennaugh, E.M. and D.L. Moffatt (1962) "On the Axial Echo Area of the Cone-sphere Shape", Proc. IRE (Correspondence), Vol. 50, 199.

Kennaugh, E.M. and R.L. Cosgriff (1958) "The use of Impulse Response in Electromagnetic Scattering Problems", IRE Nat'l. Conv. Rec. pt. I, 72 - 77.

Kleinman, R.E. (1965) "The Rayleigh Region", Proc. IEEE, Vol. 53, No. 8, 848 - 855.

Kleinman, R.E. and G.F. Roach (1974) "Boundary Integral Equations for the three-dimensional Helmholtz equation", SIAM Rev., Vol. 16, 214 - 236.

Kleinman, R.E. and T.B.A. Senior (1963) "Diffraction and Scattering by Regular Bodies - II: The Cone", Radiation Lab., The University of Michigan, Ann Arbor, Rept. 3648-2-T.

Lee, S-W. and G.A. Deschamps (1976) "A Uniform Asymptotic Theory of Electromagnetic Diffraction by a Curved Wedge", IEEE Trans. Propagat., Vol. AP-24, No. 1, 25 - 34.

Levy, B.R. and J.B. Keller (1959) "Diffraction by a Smooth Object", Commun. Pure and Appl. Math., Vol. 12, 159 - 209.

Levy, B.R. and J.B. Keller (1960) "Diffraction by a Spheroid", Can. J. Phys., Vol. 38, 129 - 144.

Magnus, W. and F. Oberhettinger (1954) "Formulas and Theorems for the Functions of Mathematical Physics", Chelsea Pub. Co.

Meixner, J. and F.W. Schäfke (1954) "Mathieusche Funktionen und Sphäroidfunktionen", Springer-Verlag.

Moffatt, D.L. and E.M. Kennaugh (1965) "The Axial Echo Area of a Perfectly Conducting Prolate Spheroid", IEEE Trans. Antennas Propagat., Vol. AP-13, 401 - 409.

National Bureau of Standards Mathematical Tables Project, Tables of Spherical Bessel Functions, Vols. I and II, Columbia Univ. Press (1947).

Rayleigh (J.W. Strutt) (1897), Phil. Mag., Vol. 44, 28.

Schwarz, L. (1943) "Zur Theorie der Beugung einer ebenen Schallwelle an der Kugel", Akust. Z., Vol. 8, 91 - 117.

Senior, T.B.A. (1965) "A Survey of Analytical Techniques for Cross-section Estimation", Proc. IEEE, Vol. 53, 822 - 833.

Senior, T.B.A. (1965a) "The Backscattering Cross-section of a Cone-sphere", IEEE Trans. Antennas Propagat., Vol. AP-13, 271 - 277.

Senior, T.B.A. (1966) "The Scattering from Acoustically hard and soft Prolate Spheroids for Axial Incidence", Can. J. Phys., Vol. 44, 655 - 667.

Senior, T.B.A. (1973) "Low-frequency Scattering", J. Acoust. Soc. Am., Vol. 53, No. 3, 742 - 747.

Siegel, K.M. (1959) "Far Field Scattering from Bodies of Revolution", Appl. Sci. Res., Sec. B, Vol. 7, Issue 4, 293 - 328.

Siegel, K.M. (1963) "Low-frequency Radar Cross Section Computations", Proc. IEEE (Correspondence), Vol. 51, 232 - 233.

Sinha, B.P. and R.H. MacPhie (1975) "Electromagnetic Scattering from Prolate Spheroids for Axial Incidence", IEEE Trans. Antennas Propagat., Vol. Ap.-23, 676-679.

Sleator, F.B. (1964) "Diffraction and Scattering by Regular Bodies - III: The Prolate Spheroid", Radiation Lab., The University of Michigan, Ann Arbor, Rept. 3648-6-T.

Spence, R.D. and S. Granger (1951) "The Scattering of Sound from a Prolate Spheroid", J. Acoust. Soc. Am., Vol. 23, No. 6, 701 - 706.

Stratton, J.A. (1941) "Electromagnetic Theory", McGraw-Hill Book Company.

Stratton, J.A., P.M. Morse, L.J. Chu and R.A. Hutner (1941) "Elliptical Cylinder and Spheroidal Wave Functions", John Wiley and Sons.

Ursell, F. (1973) "On the Exterior Problem of Acoustics", Proc. Camb. Phil. Soc., Vol. 74, 117 - 125.

Wait, J.R. (1955), Can. J. Phys., Vol. 44, 655 - 667.

ACKNOWLEDGEMENTS

The author wishes to thank his supervisor Prof. G.R. Brundrit for his help and guidance.

Thanks are also due to Mr. A. Haller of the Computer Centre, University of the Western Cape, for helpful discussions, Mr. Jan Engelbrecht who drew the graphs and Mrs. Valerie Green who typed the thesis.

Finally the author is grateful to his wife and all others who gave encouragement during the project.